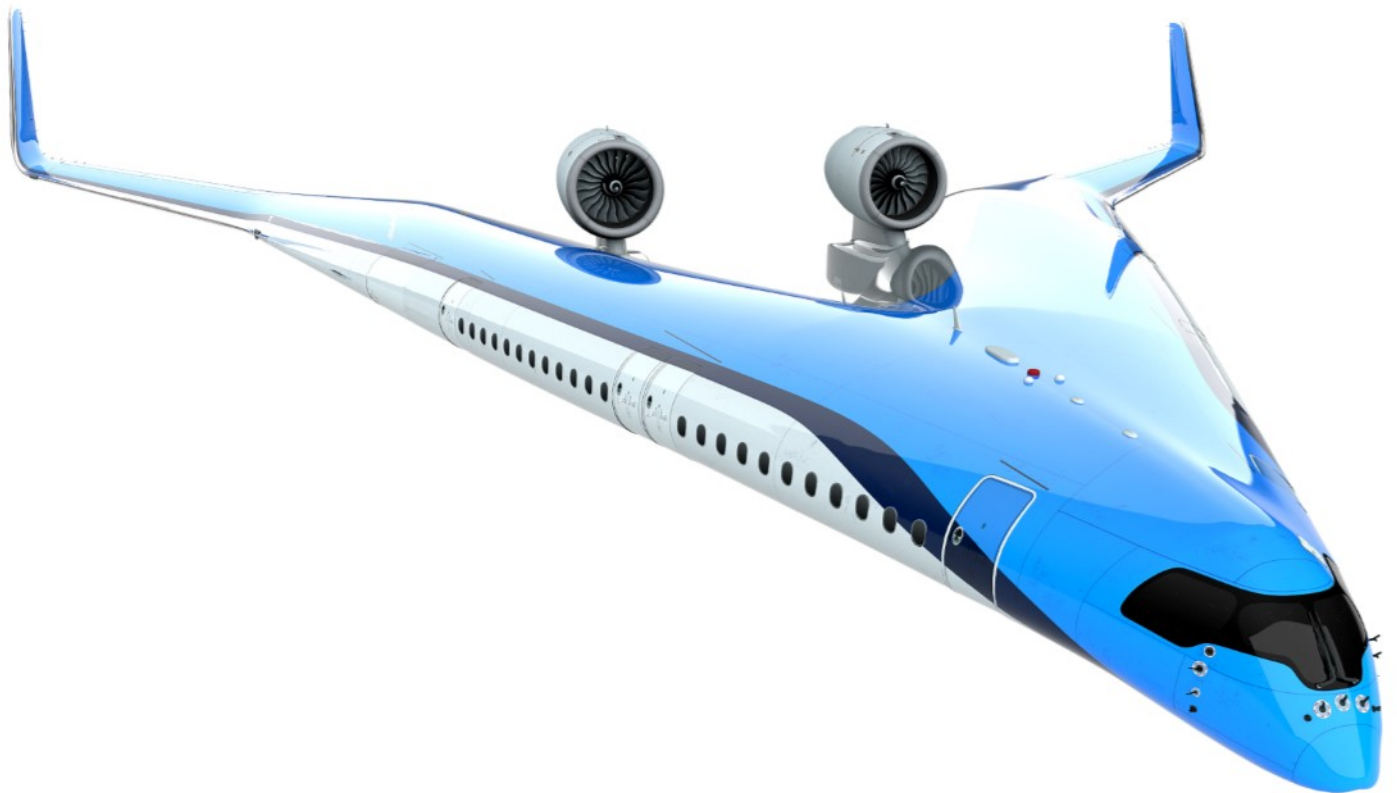


Handling Qualities of a Flying V Configuration

T. Cappuyns



Handling Qualities of a Flying V Configuration

by

T. Cappuyns

to obtain the degree of Master of Science
at the Delft University of Technology,
to be defended publicly on Tuesday December 17, 2019 at 13:00 AM.

Student number: 4290135
Project duration: June 3, 2019 – December 17, 2019
Thesis committee: Prof. dr. ir. L. L. M. Veldhuis, TU Delft, Chair
Dr. ir. R. Vos, TU Delft, Supervisor
Ir. K. Bender, Airbus Operations GmbH, Daily Supervisor
Ir. H. Mulder, TU Delft, Examiner

This thesis is confidential and cannot be made public until December 31, 2024.

An electronic version of this thesis will become available at <http://repository.tudelft.nl/>.

Equivalent word count: 29,846

Summary

Generally, performance of aircraft is optimized within the limits of adequate Handling Qualities. The dominant challenges in designing flying wings exist in their paradigm relating stability margin and the effectiveness of controls. The project, undertaken at Airbus Future Projects Office, provides a qualitative assessment of the Handling Qualities of the Flying V concept. More specifically, the centre of gravity limits for the Flying V configuration are determined. A look into the effects of the overall parametric model variables such as sweep, dihedral etc. onto the Handling Qualities is provided.

The Flying V, a tailless concept proposed by J. Benad is a recently conceived flying wing concept. The aerodynamically efficient tailless design integrates the cabin, cargo space and fuel tanks in V-shaped wings. Benefits of up to 20% in fuel consumption in comparison to the Airbus A350 were found. Further investigation focused on optimizing and maturing the conceptual design. As the design passed its first iteration, it was an appropriate time to look into the Handling Qualities.

Relevant Handling Qualities criteria were selected based on the Military Handbook MIL-HDBK-1797 and European Aviation Safety Agency, Large Aeroplanes Certification Specifications. A 6 Degrees of Freedom Flight Mechanics Toolbox was set-up. This mathematical model provides the aircraft's flight dynamics and allows for analyses in time and frequency domain. The system of equations is trimmed and subsequently linearized for the eigenvalue analyses.

Data generation was achieved through parametric models. These geometric models were fed into the Vortex Lattice Method and the lumped mass model. The lift distribution was optimized through altering the wing twist. Subsequently the stability and control derivatives were assembled. The parametric models were additionally used to create a lumped masses model providing the inertia estimation. The same methodology was repeated for a reference aircraft of conventional configuration based on the A350-900. Both time and frequency domain analysis were undertaken focusing on stability and controllability requirements.

Results revealed a similar centre of gravity range for the Flying V in comparison to the conventional configuration. It was found that with the current design of the Flying V, the Dutch Roll mode is unstable. Therefore as a possible solution, a certifiable yaw damper would be required with a failure rate of less than 10^{-9} . Furthermore, the rudder control power proved to be insufficient in case of One Engine Inoperative conditions. Rudder deflections reached excessive deflections during Steady Heading Sideslip, Trim in Coordinated Turn and Bank to Bank tests with One Engine Inoperative. As no dedicated study has been made into the design of the winglets, these lateral-directional controllability and stability discrepancies are not insurmountable.

A dedicated control surface design study is likely to resolve the bulk of these complications. Specifically, the addition of more advanced and secondary control surfaces such as spoilers and split elevons or ruddervons will reduce the rudder control power demanded.

Up to the conclusion of this research not all capabilities of the toolbox were put to the test. As there is a landing gear model included, it might be beneficial to look into take-off behaviour. Furthermore the flexibility of the toolbox allows for a rapid continuation of the Handling Qualities study. Taking into account the limitations of the toolbox, this study concludes that apart from the undersized yaw control surfaces and dutch roll damping all tested criteria are favourable.

Acknowledgements

I would like to express my gratitude to my thesis supervisor, Dr. ir. Roelof Vos. The same day as I contacted you with relation to thesis topics I was handed a fantastic opportunity. Upon informing you about being accepted into the National Test Pilot School you were supportive towards my tight deadline.

Considering this limited window, I owe a considerable amount of gratitude to my Airbus supervisor Klaus Bender. Thank you for adjusting all relevant tools for my purposes and explaining concepts time and again with great patience. I greatly enjoyed our ice cream breaks in summer and conversations about aviation history, unique aircraft and their properties. Also, thank you for monitoring my work scheme and ensuring I took enough rest.

To my parents and sister, all the achievements of the past years are as much yours as they are mine. You sacrificed a lot of time and financial resources without ever doubting my abilities. I owe you a lifelong gratitude for your endless support.

To my partner, you have taught me the art of planning and structured work. You seem tireless in your hard work and it I am grateful for being able to share a passion for aviation and engineering. Furthermore you have proven that you support me wherever I go, contributing to a large portion to the encouragement of my ambitions.



*Thibaut Cappuyns
Tongeren, December 2019*

Contents

1	Introduction	1
1.1	Problem Statement	1
1.2	Research Objective	2
1.3	Report Structure	2
2	Background	3
2.1	Flying V Configuration	3
2.2	Handling Qualities Requirements	5
2.2.1	Longitudinal Requirements	5
2.2.2	Lateral-Directional Requirements	6
2.2.3	European Aviation Safety Agency Certification Specification 25	6
3	Methodology	9
3.1	BlackSwan Parametric Models	10
3.1.1	Flying V Classes	11
3.1.2	Elevons	12
3.1.3	Reference Aircraft Classes	13
3.2	Inertia Estimation.	16
3.3	Odilila, a Vortex Lattice Method.	18
4	Flight Mechanics Toolbox	20
4.1	Transformations	21
4.2	Equations	21
4.3	Trim Functions	22
4.3.1	Longitudinal Trim	22
4.3.2	Level Coordinated Turn Trim	22
4.3.3	Sideslip Trim	23
4.3.4	State Space.	23
4.3.5	Landing Gear	23
4.4	Process	24
4.5	Limitations	24
5	Verification & Validation	25
5.1	Inertia Model Verification and Validation	25
5.2	Odilila Validation	28
5.3	Aircraft Model Validation & Verification.	30
5.3.1	Flying V Aero Data Validation	31
5.3.2	Neutral Point Verification	32
5.4	Flight Mechanics Model Verification	33
6	Results	37
6.1	Moments of Inertia	37
6.2	Performance Considerations	37
6.2.1	Optimization Point.	38
6.2.2	Maximum Specific Range	40
6.3	Longitudinal Handling Qualities	41
6.3.1	Trim on Approach	41
6.3.2	Control Anticipation Parameter	43
6.3.3	Eigenvalue Analyses	44

6.4	Lateral-Directional Handling Qualities	45
6.4.1	Lateral Control Departure Parameter	45
6.4.2	Eigenvalue Analyses	46
6.4.3	EASA CS 25.143	48
6.4.4	Proposed Solution	51
7	Conclusion & Recommendations	55
7.1	Conclusion	55
7.2	Recommendations	56
7.2.1	Flight Mechanics Toolbox	56
7.2.2	Flying V	57
	Bibliography	58
A	Cooper-Harper Rating Scale	60
B	MIL-HDBK-1797A Extractions	61
C	Parametric Model Values	63
D	A300-600 Mass & Inertia Model	66
E	Odilila Delta Wing Validation	67

Nomenclature

Greek Symbols

α	Angle of attack	[deg]
β	Sideslip angle	[deg]
δ_a	Aileron deflection	[deg]
δ_e	Elevator deflection	[deg]
δ_r	Rudder deflection	[deg]
ϵ	Wing twist angle	[deg]
η	Relative kink position along half span	[-]
γ	Flight path angle	[deg]
λ	Wing sweep angle	[deg]
ϕ	Roll attitude	[deg]
ψ	Yaw attitude	[deg]
θ	Pitch attitude	[deg]

Roman Symbols

\bar{c}	Mean aerodynamic chord	[m]
C_D	Drag coefficient	[-]
C_L	Lift coefficient	[-]
C_m	Pitching moment coefficient	[-]
b	Span	[m]
p	Roll rate	[deg/s]
q	Pitch rate	[deg/s]
r	Yaw rate	[deg/s]
S	Surface area	[m ²]
V	Velocity	[m/s]
C_l	Rolling moment coefficient	[-]
C_n	Yawing moment coefficient	[-]
C_X	Force coefficient in X-direction	[-]
C_Y	Force coefficient in Y-direction	[-]
C_Z	Force coefficient in Z-direction	[-]

Subscripts

α	Derivative with respect to angle of attack	[1/deg]
β	Derivative with respect to sideslip angle	[1/deg]
δ_a	Change in stability derivative due to aileron deflection	[1/deg]
δ_e	Change in stability derivative due to elevator deflection	[1/deg]
δ_r	Change in stability derivative due to rudder deflection	[1/deg]
p	Derivative with respect to roll rate	[s/deg]
q	Derivative with respect to pitch rate	[s/deg]
r	Derivative with respect to yaw rate	[s/deg]
u	Velocity in x-direction with respect to the body fixed reference frame	[m/s]
v	Velocity in y-direction with respect to the body fixed reference frame	[m/s]
w	Velocity in z-direction with respect to the body fixed reference frame	[m/s]



Introduction

Tailless aircraft spark interest due to their aerodynamic performance advantages in comparison to conventional Wing-Body-Tail (WBT) configurations. The exclusion of horizontal and vertical tailplanes may however evolve into stability and control authority issues [16]. The Flying V, a tailless concept proposed by J. Benad is a recently conceived flying wing concept [5]. Upon having defined the specifications for the Flying V concept, a preliminary design was created. Consequently the aerodynamic shape was defined and optimized. The primary aim of aerodynamic optimization is designing a hull holding the highest aerodynamic efficiency. The succeeding step in the aircraft design process is looking into the handling characteristics of the outer shape defined.

Performance is optimized within the bounds of adequate Handling Qualities. These handling characteristics on their own are not optimized, they should rather be viewed as boundary conditions where stability and control impose contradicting requirements.

1.1. Problem Statement

Stability margin and control effectiveness go closely together as larger stability margins require higher pitching moment control authority. A poor feature intrinsic to flying wing designs is the lacking ability to generate moments (due to the lack of dedicated tailplane). Stall of the rearward parts of the planform can lead to pitch break tendencies or other poor high angle of attack behaviours. To compensate for the limited static margin, a small linear pitching moment is sought after. This can be achieved through incorporating reflex camber airfoils that complement the longitudinal dihedral. The latter being provided by combined wing sweepback and washout.

The small distance to the centre of gravity renders the elevons less effective for pitch control than an elevator mounted on a tailplane. The increased drag due to the elevator deflection, called 'trim drag', of the tailless aircraft may be one of the factors in favour of a design with a tailplane. Additionally, the 'elevator' of tailless aircraft is situated at the trailing edge of the wing. Therefore a deflection of an elevon does not only cause a change in pitching moment. The elevator deflection also has a non-negligible influence on the direct lift.

1.2. Research Objective

The Flying V is likely to exhibit, in addition to its aerodynamic superiority, some of the adverse characteristics inherent to flying wings. Having this in mind a Master thesis request was made by Airbus' Future Project Office (FPO). The problem statement was twofold as both Airbus and TU Delft pose requirements. The Airbus objectives were outlined as follows:

- Review HQ and performance studies for flying wing aircraft while establishing a state of the art literature study
- Identify a limited but relevant set of HQ and performance criteria
- Define a flight control layout
- Collect aerodynamic, mass and centre of gravity data in addition to setting up parametric models
- Validate the models generated
- Application of the models and trade studies
- Document the entire process

To satisfy the request made by FPO, this research project aims to understand the unaugmented stability characteristics of the Flying V configuration. Doing so by assembling a representative mathematical model. This will be achieved by the development and validation of a simplified numeric simulation for flight dynamics assessment. A basic understanding of the tailless flight dynamics is created through the application of the equations of motion and eventual Handling Qualities assessment. The Flying V's handling characteristics will be verified for their adequacy with relation to relevant criteria. The ultimate goal being able to provide a forward and rearward limit of the centre of gravity in function of the demonstrated characteristics and suggesting design changes where necessary. The objectives were shaped into the following research questions.

Research Question

How do the Handling Characteristics of a Flying V configuration compare to those of a conventional Wing-Body-Tail configuration?

- *What is the applicability of current Handling Qualities and performance criteria for a Flying V configuration?*
- *What is the influence of the centre of gravity position on the handling characteristics for a Flying V configuration?*
- *How do the overall parametric model variables such as sweep, dihedral, etc., affect the Handling Qualities for a Flying V configuration?*

1.3. Report Structure

The report is initiated by introducing the Flying V's design and work performed. The Handling Qualities requirements based on the Military-Standard-1797A [19] and EASA Certification Specification [1] is treated next. The latter provides an extra insight into the objectives in mind when undertaking this dissertation. Chapter 3 discloses the general methodology adopted to arrive at all the prerequisites of the Flight Mechanics Toolbox. Here, the creation of the parametric models, Inertia estimation and Aero Data files are described. The mathematical model to describe the flight mechanics is left for Chapter 4. The verification and Validation of the Inertia model, system of equations of the 6 Degrees of Freedom model and VLM method utilized are clarified in Chapter 5. The static and dynamic analysis and its conclusions and further recommendations conclude this report in Chapters 6 and 7.

2

Background

This Chapter will introduce the timeline of developments with regards to the Flying V, starting from its conception. It is attempted to give a general idea of the developments while going more in depth into the parts on the topic of Handling Qualities. Next the selected Handling Qualities Requirements will be explained as concise as possible.

2.1. Flying V Configuration

J. Benad concluded that the Flying V concept offers a gain over the reference airframe of about 10% higher aerodynamic efficiency [5]. The reference aircraft chosen was based on the Airbus A350-900. Additionally the Flying V has roughly a 2% weight advantage. Other attractive properties of the V comprised the simplicity and compactness of its configuration. In effect not requiring High Lift Devices (HLDs) nor tailplanes.

Going from the established concept, the iteration to further develop and optimize this concept is started. It was F. Faggiano who commenced by performing an aerodynamic optimization. The objective of this research was to investigate the performance in comparison to the NASA Common Research Model (CRM). An Euler method for the CFD computation was utilized and Benad's results were verified.

Three significant alterations to the design were made. The fuselage concept was changed from two elliptic payload compartments to a single wide elliptic one. The outer wing was swept back from 15° to 30° while the wash-out was increased. Eventually the Flying V proved to be 25% more aerodynamically efficient in comparison to the NASA Common Research Model (CRM) at the specified optimization point. This was a single point during cruise, more specifically: a Mach number of 0.85, altitude of 13,000 m and lift coefficient of 0.26.

The wing loft was analyzed by a Vortex Lattice Method and Computational Fluid Dynamics package. Lift distribution and accurate inviscid coefficients were examined. The largest portion of the adaptations to the design was implemented on the outboard part of the aircraft. This since the inboard part is constrained due to cabin parameters. Finally, vertical fins were introduced. These were sized based on stability and controllability requirements.

After Faggiano addressed the aerodynamic optimization and some of the static stability particularities. M. Palermo addresses the static Stability and Control characteristics of a scaled Flying V model [20]. The presence of a vortex and pitch-up break tendencies were found. The ideal Centre of Gravity (CG) location to maximize the lift coefficient was identified under the requirement of respecting 4.4% MAC of static margin.

B.R. Pascal created a nacelle by utilizing the Class/Shape Transformation (CST) method [21]. Within the design space defined, an optimal engine location was searched while minimizing the interference drag between engine and wing. Additionally it was suggested that the landing gear and engine could share their structural rigging points.

L.A. Vanderschaft researched the structural concept for the flying V. The dual-tube fuselage which had a circular shape was changed to an oval structure, which was integrated with the skin. L. A. Vanderschaft's work was limited to the current capabilities of the ParaPy[®] and ZORRO software. Another structural feasibility study was undertaken by M. Claeys. This work provides a preliminary structural weight for the Flying V and its components together with a reference aircraft. Relevant findings on the topic of Handling Qualities were made. At low speeds the centre of gravity was found to possibly trespass the Neutral Point, therefore becoming statically unstable.

All the research on the topic of the Flying V concludes to date that the feasibility of the concept is favourable. Continuing on the work mentioned, it is an appropriate moment to look more in depth to the Handling Qualities. The most up to date configuration is displayed in Figure 2.1, while the design parameters are provided in Table 2.1.

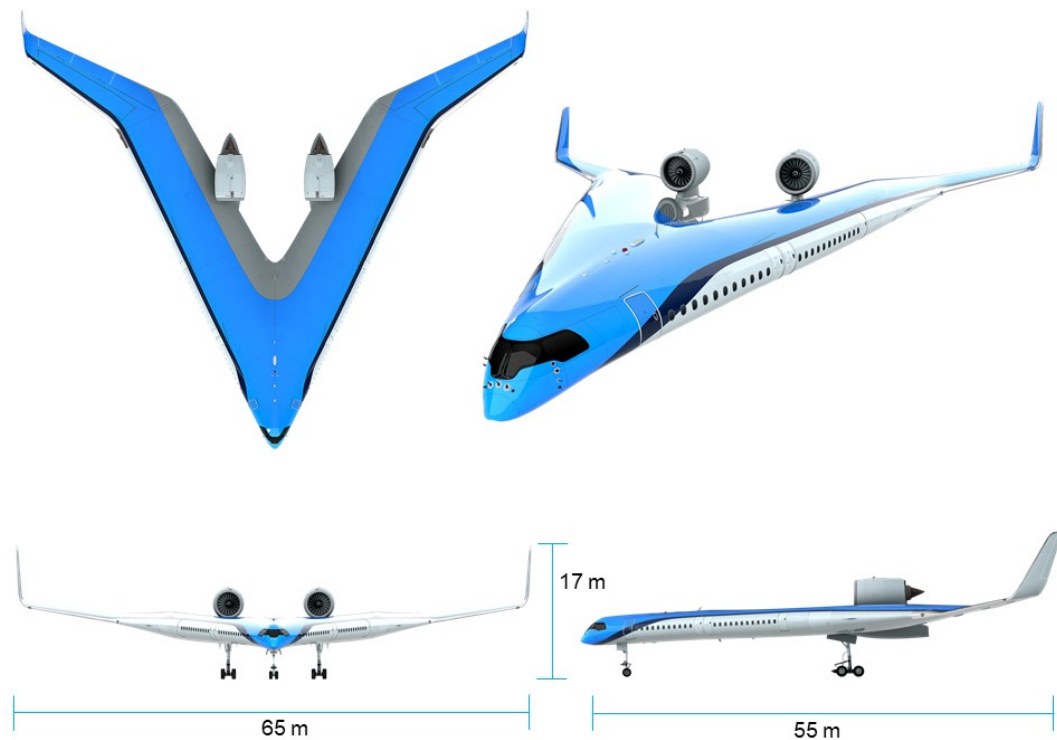


Figure 2.1: Flying-V, three view renders adopted from TU Delft; "Flying-V, flying long distances energy-efficiently", 3 June 2019, <https://www.tudelft.nl/en/ae/flying-v/>; render.

Parameter	Value	Unit
Length	55	[m]
Wingspan	65	[m]
Height	17	[m]
Pax	314	[-]
Fuel capacity	140.000	[l]
Cargo Capacity	160	[m ³]
Design Mach number	0.85	[-]
Cruise altitude	43,000	[ft]

Table 2.1: Design Parameters for Flying V conceptual design

2.2. Handling Qualities Requirements

Stability requirements can be fulfilled in an open or closed loop manner [15]. The open loop or unaugmented stability is specified as "inherent stability". If the stability is considered in closed loop, it is considered as "de facto stability". This work will mainly focus on the inherent stability of the Flying V's design in comparison to that of the reference aircraft.

The objectives of a Handling Qualities study are defined by Roskam [24] under following items. First of all the aircraft must demonstrate adequate control authority to maintain steady, straight horizontal flight. The aircraft can safely be manoeuvred from one steady state to another. The aircraft can be trimmed in certain flight conditions. Finally the cockpit control force levels are acceptable under all expected conditions, including those caused by configuration changes. The latter will be left for a more advanced design stage.

The latter objectives fall under the definition of Handling Qualities, best described by Cooper and Harper as: "those qualities or characteristics of an aircraft that govern the ease and precision with which a pilot is able to perform the tasks required in support of an aircraft role" [11]. Through criteria formalized in the late 1960s, Cooper and Harper set up a rating scale. Ever since, the Cooper-Harper Rating Scale has been used by test pilots during flight tests. The criteria and scale however are considered to be subjective. To be of added value, the rating can only be assigned to "a well defined combination of a repeatable task, a well trained pilot, that is actively engaged in accomplishing the task and a specific aircraft" [11]. As a remedy, correlation between the frequency and damping values of the modes and pilot opinion was researched and summarized in military handling qualities specifications. The most up to date version provided is the military Handbook MIL-HDBK-1797A [19].

A welcome feature of the Military specification concerned is that it provides a comprehensive assortment of requirements. Spanning all modes of motion of a conventional airplane, specifying the limits of acceptability which an aircraft should demonstrate to meet the requirements. Appendix B provides relevant requirements per mode and the subdivision into aircraft types, flight phases, etc.

Additionally a look into actual regulations is provided as well. Airworthiness regulations have a considerable leverage on the design and development of airplanes. This to such an extent that they should be considered as early as possible in the design cycle of a new concept. Failing to do so might result in exponential increase in cost or even having to abandon the project in a more advanced design stage due to its in-feasibility to meet the regulations concerned. Therefore it is advisable for this dissertation to look into these requirements.

First the aircraft classes, flight phases and the meaning of the different levels are outlined in Tables B.1 to B.3. Below the MIL-STD-1797A requirements are postulated followed by additionally selected Airworthiness requirements of EASA Certification Specification CS-25 Large Aeroplanes [1]. Sections written in *italic* indicate literally quoted extractions of CS25. The conditions that apply per requirement are explained in more detail in this document.

2.2.1. Longitudinal Requirements

Short Period

For the first longitudinal mode discussed, the longitudinal control dynamic is quantified per flight phase category and quality level according to its range of damping ratio. The damping ratios summarized in Table B.4 demonstrate a wide region of acceptable values. Cook demonstrated that the ideal damping ratio for a Short Period Oscillation (SPO) mode is 0.7. For this value, the settling time after a disturbance is minimized while ensuring a satisfactory margin for stability. Any value over 1.0 would be an indication of an over-damped system coming at the cost of longer settling times.

Phugoid

The other longitudinal mode inherits a slow sinusoidal mode. Potential and kinetic energy are interchanged while the angle of incidence remains virtually unchanged. This mode is known as the phugoid. This long periodic oscillation is occasionally unstable, as was the case for the Northrop B2 Spirit [16]. The inertia and damping forces have little influence on the Phugoid. Criteria are given in Table B.5.

Control Anticipation Parameter

The Control Anticipation Parameter criterion, as documented in the MIL-HDBK-1797A [19] defines limits for the natural frequency of the short period. It particularly intends to realise a certain longitudinal aircraft agility. Therefore, the CAP is defined, which represents the ratio of pitch acceleration and the respective steady state load factor induced by an elevator step input. It is approximately given by:

$$CAP = \frac{\ddot{\theta}(t=0)}{n_z(t \rightarrow \infty)} \approx \frac{\omega_{sp}^2}{n_{z_a}} \quad (2.1)$$

The CAP can generally be interpreted in such a way that the aircraft's response is too sluggish in case of a small CAP (below "Level 2" band). As a consequence the pilot tends to over-steer. On the other hand, for too large values of the CAP (above "level 2" band), the aircraft reacts too agile and under-steering is an issue.

2.2.2. Lateral-Directional Requirements

Dutch Roll

Flying qualities for the dutch roll have been specified in a number of ways. The undamped natural frequency and damping ratio specify the pace and oscillatory decay of the Dutch roll. A summary of the recommended minimum dutch roll frequency and damping [19] is provided in Table B.6. John Hodgekinson [15] prefers to plot the dutch roll damping ratio against dutch roll frequency, while the MIL-Handbook-1797 provides them with the axis inverted.

Lateral Control Departure Parameter

$$LCDP = C_{n_\beta} - C_{l_\beta} \frac{C_{n_{\delta_a}}}{C_{l_{\delta_a}}} \quad (2.2)$$

When yaw due to aileron gets large, commanded roll produces a motion in the opposite direction. As can be noted from Equation 2.2, the value depends completely on static aerodynamic coefficients. The LCDP is a coefficient which describes aircraft response on correct pilot's ailerons deflection in a case of sideslip, it should be positive. Negative values imply roll reversal.

In case the inherent LCDP is not positive, there are two ways to arrive at positive values. One is the augmented LCDP and the other the Aileron Rudder Interconnect (ARI) LCDP as shown in Equations 2.3 and 2.4. Here the damping derivatives are $C_{nr} < 0$, the yaw damping which should not be too negative. C_{lp} , the roll damping, preventing wing rock. ¹

$$LCDP_{Aug} = C_{n_\beta} - C_{l_\beta} \frac{C_{n_{\delta_a}}}{C_{n_{\delta_a}}} + k_1 \left(\frac{C_{n_{\delta_a}}}{C_{n_{\delta_a}}} C_{l_{\delta_r}} - C_{n_{\delta_r}} \right) \quad (2.3)$$

$$LCDP_{ARI} = C_{n_\beta} - C_{l_\beta} \left(\frac{C_{n_{\delta_a}} + k_2 C_{n_{\delta_r}}}{C_{l_{\delta_a}} + k_2 C_{l_{\delta_r}}} \right) \quad (2.4)$$

2.2.3. European Aviation Safety Agency Certification Specification 25

Relevant extractions of some of the test points are cited below. Where necessary, extra information is provided. More straightforward requirements will be explained during the Methodology and Results Chapters 3 and 6.

One Engine Inoperative (OEI)

The effect of an engine failure on the lateral directional behaviour is briefly explained. When flying at steady state, the ψ_{target} would be zero, more specifically the sideslip angle is zero. When at this point an engine failure occurs, a yaw rate ($\dot{\psi}$) in the direction of the inoperative engine is created. Additionally the wing on the same side rolls downward. A sideslip angle is created on the opposite side of the engine failure. The pilot's response should be to apply a roll input to stop the roll angle from increasing. However with One Engine Inoperative (OEI) and wings level, the asymmetrical thrust makes that the aircraft slip and the aircraft sets out on a curved flight path. To counteract this, the pilot or flight control system provides a rudder deflection

¹http://www.dept.aoe.vt.edu/mason/Mason_f/HiAlphaBasicsPres.pdf

input. Flying wings level with zero sideslip creates however more drag than establishing zero sideslip with a small specific bank angle. This angle can in fact be optimized. Therefore most Flight Control Systems on large aircraft provide a β_{target} . This translates to the sideslip angle that provides the least amount of drag for which the aircraft can be trimmed to achieve equilibrium again.

On this behalf, the most relevant requirement is the CS 25.121 Climb One-Engine-Inoperative [1]. This certification specification mainly focuses on the minimum climb gradient to be demonstrated in different phases of flight in the event of an engine failure. However a constraint is put on the maximum bank angle that is allowed during these climbs, the AMC state a bank angle of 2 to 3° to be acceptable. The sideslip to be assumed is a steady heading sideslip, meaning the aircraft maintains a constant track in no wind conditions.

Additionally, a look was given into CS 25.143. More specifically in CS 25.143(h) *The manoeuvring capabilities in a constant speed coordinated turn at forward centre of gravity, as specified in Table 2.2, must be free of stall warning or other characteristics that with interfere with normal manoeuvring.*

Configuration	Speeds	Manoeuvring bank	
		angle in a coordinated turn	Thrust/Power Setting
Take-Off	V_2	30°	Asymmetric WAT-Limited
Take-Off	$V_2 + XX$	40°	All Engines Operating Climb
En-Route	V_{FTO}	40°	Asymmetric WAT-limited
Landing	V_{REF}	40°	Symmetric for -3° Flight Path Angle

Table 2.2: Manoeuvring Bank Angle CS 25.143 requirements [1]

In summary, amendment 23 of CS 25 specifies the Acceptable Means of Compliance [1] for this requirement (Lateral Control Roll Capability One Engine Inoperative CS 25.147(d) [1]) as: *"With the aeroplane in trim, all as nearly as possible, in trim, for straight flight at V_2 , establish a steady 30° banked turn. It should be demonstrated that the aeroplane can be rolled to a 30° bank angle in the other direction in not more than 11 seconds. In this demonstration, the rudder may be used to the extent necessary to minimise sideslip. The demonstration should be made in the most adverse direction. The manoeuvre may be unchecked. Care should be taken to prevent excessive sideslip and bank angle during the recovery."*

First some insight on Table 2.2 is provided. The asymmetric WAT-Limited Thrust Setting stands for a combination of Weight, Altitude and Temperature (WAT). Practically this means that the thrust setting is able to provide for the minimum climb gradient specified in CS 25.121.

Next for the required speed of the second configuration the speed must be the approved airspeed for all-engines-operating initial climb. Note that for every aircraft type, V_1 , V_R and V_2 are computed for every take-off and vary with amongst other weight and balance, atmospheric and runway conditions. Before going into the next point a bit of background on reference speed is provided. V_2 is the minimum take-off speed that the aircraft must obtain when 35 ft above the runway surface is reached with One Engine Inoperative. This speed is always greater than V_{MCA} and therefore should guarantee controllability in flight. Additionally Airworthiness Authorities such as in this case, the EASA, demand that operating speeds are referenced to a demonstrable stall speed in flight test. This stall speed is the V_{S1g} or in other words the lowest speed at which a normal acceleration of 1 g can be maintained. The relation between V_2 and V_{S1g} is $1.13 V_{S1g} \leq V_2$. A more detailed look into take-off speeds is provided in Figure 2.2.

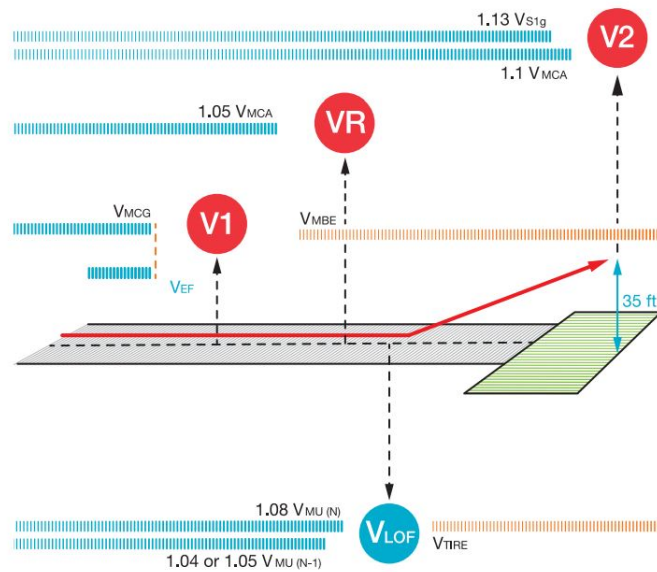


Figure 2.2: Take-Off reference speeds [14]

Roll Capability

Following method for demonstrating compliance with CS 25.147(d) demands that the aircraft is trimmed in a level turn at V_2 (for straight flight) with a bank angle of 30° and with One Engine Inoperative. Next a step input of the ailerons in the opposite roll direction is made. The aircraft should demonstrate that it can roll to the other direction in not more than 11 seconds. The roll will be made towards the side with the operative engine as this is the most adverse direction. The same test is undertaken with all engines operative and its demonstration (Lateral Control All Engines Operating EASA CS 25.147(f) [1]) is described as follows: *"It should be possible in the conditions specified below to roll the aeroplane from a steady 30° banked turn through an angle of 60° so as to reverse the direction of the turn in not more than 7 seconds. In these demonstrations the rudder may be used to the extent necessary to minimise sideslip. The demonstrations should be made rolling the aeroplane in either direction, and the manoeuvres may be unchecked."*

Note that some of these test points allow for using a Yaw Stability Augmentation System (SAS). Hereby excessive sideslip angles are prevented by the pilot or in this case, by a basic controller, invoking a rudder deflection to limit the sideslip angle.

3

Methodology

This Chapter comprises the complete set of tools required for setting up the Flight Mechanics Toolbox. Starting out with the parametric models which are later on used for the inertia and aerodynamic models. Finishing with the assembly of all data required to provide the input for the toolbox itself.

The fundamental purpose of the flight mechanics model is to assess the Handling Qualities of a Flying V configuration in the preliminary design phase. In order to set-up a valuable Flight Mechanics Toolbox, information of different fields is required. Next to the aircraft's dimensions and reference values, its mass and inertia are required. Another requisite is the aero data, holding the Stability and Control derivatives.

The complete process is displayed in Figure 3.1. Starting from the geometry defined by previous work, it is translated into BlackSwan. This parametric geometry model is converted into an input file for the Vortex Lattice Method, which transforms it into a panel model. Additionally the parametric model is translated into a strip model for the inertia estimation. The aero data, mass and inertias are fed into the Flight Mechanics Model. In case a shift in centre of gravity is required, the user can define it in the BlackSwan model or hard code it into the inertia and Odilila models. Should the current geometry not hold the desired properties, the geometry is changed and the process is reinstated.

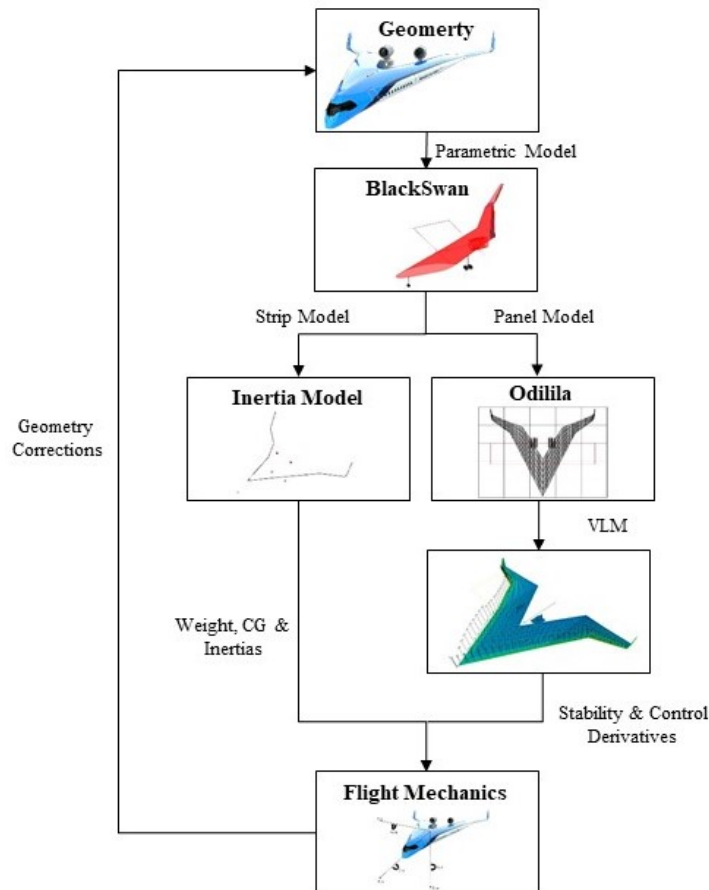


Figure 3.1: The complete Flight Mechanics Toolbox process

3.1. BlackSwan Parametric Models

When transferring the geometry between different tools, the origin and axes of the reference frames had to be monitored closely. The BlackSwan and Inertia Model for example share the same reference frame while Odilila's origin is placed at the reference point, i.e. at the defined CG location. The S&C derivatives are outputted with respect to the experimental reference frame. This frame is a commonly used body-fixed reference frame. Here a steady flight reference conditions is chosen together with the orientation of the reference frame which remains fixed thereafter [30]. In effect this is the stability reference frame. The S&C are then transformed to the body carried normal Earth reference frame by firstly being transformed to the body axis reference frame.

Different configurations can be examined with ease by modelling the aircraft parametrically. The user constructs dependencies in a system. Next the variables in that system are altered to swiftly explore different solutions. The parametric model is constructed using variables and functions [17]. The response surface equations for example will ensure that the total surface area will be valid for any configuration defined [18].

Before Parapy models were set-up through continuous work of several students with specific contributions to their research topic. The traits sought after in setting up a parametrization scheme are its conciseness, robustness and flexibility. It was found that the flexibility to use ParaPy in combination with Airbus tools was lacking. The first task was therefore to set up parametric models in a more user friendly tool with respect to Airbus software. This was acquired in the MATLAB[®] based tool, BlackSwan. It assembles aircraft from different components. These components are entities such as the landing gear, nacelle, etc.

3.1.1. Flying V Classes

Planform Class

The created Object Oriented classes specific to the Flying V are the *Planform* and *Winglet* Classes. The *Landing Gear*, *Nacelle* and *Elevon* classes are common classes, also defined for the reference aircraft. The only change being made to the global locations of the nacelle and gear.

The airfoils are adopted from the splines provided by the Catia model. The winglet's root airfoil needs to be inherited from the parent's "Flying V" class to ensure a seamless transition. The BlackSwan Flying V planform class created only utilizes 9 variables while 10 are required in the Parapy[®] model. Below the parametric values for the optimized Flying V model by Faggiano are repeated in Table 3.1. Additionally a design iteration in BlackSwan of the Flying V is displayed in Figure 3.2.

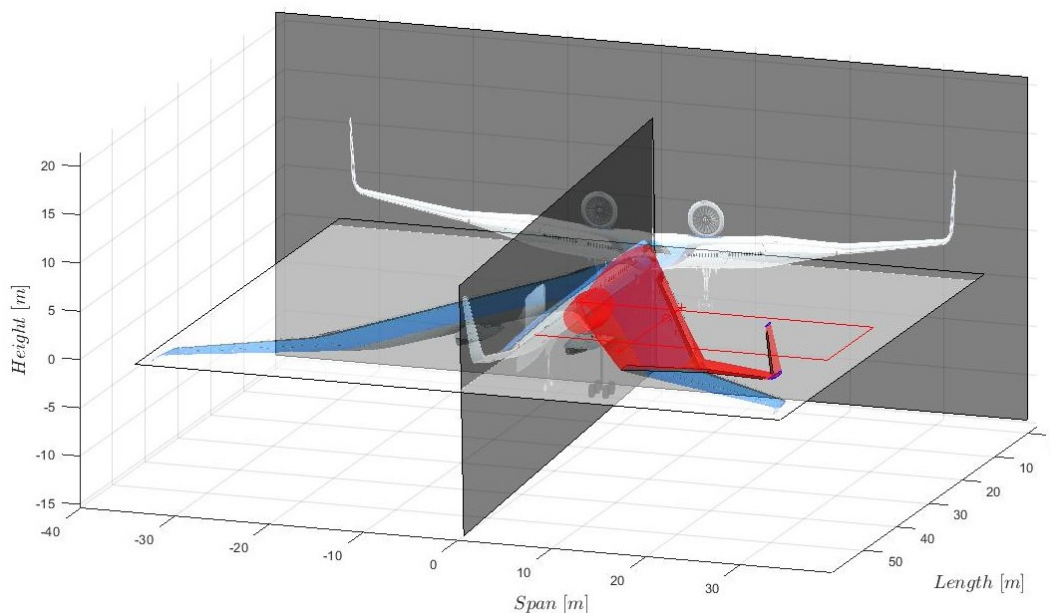


Figure 3.2: Flying V Parametric Model during set-up in BlackSwan

Name	Variable	Value	Unit
Wing area	S	883.3	[m ²]
Wing span	b	65	[m]
Root Chord	C_r	24	[m]
Aspect Ratio	AR	4.78	[-]
Relative Kink Position 1	η_1	0.386	[-]
Relative kink Position 2	η_2	0.623	[-]
Leading Edge Sweep 1	λ_1	64.4	[deg]
Leading Edge Sweep 2	λ_2	37.8	[deg]
Twist Kink 2	ϵ_{IV}	-4.3	[deg]
Twist tip	ϵ_V	-4.4	[deg]

Table 3.1: Planform Design Variables of Faggiano's 4th configuration optimization [12]

Winglet Class

The Winglet Class is addressed first since it will justify the adjustments made to the values used in the planform class. The winglet's shape is approximated by using the three splines provided by the Catia model. The curvature of the real winglet is approximated by defining a radius in the winglet's class.

The Flying V's planform without winglet then results into a reference span of 62.2 m. Therefore the total span of both winglets amounts to 1.8 m. Later on the difference between jig-shape and loaded wing with cargo, passengers, fuel, etc needs to be considered. As the planform is likely to exceed the allowed 65 m of span if the total span is already at 65 m.

The calculated reference area of the winglet's was subtracted from the initial value for the complete aircraft as defined by Faggiano. As the total span of the planform changed, values for spanwise locations of e.g. the kinks are tweaked so that the final result resembles Faggiano's optimized planform with winglets.

A three-view was imported into BlackSwan's Graphical User Interface (GUI) in order to make sure that the calculated values were correct. With the above mentioned adjustments in mind it was possible to define the planform sufficiently to start a flexible yet robust research for the aerodynamic stability derivatives in Odilila.

For simplicity and purpose of repeatability it was chosen to adopt the design of the Airbus A350-900 as reference aircraft [25]. The reference aircraft's High Lift Devices (HLD) will become of significant importance once the stability in different flight phases will be assessed and are therefore modelled as well.

Rolls-Royce Trent XWB Nacelle Class

The nacelle class created is based on the Engine and Nacelle dimensions of the Rolls Royce Trent XWB-84 as defined in the Aircraft Characteristics - Airport and Maintenance Planning document for the A350-900 and A350-1000 [25]. Its location in the parametric model is based on the relative spanwise location and distance from the wing's trailing edge at the location specified. Kindly note that since this Class is a common Class for the Reference Aircraft and Flying V, the values for both models are provided.

Landing Gear Classes

The Landing Gear's dimensions are equally adopted from the Aircraft Characteristics - Airport and Maintenance Planning document [25]. The locations are kept to their original values for the Reference Aircraft. The Nose Landing Gear (NLG) tyre assumed is: 1,050 x 395 R16, while the Main Landing Gear (MLG) tyre assumed is: 1,400 x 530 E23. The wheel spacing defined in BlackSwan accounts for the thickness of the tyres, in fact they should be added up. Moreover when dimensions of wheel basis, stroke, etc. are provided it should be noted that these values are highly dependent of the weight on wheels and CG location. The initial Landing Gear location utilized for the Flying V was based on the Catia model.

3.1.2. Elevons

Figure 3.3 provides the dimensions of the inner and outer elevon created, together with the Mean Aerodynamic Chord dimension of 18.74 m of the Flying V's planform without winglet. It was chosen to simplify the number of control surfaces as much as possible. In Chapter 6 the use of a control mixer will be introduced. Here the elevons can take up more than 1 function. Note that it is currently only possible to model primary control surfaces such as elevator, aileron, rudder in Odilila. As a result no split elevons, spoilers, etc. can be implemented in the current models.

Note that the red rectangle indicated the reference area in Figure 3.3. Furthermore, the Mean Aerodynamic Chord (MAC) is drawn in between the "+" markers. Lastly, the quarter chord position is indicated by the red circle.

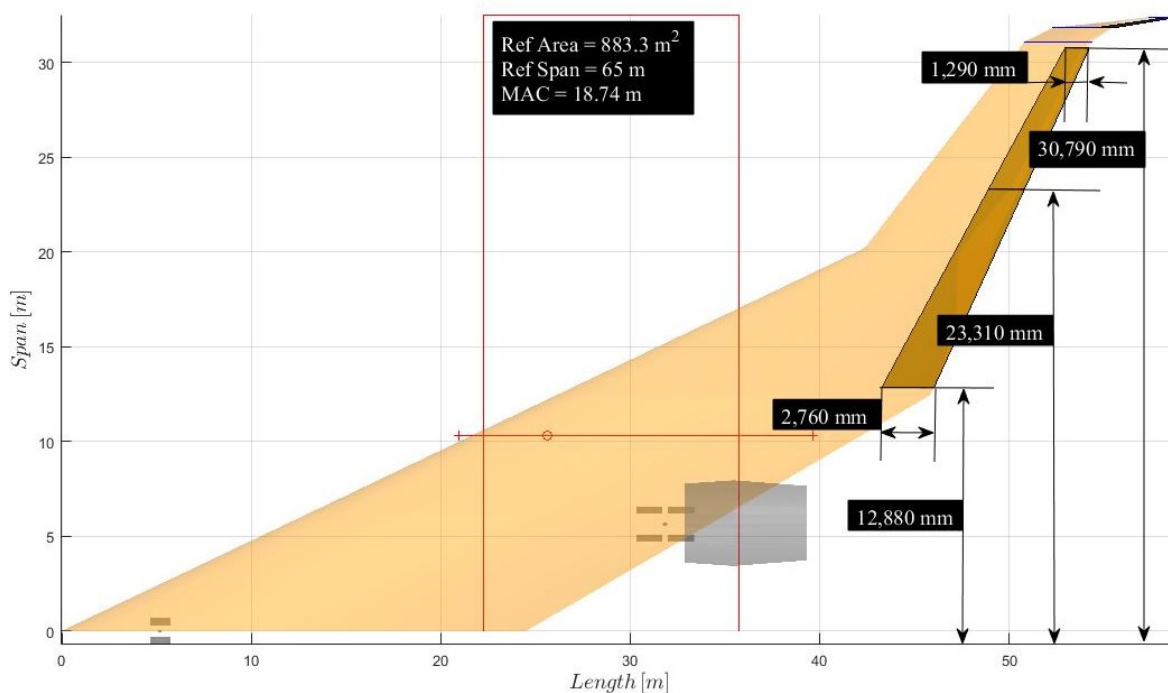


Figure 3.3: Flying V elevon dimensions expressed in mm

3.1.3. Reference Aircraft Classes

For the sake of comparison of the flying V's general Handling Qualities and take-off behaviour, a reference model is created. For simplicity and purpose of repeatability it was chosen to adopt the design of the Airbus A350-900. Additionally, M. Claeys already provided a reference aircraft model, developed in Mares. This is another Airbus tool like BlackSwan used as Finite Element Method (FEM). Here a numeric model of the A350 was created. The Classes left to describe for this Reference Aircraft are again based on the Airbus document [25]. Values for which no reference could be found such as the body fairing are based on three views, imported as background images in BlackSwan. Kindly note however that the body fairing is at this point is only an aesthetic feature as Odilila will not take its shape into account. Below all initial values utilized are tabulated per Class.

High Lift Devices

Table 3.2 provides the different High Lift Devices settings for the A350-900. This Table will become of significant importance once the stability in different flight phases will be assessed. These slats, flaps and Droop Nose Devices (DND) were introduced in the parametric model as well together with their configurations. The location of the High Lift Devices is presented in Figure 3.4. Furthermore, the ailerons droop downwards 5° in CONF 1+F and 10° in CONF 2 to FULL. When the flaps are extended they naturally continue to perform their roll function.

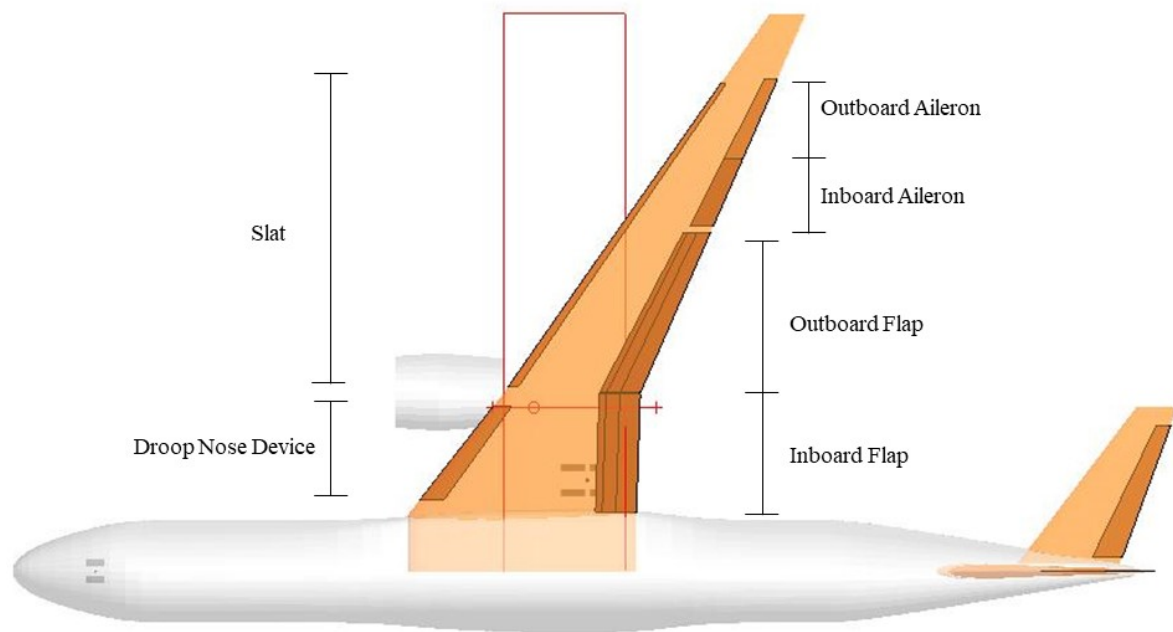


Figure 3.4: Wing movables of the reference aircraft

Configuration	Flight Phase	DND [°]	Slats [°]	Flaps [°]	
				Inboard	Outboard
Clean	Cruise	0	0	0	0
1	Hold/APP	16.7	18	0	0
1+F	TO/APP	16.7	18	6 TO / 9 APP	12 TO / 9 APP
2	TO/APP	16.7	18	20	20
3	TO	16.7	18	26	26
3+S	APP/LDG	25	27	26	26
Full	LDG	25	27	37.5	37.5

Table 3.2: A350-900 High Lift Devices Configurations, adopted from A350-900 Flight Deck and Systems Briefing for pilots [3]

Figures 3.5 and 3.6 provide the reader with a comparative look into the dimensions of the Flying V and A350-900 Reference Aircraft. The red rectangle indicates the reference area and span. The red line with crosses as end points shows the Mean Aerodynamic Chord (MAC) while the circle illustrates the 25% MAC position.

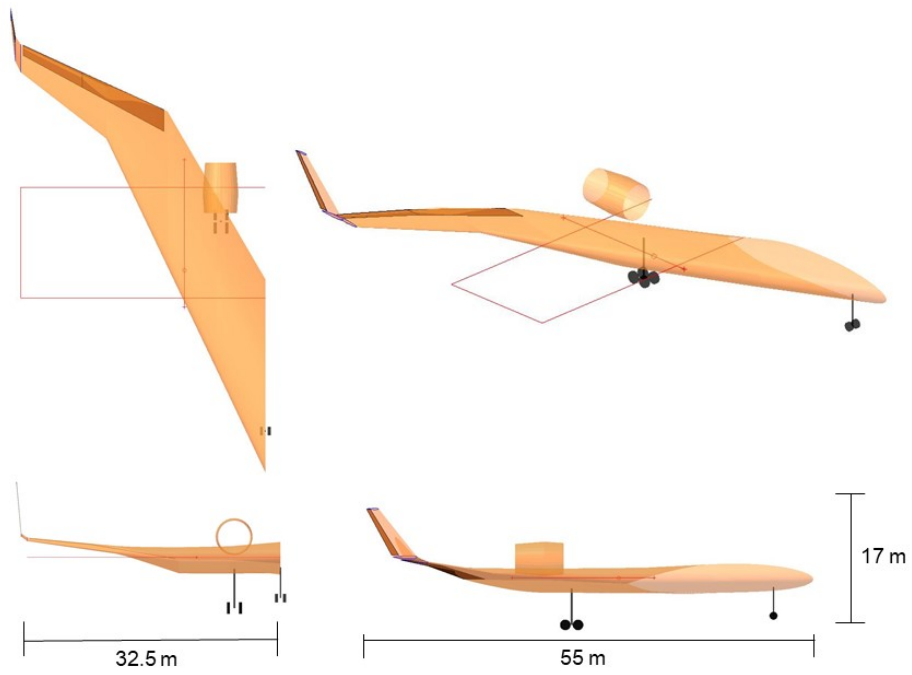


Figure 3.5: Flying V BlackSwan Parametric Model

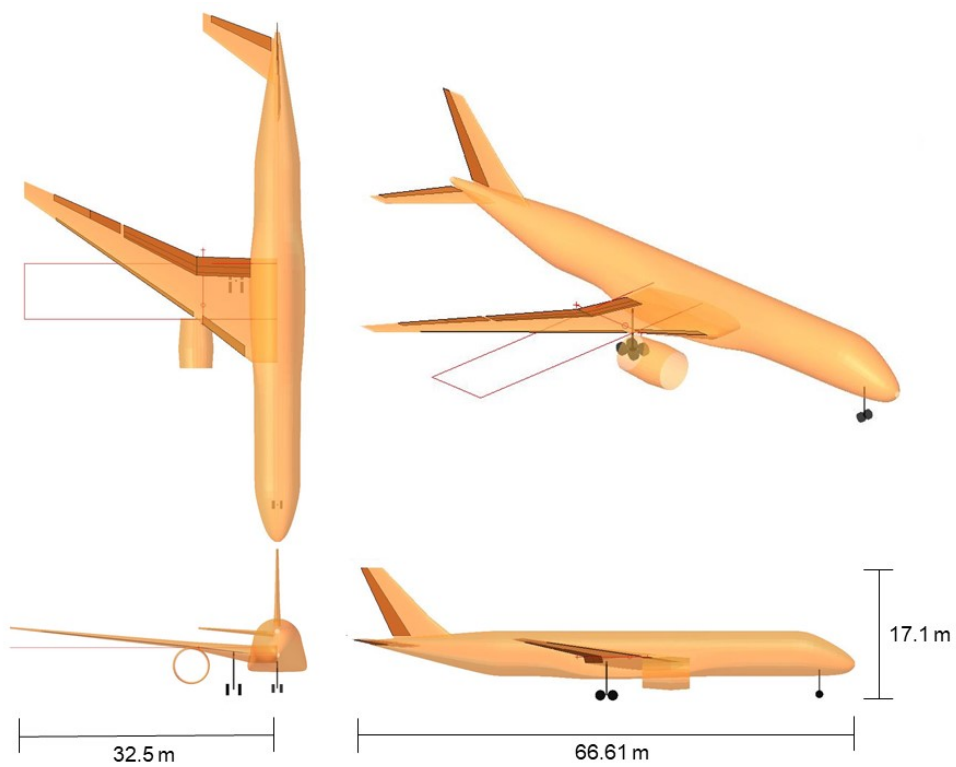


Figure 3.6: Reference Aircraft BlackSwan Parametric Model

3.2. Inertia Estimation

Acquiring sufficiently accurate Moments of Inertia (MOI) are of predominant importance for the dynamic analysis to be of value. A custom method for collecting the inertias was created. The method is believed to be a well-considered simplification in relation to the accuracy of the rest of the toolbox. The general idea is to consider the powerplant and landing gear as point masses. The rest of the aircraft is divided in lumped masses, placed at the half chord locations.

The mass distribution was adopted from M.B.P. Claeys's Master thesis on the Structural Analysis of the Flying V [8]. Next the entities are retrieved from the BlackSwan created Flying V model. For the wing planform and winglet, a number of lumped masses per meter span is defined. Hereby a linearly spaced vector can be set-up when running from the root to the tip section. Based on BlackSwan's generated planform, points are created from root to tip at 50% chord of each considered location. At these locations the local chord length is calculated.

Next the mass per local chord can be calculated by distributing the masses per wing section. Table 3.3 and Figure 3.7 provide the allocation of the weights per wing section. Taking for example the fuel mass. Assume for now that this mass is evenly distributed over the chords of Section 3 on the left and right wing. Therefore this mass can be divided by the total length of all chords located within Section 3. This mass per chord-length provides a factor with as units [kg/m]. These K-factors can be superimposed. The K-factor of the fuel needs to be added to the K-factor of the Structure. The latter is obtained from dividing the structural mass over the summation of all chord lengths of the planform. This process is repeated for all masses and Sections. Resulting in a vector, holding the K-factor per chordwise location. This together with the coordinates of the lumped masses and local chord length allows for calculating the actual CG and Moments of Inertia.

The MOIs off the engines and landing gear are added to those retrieved from the lumped masses. These are considered to be point masses and can directly be added by utilizing Equations 3.1 to 3.5. These are valid on the assumption that the weight breakdown contains a sufficiently large number of parts so that the inertia of each part around its own CG location is negligible.

When assuming that the masses are evenly distributed between the left and right side, I_{xy} and I_{yz} amount up to zero because of the symmetry assumed. As soon as a mass imbalance is created by e.g. assuming more fuel or payload on either side, these MOI become nonzero.

M.B.P. Claeys created a mass breakdown, which was required to determine the aircraft's overall CG. Here the foremost determining weights were known, being the payload, fuel, operational and maximum take-off masses [8].

This complete process is repeated for the reference aircraft with some minor changes. An additional category was added, a body of revolution. The fuselage is assumed to be a cylinder with a radius equal to the average of the fuselage's height and width. The Moments of Inertia of the cylinder are calculated separately around its centroid. Next Steiner's theorem is used to calculate the MOI around the reference location.

Group	Subgroup	Mass [kg]	Section #
Landing Gear	Nose	2,493	n.a.
	Main	4,985	n.a.
Propulsion	Engine	9,900	n.a.
Cabin	Operational Items	12,255	1
	Furniture	3,770	1
Payload	Cargo	32,326	2
	PAX	11,9326	1
Structure		58,457	1-6
Fuel		97,065	3

Table 3.3: Flying V Mass Breakdown per Section as indicated in Figure 3.7 [8]

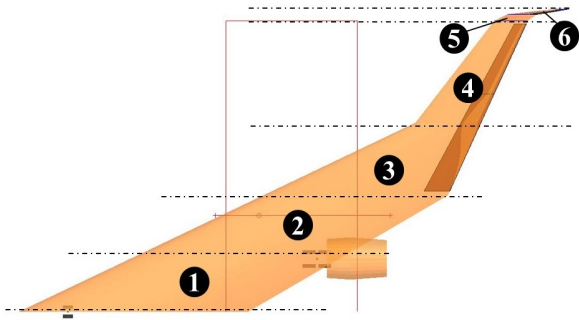


Figure 3.7: Flying V planform section breakdown for inertia estimation

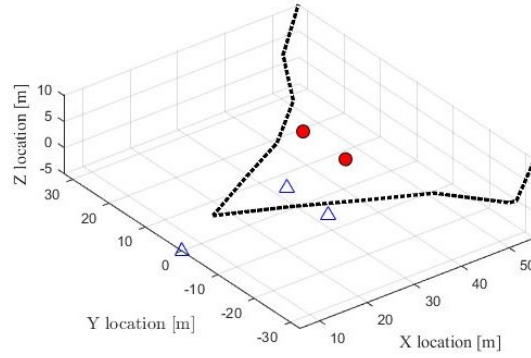


Figure 3.8: Point and lumped masses distribution of Flying V

Equations 3.1 to 3.6 are valid on the assumption that the weight breakdown contains a sufficiently large number of parts so that the inertia of each part around its own cg location is negligible.

$$I_{xx} = \sum_{i=1}^{i=n} m_i [(Y_i - Y_{ref})^2 + (Z_i - Z_{ref})^2] \quad (3.1)$$

$$I_{yy} = \sum_{i=1}^{i=n} m_i [(Z_i - Z_{ref})^2 + (X_i - X_{ref})^2] \quad (3.2)$$

$$I_{zz} = \sum_{i=1}^{i=n} m_i [(X_i - X_{ref})^2 + (Y_i - Y_{ref})^2] \quad (3.3)$$

$$I_{xy} = \sum_{i=1}^{i=n} m_i [(X_i - X_{ref})(Y_i - Y_{ref})] \quad (3.4)$$

$$I_{yz} = \sum_{i=1}^{i=n} m_i [(Y_i - Y_{ref})(Z_i - Z_{ref})] \quad (3.5)$$

$$I_{zx} = \sum_{i=1}^{i=n} m_i [(Z_i - Z_{ref})(X_i - X_{ref})] \quad (3.6)$$

Figures 3.9 and 3.10 illustrate the above described method. For the Flying V, the lumped masses form a line at the mid-chord position. The star-markers illustrate point masses at the locations of landing gear and nacelle. The same is outlined for the reference aircraft with the addition of the cylinder, approximating the fuselage's inertia.

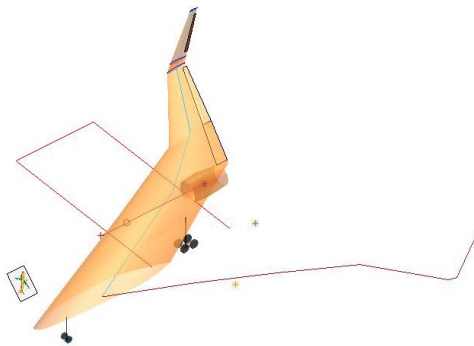


Figure 3.9: Flying V Inertia estimation model

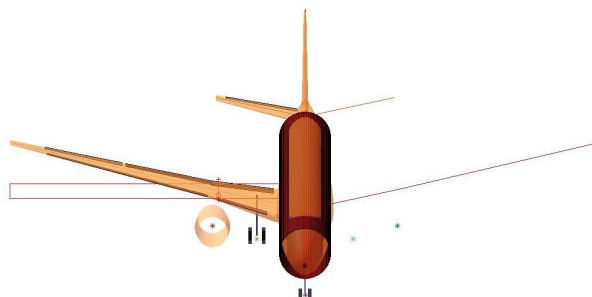


Figure 3.10: Reference Aircraft Inertia estimation model

3.3. Odilila, a Vortex Lattice Method

Odilila is a Vortex-Lattice Method (VLM) used to analyze and optimize aerodynamic performance. In this case during the conceptual and preliminary design phase. The software has been created and validated by Airbus FPO expert K. Bender. VLMs are especially attractive in the initial stages of aircraft design and analysis.

The shape under consideration is approximated by discrete vertices spread over an infinitely thin sheet. They allow for computing lift and induced drag while omitting the thickness and viscosity. Odilila can be considered as a complex VLM. It is able to take into account taper, twist, camber, control surfaces, high lift devices and nacelles. The principle is based on ideal flow theory, in effect potential flow. Here no turbulence, dissipation nor boundary layers are resolved and is therefore an ideal approximation of nature with limitations.

After the geometries of both aircraft are defined the next step is to optimize the lift distributions. When optimizing the lift distribution an alteration to the twist and camber distribution is made by Odilila. The optimizer utilized is a Sequential Quadratic Programming (SQP) method for constrained linear optimization. The components for which the drag should be minimized have to be defined and constraints can be implemented. Induced drag is minimized by altering the wing twist while the C_L and C_m can be prescribed as constraints. As the twist is changed, the cabin integration into the wing might be jeopardised. The induced drag is acquired through the down- and sidewash analyzed in the Trefftz-plane.

The input from BlackSwan to Odilila was automated and eventually the aerodata output is inputted into the Flight Mechanics Toolbox. All components are therefore modelled with vortex lattice elements. The geometry is based on providing the trailing edge points in 3D coordinates and the chord at those locations. This chord is provided with its length parallel to the x-axis. The panels created are linked to a section and a row is defined going from leading to trailing edge. A wing section has additional features such as twist and camber. The camber distribution can be provided or imported from airfoils defined by coordinates on the trailing edge points defined earlier.

The aero data consists of the stability and control derivatives. These are outputted for the specified range of Mach numbers, conventionally obtained through applying finite differences to the flight conditions. Moments are obtained through the estimating the lift of single bound vortex elements at the leading edge of the panel. In order to simulate a shift in CG, the reference point in Odilila is altered. In effect the S&C derivatives are calculated around this specified reference point. The neutral point, aerodynamic efficiency etc. could be directly analyzed from the automatically generated reports. The sign convention of the stability and control derivatives utilized is illustrated in Figure 3.11.

$$C_x = \frac{F_x}{qS}, \quad C_y = \frac{F_y}{qS}, \quad C_z = \frac{F_z}{qS} \quad (3.7)$$

$$C_l = \frac{M_x}{qSc}, \quad C_m = \frac{M_y}{qSc}, \quad C_n = \frac{M_z}{qSc} \quad (3.8)$$

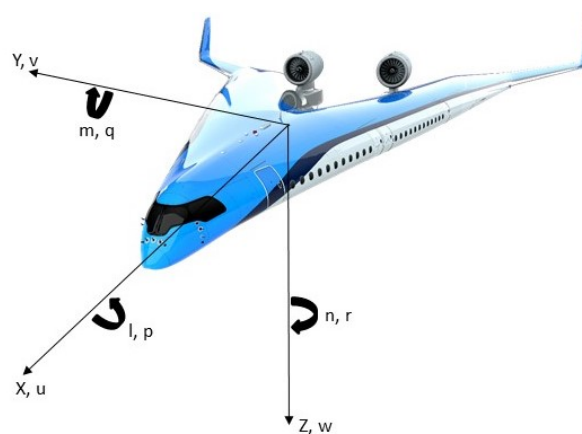


Figure 3.11: Stability and Control Parameters sign convention

Conventionally, when utilizing Lifting Line Theory, the minimum induced drag solution for lift distribution is given by an elliptic spanwise loading. In 1933 however, Prandtl presented a superior spanwise loading [7]. Here, the span was allowed to vary and lift and local bending moment are provided instead. The solution now evolves from an elliptic span loading to a bell-shaped curve, yielding less induced drag for a certain structural weight. The solution is provided by utilizing non-linear twist distribution along the span.

The same type of twist distribution should be sought after for performance optimization. Kindly note that the twist distribution provided in Figure 3.13 is the net distribution. In effect, the twist of the airfoils was removed before providing them to the Odilila model. This however also means that the cabin section is no longer guaranteed to fit into the fuselage. Note that the twist of the winglets is optimized as well. Figure 3.13 and 3.14 show an optimization for a mass of 230 tons. The twist optimization is however not the scope of this thesis. These high twist values are problematic to implement with regards to e.g. cabin accommodation and therefore deserve specific investigation in the future. For now the acceptable twist distribution of the optimization for 200 tons is adopted.

As additional note, the only feasible alternative to designing inherently stable flying wings is to implement sweep-back with washout (longitudinal dihedral). When the CG is placed in front of the neutral point, a moment couple is created by the part of the wing in front of the CG and the parts aft of it that stabilizes the aircraft.

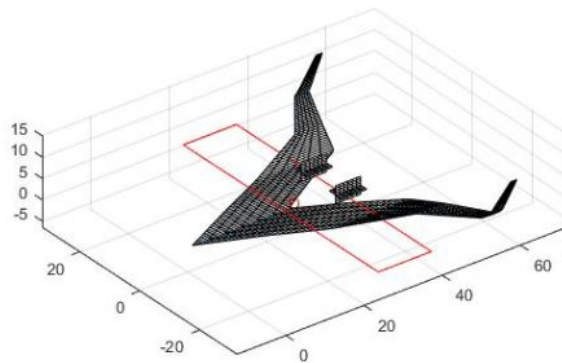


Figure 3.12: Odilila Flying V panel model

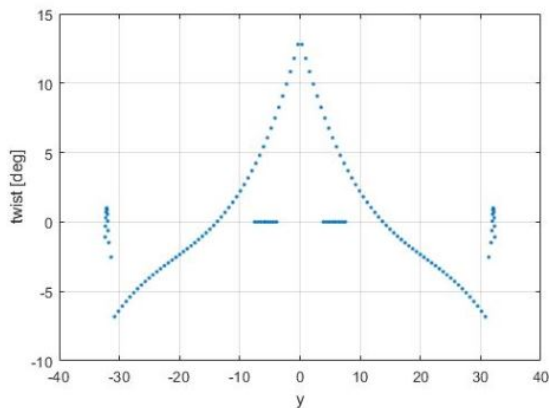


Figure 3.13: Odilila optimized twist distribution (mass=230 t)

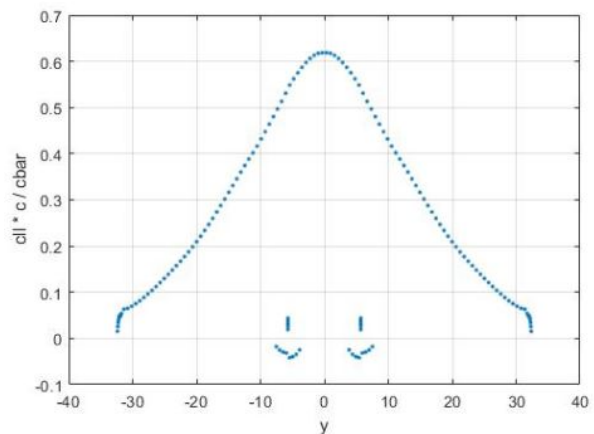


Figure 3.14: Flying V lift distribution (mass=230 t)

4

Flight Mechanics Toolbox

In the Flight Mechanics Toolbox, the aero data, inertias and equations of motion are brought together. This process forms the content of subsequent Sections. Economy of notation was preserved by providing all equations of motion in their matrix notation. They serve the purpose of creating a 6 Degree Of Freedom (6 DOF) mathematical model of the aircraft's flight dynamics. This system of equations is trimmed and subsequently linearized before conducting the Eigenvalue analysis. Facilitating the Handling Qualities analysis, where the longitudinal and lateral characteristics are separated.

Following assumptions were made when setting up the toolbox [30]:

1. Vehicle is a rigid body of constant mass
2. Flat Earth
3. Non rotating Earth
4. Zero wind velocity, perfect atmosphere
5. Resultant thrust lies in the symmetry plane (this is not the case for One Engine Inoperative conditions)
6. Gravity vector magnitude is constant

The forces acting on an aircraft exist of gravity, propulsion and aerodynamic forces. It is assumed that these distributed forces can be replaced by point forces generating forces and moments around the centre of gravity. Therefore no additional reference frames are required [30].

Keeping track of origins and reference frames in between Odilila, BlackSwan and the flight dynamics reference frames was challenging. Two transformation matrices were specified, provided by Equations 4.1 and 4.12. Furthermore the derivatives coming from the aero model had to be transformed from their experimental reference frame to the body fixed frame. The presented model and its notations are adopted from "Analyse der Handling Qualities im Flugzeugvorentwurf" [6] and "General Equations of Motion for a Damaged Asymmetric Aircraft" [4].

The propulsion model has a limited level of fidelity and represents an ideal engine. Hereby instantaneously providing the amount of thrust in order to maintain a certain True Airspeed (TAS). No spool-up time, throttle transients, etc. are present. This is modelled by a mere thrust vector, instantaneously reacting to throttle changes.

The International Standard Atmosphere (ISA) is modelled based on the geopotential altitude. The model goes from sea level up to and including the stratosphere. No turbulence, wind (shear) are currently modelled.

4.1. Transformations

Aerodynamic to body fixed frame

$$\Gamma_{ba} = \begin{bmatrix} \cos \alpha \cos \beta & -\cos \alpha \sin \beta & -\sin \alpha \\ \sin \beta & \cos \beta & 0 \\ \sin \alpha \cos \beta & -\sin \alpha \sin \beta & \cos \alpha \end{bmatrix} \quad (4.1)$$

Vehicle carried normal Earth to body fixed

$$\Gamma_{be} = \begin{bmatrix} \cos \psi \cos \theta & \sin \psi \cos \theta & -\sin \theta \\ \cos \psi \sin \theta \sin \phi - \sin \psi \cos \phi & \sin \psi \sin \theta \sin \phi + \cos \psi \cos \phi & \cos \theta \sin \phi \\ \cos \psi \sin \theta \cos \phi + \sin \psi \sin \phi & \sin \psi \sin \theta \sin \theta \cos \phi - \cos \psi \sin \phi & \cos \theta \cos \phi \end{bmatrix} \quad (4.2)$$

4.2. Equations

The aerodynamic forces are calculated from the S&C derivatives. They take into account the control surface deflections, aircraft's velocity and rates in relationship to the atmosphere. Equation 4.3 provides the complete system of equations. Here the subscript "e" refers to vectors expressed in the body carried Normal Earth reference system. "b" then stands for vectors with respect to the body fixed reference frame. Conventionally I_{xy} and I_{yz} would be set to zero for a mass-symmetrical vehicle, which is not necessarily the case. This allows for analyzing the flight dynamics of e.g. a fuel or cabin load imbalance, to which the design of the Flying V is more prone. The angular velocity vector is outlined in Equation 4.6.

$$\begin{bmatrix} \dot{\mathbf{P}}_e \\ \dot{\mathbf{v}}_b \\ \dot{\boldsymbol{\omega}}_b \end{bmatrix} = \begin{bmatrix} 0 & \Gamma_{be}^{-1} & 0 \\ 0 & -\boldsymbol{\Omega}_b & 0 \\ 0 & 0 & \mathbf{I}^{-1} \boldsymbol{\Omega}_b \mathbf{I} \end{bmatrix} \cdot \begin{bmatrix} \mathbf{P} \\ \mathbf{v}_b \\ \boldsymbol{\omega}_b \end{bmatrix} + \begin{bmatrix} 0 \\ -\mathbf{g}_b + \frac{\mathbf{F}_b}{m} \\ \mathbf{I}^{-1} \mathbf{T} \end{bmatrix} \quad (4.3)$$

To get the Euler angles from the rotational rates:

$$\frac{d\boldsymbol{\phi}}{dt} = \begin{bmatrix} \dot{\phi} \\ \dot{\theta} \\ \dot{\psi} \end{bmatrix} = \begin{bmatrix} 1 & \sin \phi \tan \theta & \cos \phi \tan \theta \\ 0 & \cos \phi & -\sin \phi \\ 0 & \sin \phi / \cos \theta & \cos \phi / \cos \theta \end{bmatrix} \begin{bmatrix} p \\ q \\ r \end{bmatrix}_b \quad (4.4)$$

$$\mathbf{g}_b = \Gamma_{be} \begin{bmatrix} 0 \\ 0 \\ g_0 \end{bmatrix} \quad (4.5)$$

$$\boldsymbol{\Omega}_b = \begin{bmatrix} 0 & -R & Q \\ R & 0 & -P \\ -Q & P & 0 \end{bmatrix} \quad (4.6)$$

$$\mathbf{I} = \begin{bmatrix} I_{xx} & -I_{xy} & -I_{xz} \\ -I_{xy} & I_{yy} & -I_{yz} \\ -I_{xz} & -I_{yz} & I_{zz} \end{bmatrix} \quad (4.7)$$

This basic model outputs the twelve states, i.e. the position, velocity, Euler angles and rates. On top of the twelve states, the Angle of Attack (AoA), Sideslip Angle (SSA), Flight Path Angle (FPA), True Airspeed (TAS) and Rate Of Climb (ROC) are calculated with following relations 4.8 to 4.10.

$$\tan \alpha = \frac{v_{zb}}{v_{xb}} \quad (4.8)$$

$$\sin \beta = \frac{v_{yb}}{|\mathbf{v}|_f} \quad (4.9)$$

$$\sin \gamma = -\frac{V_{ze}}{|\mathbf{v}|} \quad (4.10)$$

4.3. Trim Functions

The different trim functions created are discussed next. A trim function with wings level, specifying FPA, altitude and TAS was the most simple one. Additionally a trim in coordinated turn and a Steady Heading Sideslip (SHS) function were created. The trim in turn and SHS functions can be imposed with both engines running or with One Engine Inoperative (OEI). Additionally basic controllers were set-up when simulating a bank to bank turn, where the aircraft is trimmed with a bank angle in one direction and is made to roll to the other direction, possibly with OEI. Here a basic Yaw Stabilization Augmentation System (SAS) and pitch controller were implemented together with differential deflections for the ailerons to limit roll induced yaw.

4.3.1. Longitudinal Trim

For the longitudinal trim, a specific altitude, Flight Path Angle (FPA) and TAS are provided. Here the roll, yaw and sideslip angle are zero (ϕ, ψ & $\beta = 0$). The TAS and FPA are then utilized to find the velocities in body fixed reference frame, as given in Equation 4.11. Next the pitch attitude, elevator and throttle input are sought after iteratively. The pitch attitude is said to change with the body fixed z-axis velocity. The elevator input is iterated with respect to the pitch rate acceleration and the throttle varies with the body fixed x-axis acceleration. When the derivatives of the state are all sufficiently close to zero, the aircraft is said to be in trim.

$$\begin{bmatrix} u \\ v \\ w \end{bmatrix} = \Gamma_{be} \cdot \begin{bmatrix} V \cdot \cos(\gamma) \\ 0 \\ -V \cdot \sin(\gamma) \end{bmatrix} \quad (4.11)$$

With,

$$\Gamma_{be} = \begin{bmatrix} \cos\theta & 0 & -\sin\theta \\ 0 & 1 & 0 \\ \sin\theta & 0 & \cos\theta \end{bmatrix} \quad (4.12)$$

4.3.2. Level Coordinated Turn Trim

Utilizing the transformation which was already provided in Equation 4.4, to transform the pitch and bank to angular rates. In order to acquire the velocities in body fixed reference frame, the Euler and flight path angle (equal to zero in a level turn) are taken into account. Next the bank, pitch and yaw angles together with the control surface deflections and throttle setting are sought after. To adjust the control surface deflections, the angular rates are used. For adjusting the aircraft's attitude, the pitch attitude is changed with the opposite of the acceleration in z-direction. The yaw angle is made such that sideslip is reduced to zero and the bank reduces the lateral acceleration to zero.

In a level coordinated turn, the accelerations ($\dot{u}, \dot{v}, \dot{w}$) and ($\dot{p}, \dot{q}, \dot{r}$) are equal to zero. Since the angular rates are required to be zero, the aerodynamic and thrust moments must be constant. Additionally the steady state conditions require the airspeed and angle of attack to be constant and the sideslip to be zero.

The same result could be achieved through utilizing unconstrained nonlinear optimization (e.g. Matlab's `fminunc`). However, viewing the trends and monitoring the behaviour of the aircraft is facilitated through simply iterating sufficiently. Figure 4.1 provides such behaviour and the convergence towards a trimmed state. Here the reference aircraft is making a coordinated turn at 5,000m at a velocity of 200m/s with a bank angle of 10°. The THS deflection can be seen to be increasing toward a trailing edge up deflection of almost 4°. While the change in aileron deflection is almost unnoticeable at this scale and is close to zero, while ensuring that the lateral acceleration is decreased to zero.

$$\begin{bmatrix} p \\ q \\ r \end{bmatrix}_b = \begin{bmatrix} 1 & \sin\phi \tan\theta & \cos\phi \tan\theta \\ 0 & \cos\phi & -\sin\phi \\ 0 & \sin\phi / \cos\theta & \cos\phi / \cos\theta \end{bmatrix}^{-1} \cdot \begin{bmatrix} 0 \\ 0 \\ \dot{\psi} \end{bmatrix}_b \quad (4.13)$$

Where,

$$\dot{\psi} = g_0 \frac{\tan(\phi)}{V} \quad (4.14)$$

$$\begin{bmatrix} u \\ v \\ w \end{bmatrix}_b = \Gamma_{be}(\psi, \theta, \phi) \begin{bmatrix} V \cdot \cos(\gamma) \\ 0 \\ -V \cdot \sin(\gamma) \end{bmatrix} \quad (4.15)$$

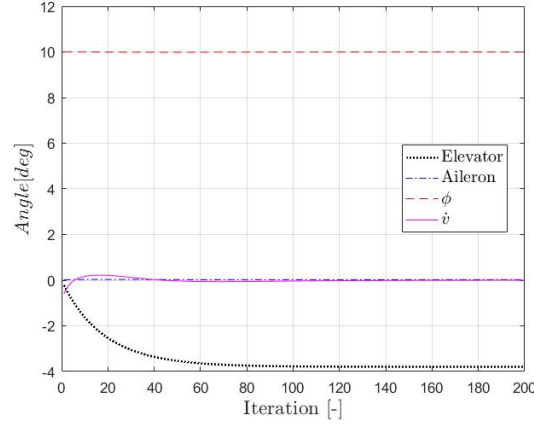


Figure 4.1: Steady turn state and input trim function iteration

4.3.3. Sideslip Trim

One trim function allows for specifying a sideslip angle at certain TAS. Again the Earth fixed specified velocity was transformed to the normal Earth body fixed reference frame. Now however, the roll and pitch attitude are unknown together with control input deflections on all axis. Pitch and power were treated as in the longitudinal trim function. Roll input was chosen to iterate based on the roll rate acceleration. Likewise the rudder input iterated with respect to the yaw rate acceleration. The roll angle itself was said to adapt for the lateral velocity in the body fixed reference frame. The aircraft can now be flown on a straight line with a certain sideslip angle and cross control inputs.

$$\begin{bmatrix} u \\ v \\ w \end{bmatrix}_b = \Gamma_{be}(\psi, \theta, \phi) \cdot \begin{bmatrix} V \cdot \cos(\beta) \cdot \cos(\gamma) \\ 0 \\ -V \cdot \sin(\gamma) \end{bmatrix} \quad (4.16)$$

4.3.4. State Space

For the modal analysis, the system of equations is transferred to a State Space notation where it is also split up into the longitudinal and lateral-directional system. A linear aircraft model is obtained from the nonlinear model when the appropriate states are trimmed and then numerically linearized. The linearized model is represented by a State Space system. This mathematical model existing of first-order differential equations grants a more straightforward identification of the Eigenvalues. It is acquired through numerical perturbation of the nonlinear model. After imposing the perturbation the system is transferred to State-Space form by utilizing the "SS" MATLAB[®] command. The inputs for the longitudinal model exist of the longitudinal control surface deflection and throttle setting. For the lateral-directional model, the aileron and rudder deflections are utilized.

4.3.5. Landing Gear

A landing gear model is available. Here the position of the landing gear is based on the BlackSwan model, providing the coordinates in body fixed coordinates. Other specified values are the direction of the landing gear vectors and height of the CG above the ground when the aircraft is stationary on its landing gear. This model is tuned to find the stiffness and damping of the landing gear based on above given values and the CG location. The landing gear model itself is able to calculate forces and moments in the body fixed coordinates as soon as the landing gear makes contact with the ground plane. Kindly note that no side forces nor rolling resistance are taken into account for now.

4.4. Process

A MATLAB[®] script is created for the configuration to be analyzed. First the BlackSwan geometry is called. Based on the entity defined, the reference values and position of landing gear and nacelles are collected. Subsequently the Odilila file containing the stability and control derivatives is collected. Next the Control Mix function is called, defining the allocation per control surface, possibly imposing differential deflections. Thereafter the mass distribution is defined after which the total mass and Inertia matrix are set-up. In Chapter 6 the use of Events, Stabilization Augmentation Systems and One Engine Inoperative trim functions will be introduced.

4.5. Limitations

When utilizing and interpreting results of the complete Flight Mechanics model, it is crucial to keep its limitations in mind. When considering the flight envelope together with the weight and balance it becomes clear that there exists an infinite amount of combinations of weight, CG, altitude and speed to test. Since the aero data is linearized, there is no added value into looking into corners of the flight envelope where behaviour is highly nonlinear. Additionally, ground effect, compressibility and aeroelasticity effects are not accounted for. Therefore high velocity test points are also more unlikely to pose significant issues. When considering for example a bank to bank turn at high velocity no roll reversal or wing deformation can be present as there is no structural model introduced.

The computation time of Odilila is low when compared to non-linearized models such as Computational Flow Dynamics (CFD). This method however allows for analyzing many different configurations in a short time, in this case with different locations of centre of gravity and changing key parametric values. The level of fidelity of Odilila, an extended VLM is in proportion to the accuracy of the rest of the toolbox. However, since there is no compressible drag prediction in the VLM but only a correction for lift and moments, the S&C are only roughly accurate for $M < M_{\text{cruise}}$. Additionally, it is not uncommon for toolboxes to use different choices of the adequate aerodynamic model dependent on the purpose of the model. When utilized for a control allocation optimization a panel method would still be beneficial due to its low running time, while CFD calculations could be used for piloted simulation.

The propulsion system could be enhanced to a static engine model, where the thrust vector is based on the flight condition. This makes the thrust dependent on Mach number, altitude and fuel flow. When analyzing OEI conditions or manoeuvres where engine dynamics affect the performance require dynamic models. This could be assessed through a Gas Turbine Simulation program.

The atmospheric model does currently not include wind, turbulence nor wind shear and is based on the International Standard Atmosphere.

The landing gear and fairing are currently not modelled aerodynamically but can be utilized in the future for take-off behaviour as they are implemented as vectors with a spring and damping ratio, where the normal forces and moments are fed back into the model. This does not include side loads nor roll friction.

5

Verification & Validation

The different tools utilized and developed to perform the investigation concerned are validated and verified in the Sections to follow. The validation of the Flight Dynamics is based on a rate 1 coordinated turn and load factor/bank angle relationship. Besides the verification of the Flight Mechanics Model itself, the Vortex Lattice Method is validated based on mainly wind tunnel data. As the Inertia model seemed to be a crude simplification, effort was put into both verification and validation for which an Airbus A300-600 model was created.

5.1. Inertia Model Verification and Validation

It was chosen to validate the Inertia model by creating a Airbus A300-600 model [26] in BlackSwan. Weights were estimated through Torenbeek's Class II [22] method for component weight estimation, as was utilized by B. Claeys [8]. Next the same method of approaching the A300's geometry by lumped, point masses and body of revolution was utilized. The achieved Moments of inertia (MOI) around all axes were then compared to K.Bender's findings of "Analyse der Handling Qualities im Flugzeugentwurf" [6]. K.Bender's method existed of defining Radii of Gyration as proposed by Torenbeek's Class I method [23].

The airplane characteristics for airport planning [26] is property of Airbus S.A.S. and can be retrieved by the public, providing high fidelity characteristics of the A300-600. The above mentioned values together with a three view were utilized to set-up the BlackSwan model of the A300-600. Additionally, a document ¹ by FedEx on the A300-600 Airframe Systems for the Air Transport Association provided detailed landing gear weights. As most weights could be deduced from documentation, it was only required to find weights for the fuselage, wing structure, systems and empennage. The equations utilized are explained in detail in Appendix C.

Additionally, reference values of the Moments of Inertia of the Airbus A300-600 were retrieved from A. Filippone's "Advanced Aircraft Flight Performance" [13]. Figure 5.3 displays these reference aircraft by circles. The MOI estimated by the custom lumped masses method (Method 1) is denoted by a "+", while K.Benders MOI for the A300-600 is provided by the diamond shaped marker (Method 2). The correspondence of the I_{zz} and I_{yy} values to the reference aircraft were deemed satisfactory. The mutual agreement between K.Bender's values and the author's method is striking. The agreement between the I_{xx} values to the reference A300-600 was found to be disappointing. Nonetheless, it should be noted that limited insight is provided to the calculation of the reference value for the A300-600 (e.g. amount of fuel in the wing). For this reason it was decided by K.Bender to implement the lumped masses method into Odilila (Method 3). Therefore the MOI method suggested is programmed independently in another language. Possibly also providing more capabilities to Odilila in the future. Here it was found that the models created by the author and K. Bender resulted in well grouped clusters for all Moments of Inertia. Additionally a rough estimate for I_{zz} can be provided by the sum of I_{xx} and I_{yy} . This estimate holds for the Inertia Model designed but not for the values adopted from literature. This strongly suggests that the I_{xx} from literature is not accurate, as displayed in Figure 5.2. Furthermore it can be concluded that the I_{yy} and I_{zz} of the Flying V and Reference Aircraft correlate well with the first order estimates as given in Figures 5.3 and 5.4.

¹<https://de.scribd.com/doc/287052535/Airbus-32-A300-A310-Landing-Gear>

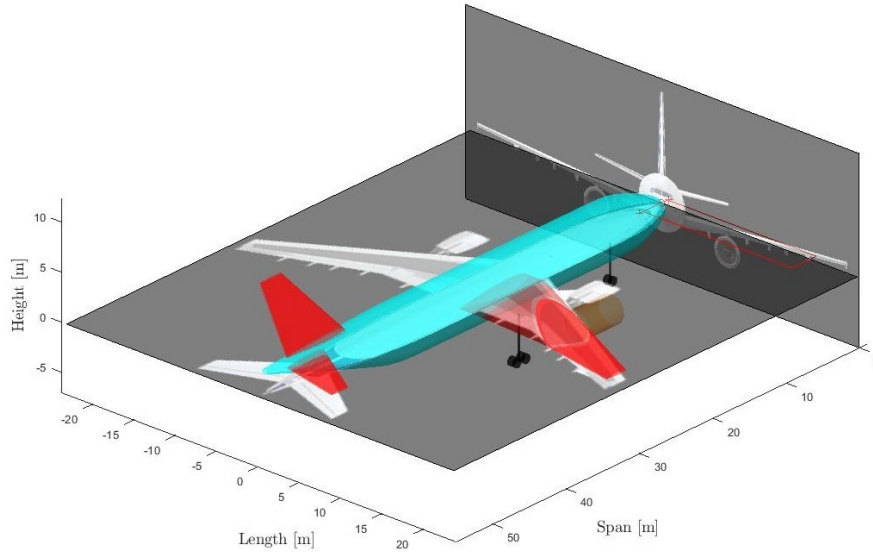


Figure 5.1: A300-600 Parametric Model during set-up in BlackSwan

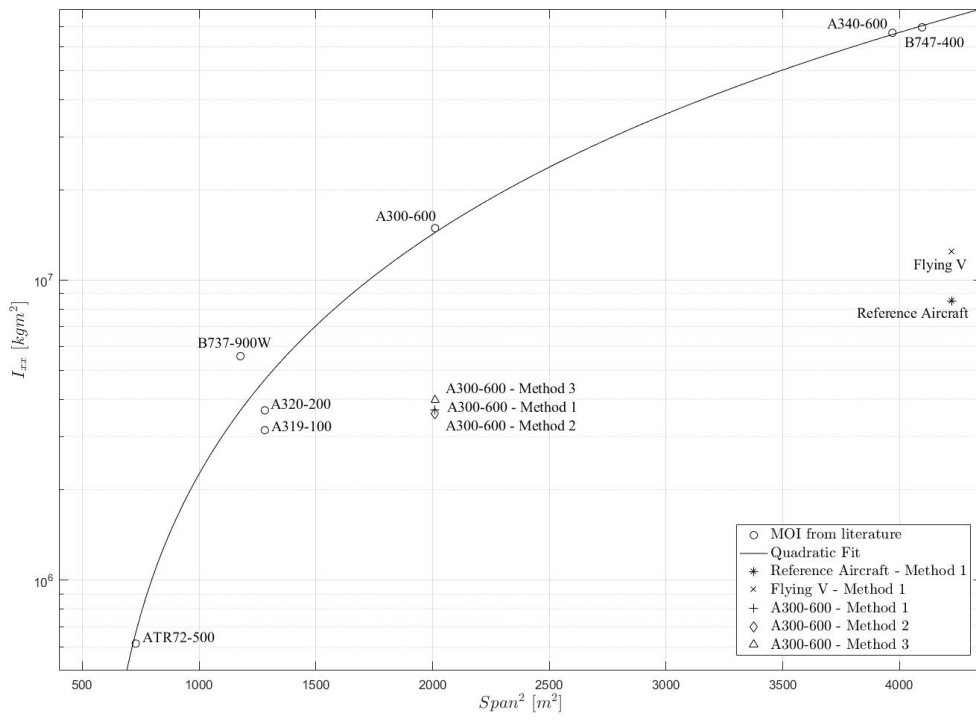


Figure 5.2: I_{xx} estimates and validation

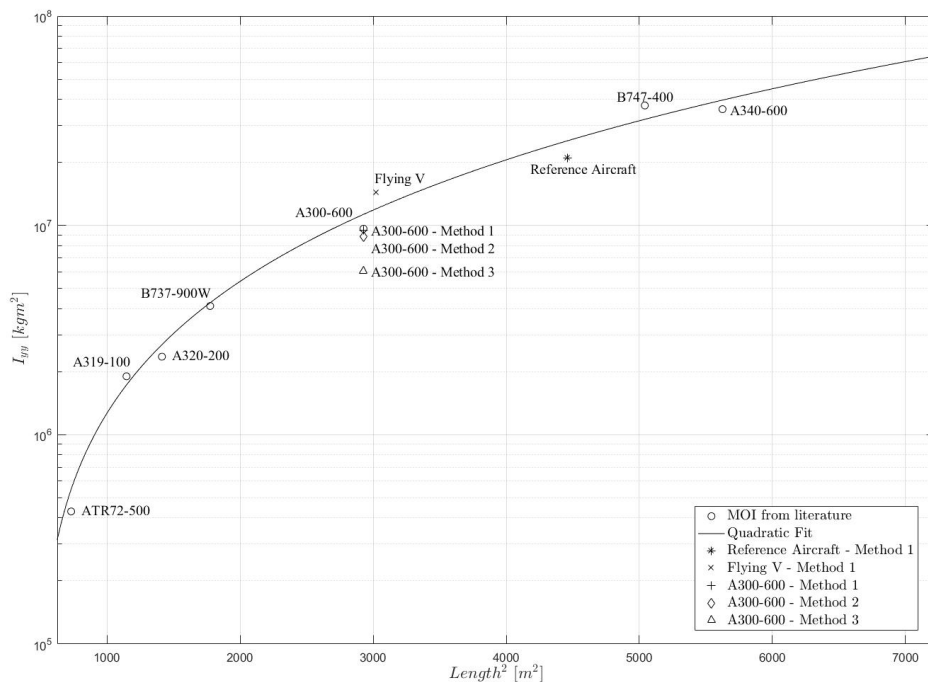


Figure 5.3: I_{yy} estimates and validation

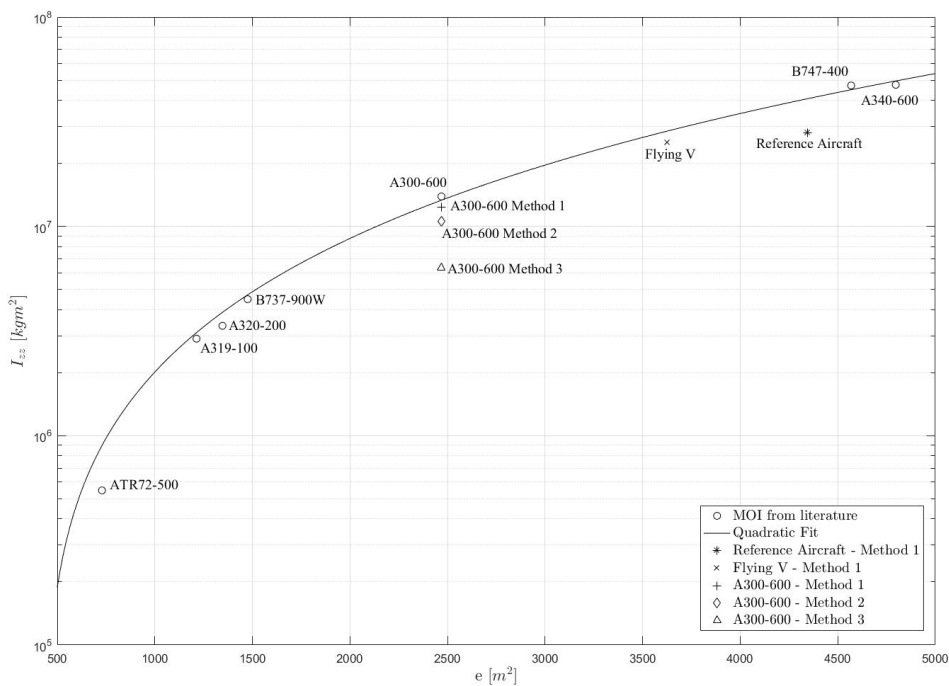


Figure 5.4: I_{zz} estimates and validation

5.2. Odilila Validation

The next portion of the validation is dedicated to Odilila. Results delimiting sweep and aspect ratio effects in comparison to benchmarks are discussed. It was already discussed by M. Claeys [8] that Odilila's lift gradient matches well with wind tunnel test data. More specifically, the k-factor is accurate to less than 1% by utilizing the inverse downwash method. Here the desired downwash is defined and the twist and camber are altered in Odilila until it is achieved.

Verification by K. Bender and M. Claeys [8] are repeated below. The Figures shown serve to verify the lift prediction of a straight untapered wing. Figure 5.7 shows the comparison of Odilila results to "Aerodynamik des Flugzeuges" [27], [28]. The red line indicates the Odilila calculation for unswept untapered wings. The markers indicate Wind Tunnel Tests of various wings with different airfoils. An accurate match between the wind tunnel results is shown for all aspect ratios. M. Claeys made this discretization with 50 elements per half wing and 6 elements in the chord-wise direction. Additionally, the theoretical formulation for the lift curve slope is adopted from Raymer [22] and is given in Equation 5.1. Here A denotes the aspect ratio and ϕ outlines the wing sweep angle. Figure 5.5 shows again the C_{L_α} of an unswept and untapered wing as a function of aspect ratio. Only this time the Figure was provided by the creator of Odilila, K. Bender. The lift gradient of an untapered wing as a function of sweep is provided by Figure 5.6. Here a satisfactory match is shown which increases for aspect ratio's of about 2 and remains almost constant from aspect ratio's in the range of 6 to 10. The discrepancy between the theoretical curve and the Odilila estimation is shown to decrease with sweep angle.

$$C_{L_\alpha} = \frac{2\pi A}{2 + \sqrt{4 + A^2(1 + \tan^2 \phi)}} \quad (5.1)$$

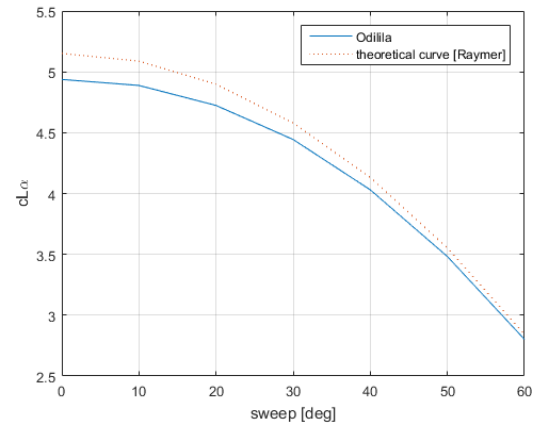
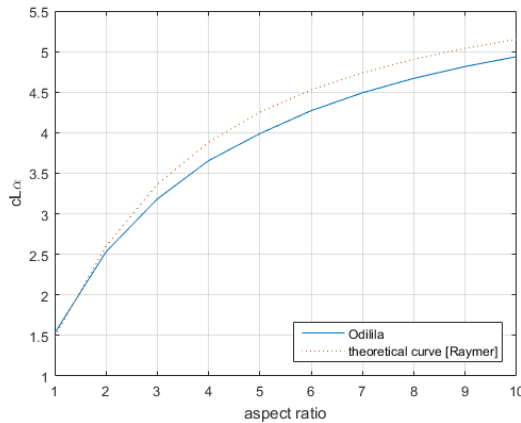


Figure 5.5: Odilila lift curve slope validation as a function of aspect ratio Figure 5.6: Odilila lift curve slope validation as a function of wing sweep

A wind tunnel test of a NACA TN 1046 in comparison to an Odilila estimate is provided in Figure 5.8. The same discretization was used as for Figure 5.7. The reference wing tested in the wind tunnel had an aspect ratio which varied with span. The Odilila wing accommodated for this and a good match is shown, slightly deviating for the higher sweep angles.

The induced drag as a function of number of panels used in the spanwise direction is demonstrated by Figure 5.9. Claeys utilized a wing with an aspect ratio of 10. Odilila's inverse normal-wash calculation was utilized to alter the twist in such a way that constant-downwash was obtained. It was found that the Odilila estimate is within 1% of the theoretical induced drag. Low discretization lead to under estimation and vice versa for high discretization numbers.

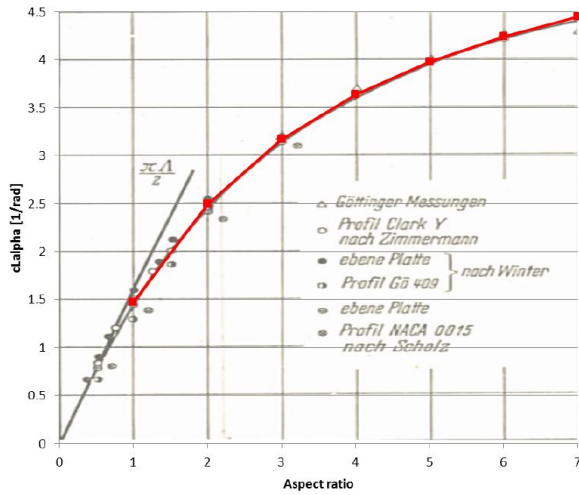


Figure 5.7: Odilila and Wind Tunnel Data comparison of lift slope versus aspect ratio [8]

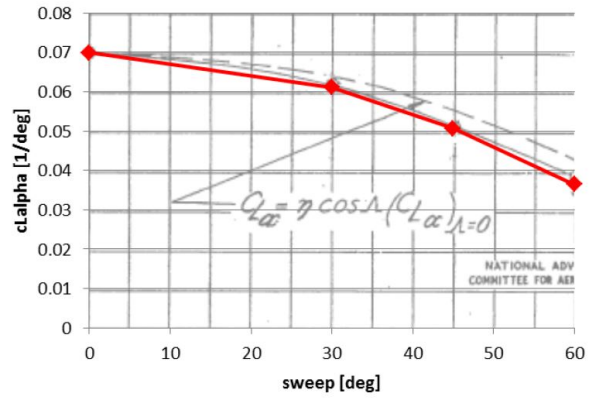


Figure 5.8: Odilila and Wind Tunnel Data comparison of lift slope versus sweep [8]

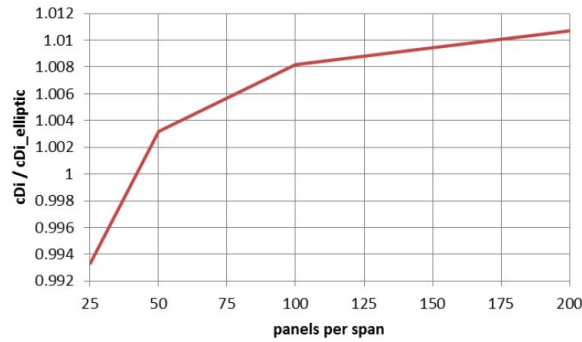


Figure 5.9: Odilila spanwise discretization effect on induced drag [8]

The number of panels in chord- and spanwise direction was altered to capture the effect on the lift gradient. It was concluded that the number of panels in chordwise direction has no noticeable consequence. The spanwise discretization was found to mainly affect higher aspect ratio wings. A maximum discrepancy of about 1% was found.

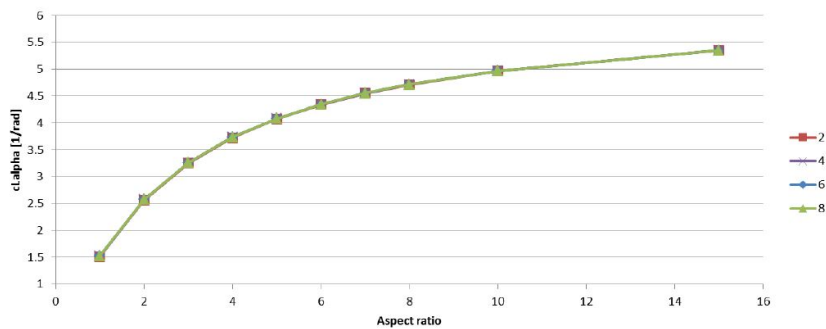


Figure 5.10: Odilila chordwise discretization effect on lift gradient [8]

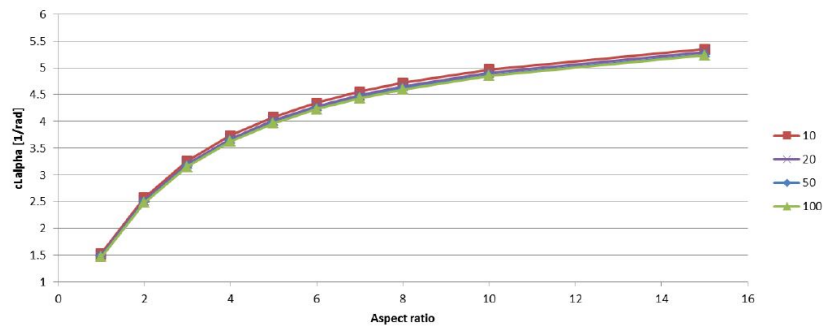


Figure 5.11: Odilila spanwise discretization effect on lift gradient [8]

Lastly, additional validation of a delta wing was provided by Odilila's creator. The variation in lift gradient and change in neutral point location with variation of the aspect ratio is provided in Appendix E. This data was validated with respect to "Aerodynamik des Flugzeuges" [27] and [28]. Note that wing aspect ratio and sweep back of delta wings cannot be varied independently. Increasing sweepback decreases aspect ratio, leading to a rearward shift of the aerodynamic centre.

5.3. Aircraft Model Validation & Verification

Even though continuous effort was put into harmonizing the parametric models in between BlackSwan and Parapy©, it should be noted that they are not equal. Different definitions of e.g. twist are certain to have been utilized. Furthermore the lift distribution optimization and therefore twist distribution is different. The number of variables for the Flying V planform was reduced from 10 to 9 variables for the Flying V. Both models were created based on reference data where possible. For other data such as landing gear position on the Flying V, three views were utilized. Figures 5.12 to 5.13 show a comparative view of the models to three views of the aircraft during the first design iteration.

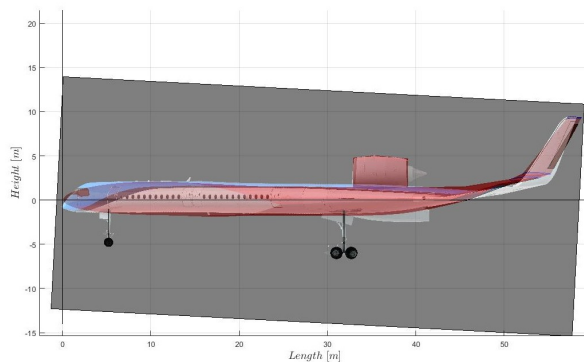


Figure 5.12: Flying V Parametric Model during set-up in BlackSwan, Side view

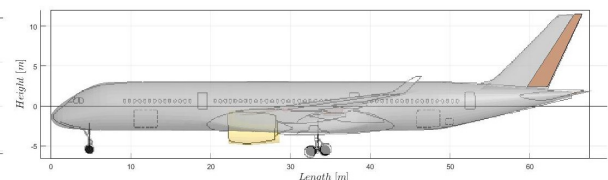


Figure 5.13: Reference Aircraft Parametric Model during set-up in BlackSwan, Side view

Next the purpose of repeating all simulations for the reference aircraft serves as a validation and verification method. Analyzing the Handling Qualities of the reference aircraft at the corners of the weight and balance envelope and critical assessment of the results found provides understanding of the reliability of the complete model and are discussed in Chapter 6. Being able to demonstrate sizing handling qualities criteria at borderline values of deflections, angle of attack etc. should however be interpreted with care, since for example no spoilers are modelled.

5.3.1. Flying V Aero Data Validation

Verifying results with respect to previous results of the Flying V was found to be ambiguous. This since it is unlikely that Parapy models and the BlackSwan generated parametric model correspond. Additionally, Faggiano's aerodynamic optimization did not yet include vertical fins nor did Palermo's wind tunnel model. Nonetheless, results were investigated for their correspondence to previously obtained results. For example, palermo's lift curve slope from wind tunnel testing and Odilila's were found to correspond satisfactory. At the lower Reynolds number a maximum lift coefficient of about 0.7 was found with the centre of gravity at the most forward location [20]. In order to calculate the reference stall speed, a maximum lift coefficient of 0.95 was found at 18° . Allowing for a margin of 2° to the start of pitch-up break tendencies, shown in the wind tunnel model. The aerodynamic efficiency found was within 1% of Faggiano's value. This should however be put in perspective as the twist and lift distribution will presumably be completely different. The pitch-break tendency beyond 20 degrees angle of attack from Palermo's tests are repeated in Figure 5.14. This phenomenon is naturally not captured in the VLM, but should be considered in the results nonetheless.

Figures 5.15 and 5.16 provide the lift and moment coefficient comparison between the wind tunnel test of Palermo and Odilila. Not only the planforms are different, but also the conditions. Palermo's tests were undertaken at a free stream velocity of 20 m/s and Reynolds number of $Re = 1 \cdot 10^6$. Odilila's results are undertaken at a velocity of 250 m/s and $Re = 6.5 \cdot 10^6$.

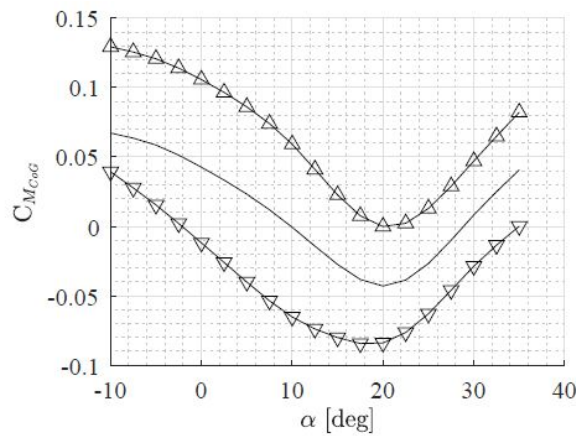


Figure 5.14: Flying V pitch break tendency beyond 20° Angle of Attack [20]

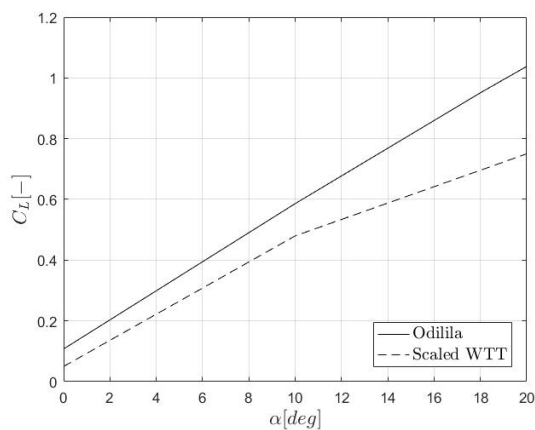


Figure 5.15: Lift coefficient comparison between scaled Wind tunnel model and Odilila

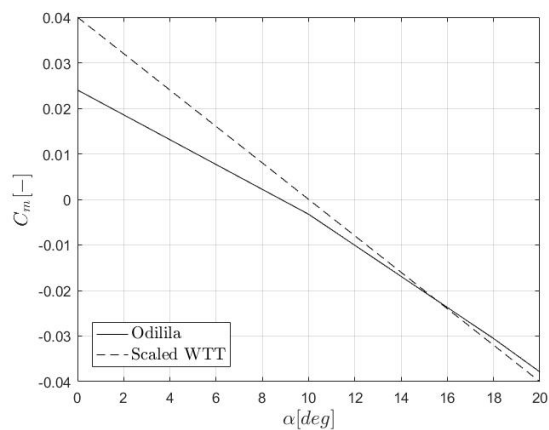


Figure 5.16: Moment coefficient comparison between scaled Wind tunnel model and Odilila

5.3.2. Neutral Point Verification

In order to verify whether the neutral point calculation, based on the automated Odilila report is correct, a trim plot is made based on the aero data output. More precisely, the reference point is placed on top of the calculated Neutral Point and the pitching moment coefficient is checked for different lift coefficients. The solid black line in Figure 5.17 indicates neutral elevon deflections (0°). Here the pitching moment coefficient is indifferent of the lift coefficient. In effect the aircraft exhibits neutral static stability, as expected for a static margin of 0%. It can also be noticed that in case the elevons 1 and 2 are deflected 30° trailing edge up, the aircraft becomes slightly statically unstable (upper dashed line). This since the control surface deflections influence the aerodynamic centre location. The lightly negative slope of the point-dash line shows slight positive stability. This is likely due to the aerodynamic centre moving forward with trailing edge up deflections.

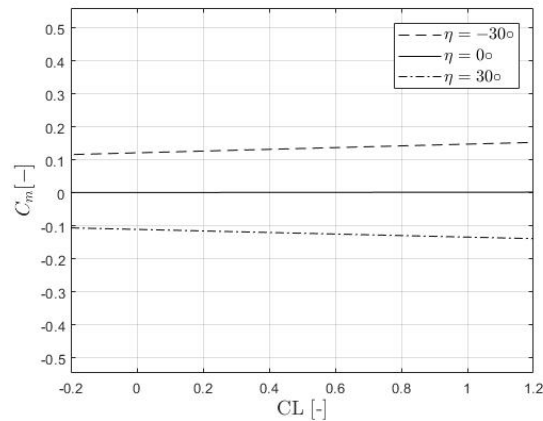


Figure 5.17: Trim plots for zero static margin

5.4. Flight Mechanics Model Verification

Throughout the creation of the Flight Mechanics Model, tests were made to verify the correctness of all functions. The simplest example being, the removal of all forces except for gravity, where the aircraft would be treated as a point mass. Here, from a certain altitude, velocities and accelerations could be assessed in the different reference frames.

Some examples are demonstrated such as load factor in a coordinated turn, Rate Of Turn (ROT) and turn radius. The load factor as a function of bank angle is represented in Equation 5.2. Here it can be derived that the load factor equals 2 times the gravitational acceleration when the coordinated turn is performed at $\phi = 60^\circ$. Figures 5.19 and 5.20 show a simulation with a bank angle of 60 degrees and the consequential load factor of 2g. From the vertical scales of Sideslip Angle (SSA), Flight Path Angle (FPA) and Rate of Climb (ROC), it can be derived that the aircraft is indeed in a coordinated turn.

$$n_z = \frac{1}{\cos\phi} \quad (5.2)$$

A rate one turn is defined as a 360° turn completed in 2 minutes, which results in an angular rate of $3^\circ/\text{s}$. The bank angle required to perform such turn is dependent on the Velocity (TAS) and the relationship is presented in Equation 5.3².

$$ROT = \frac{1,091 \cdot \tan(\phi)}{V} \quad (5.3)$$

A simulation of a coordinated turn at 200kt was made. The required bank angle equalled $\phi = 28.8^\circ$ and the turn resulted in a radius of 1.96 km, according to Equations 5.3 and 5.4. Figure 5.18 shows the aircraft flight path from which this value can be derived. Furthermore the yaw Euler angle is shown to increase linearly from 0 to 360° as displayed in Figure 5.21. The behaviour of the Flight Mechanics Model is therefore as expected.

$$R = \frac{V^2}{11.26 \cdot \tan\phi} \quad (5.4)$$

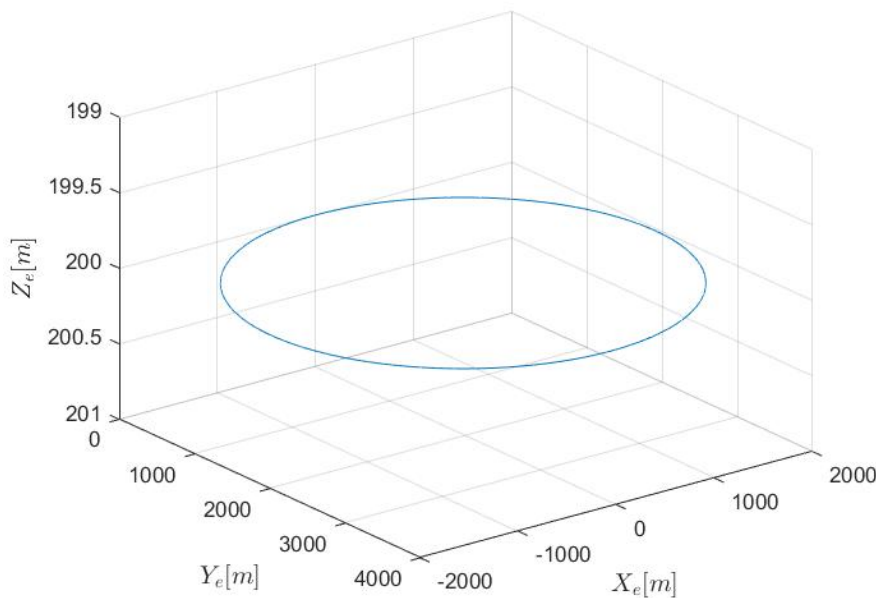


Figure 5.18: Aircraft flight path in a rate one turn

²<http://adl.stanford.edu/sandbox/groups/aa241x>

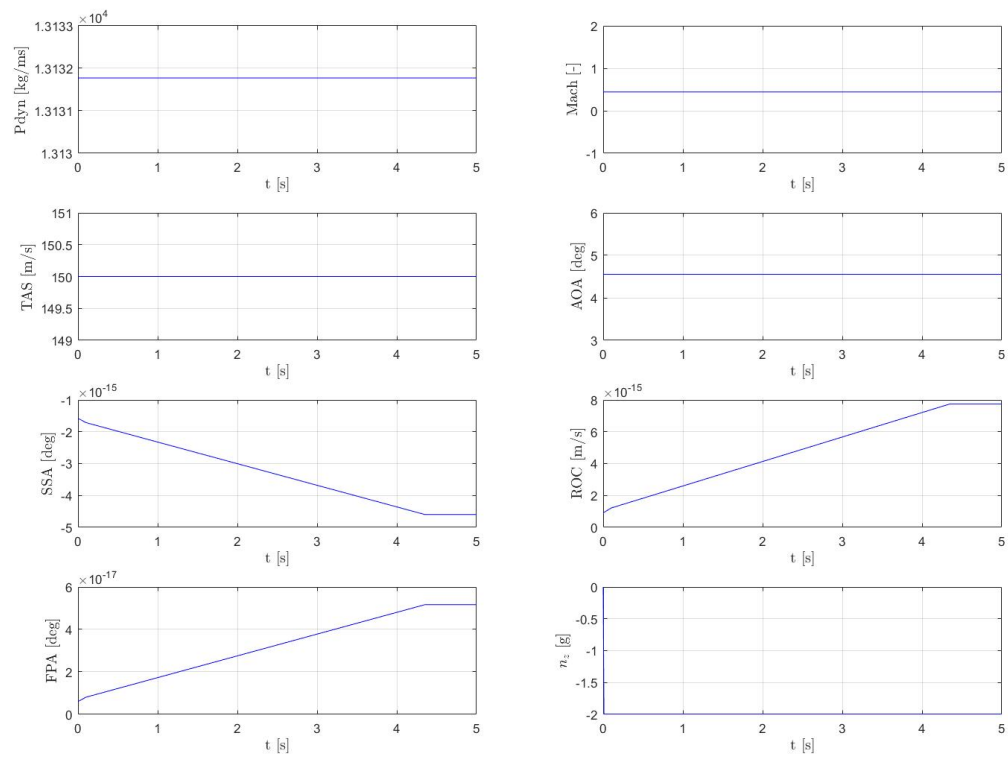
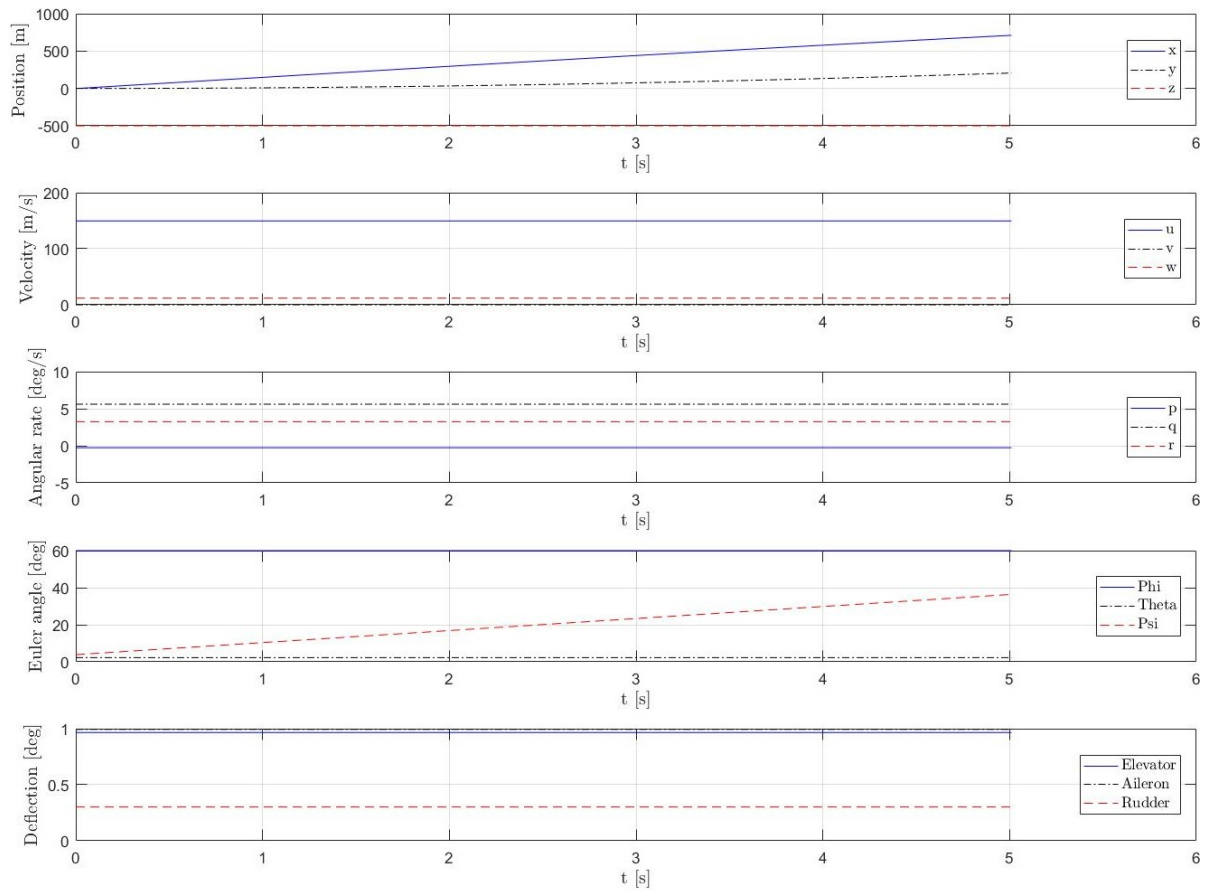


Figure 5.19: Load factor of 2 in a coordinated turn with $\phi = 60^\circ$

Figure 5.20: Time domain plot, demonstrating a bank angle of $\phi = 60^\circ$

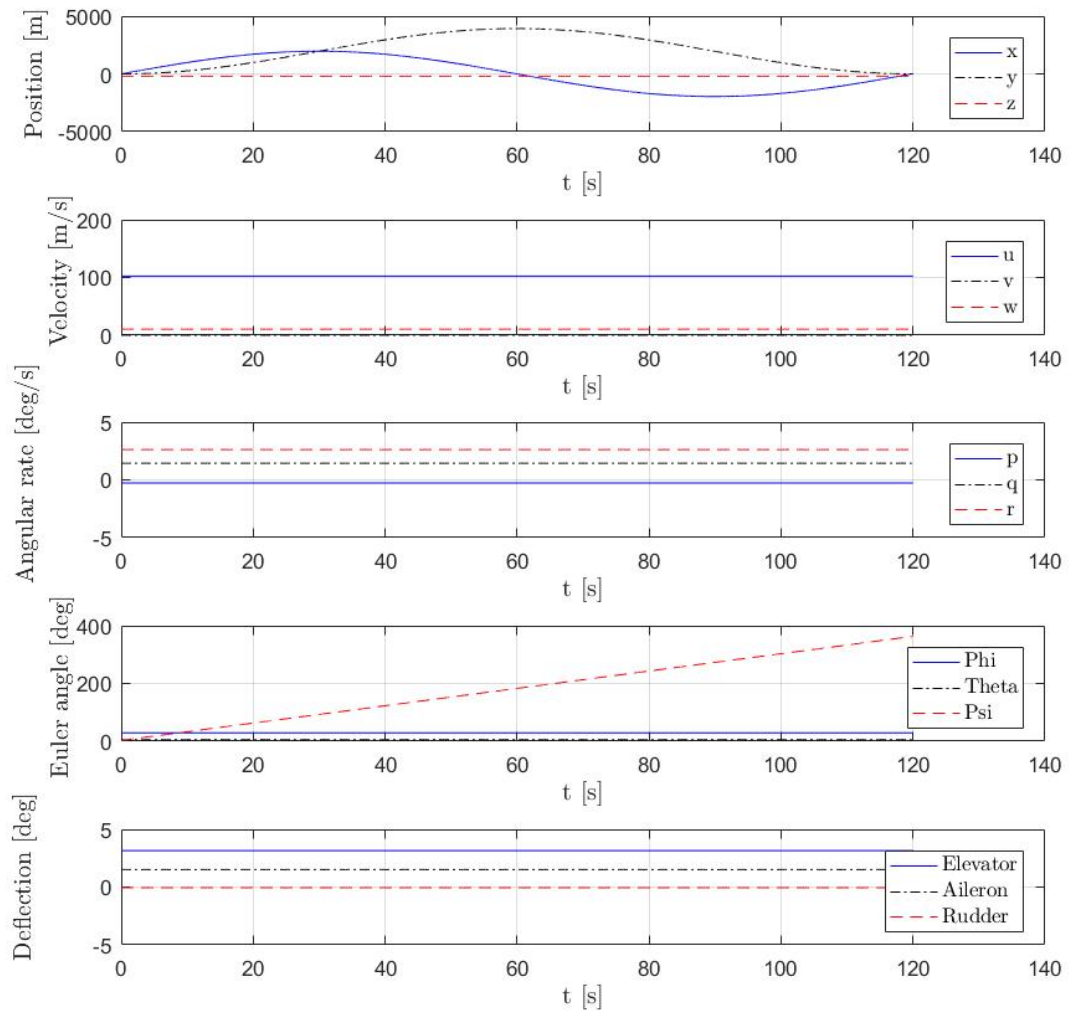


Figure 5.21: Yaw Euler Angle (ψ) increasing from 0 to 360° throughout the rate 1 turn

6

Results

In this chapter the results of the complete Flight Mechanics Toolbox are addressed. First a glance into the performance of both aircraft is provided. Thereafter the longitudinal and lateral-directional Handling Qualities are discussed. The results are provided with respect to static and dynamic Handling Qualities criteria, introduced in Chapter 2. The forward and rearward CG limits for the flying V are established by ensuring sufficient longitudinal stability while safeguarding control power.

The first iteration of results for the Flying V will show that the forward CG was limited by the pull up manoeuvres outlined in CS 25.143 [1]. A new iteration, having adapted the chords of the control surfaces found that when the chords of the elevons was increased, the pull up manoeuvres were no longer limiting. This time the coordinated turn with a bank angle of 40° at V_{app} lead to elevated angles of attack and the forward CG limit will be adjusted accordingly. Subsequently, the limited lateral-directional control power of the Flying V will be addressed. The chapter is finalized with the conclusion and potential solutions for the lateral-directional controllability issues.

6.1. Moments of Inertia

Table 6.1 provides the Moments of Inertia of both aircraft around their principle axes. At Maximum Take-off Weight (MTOW) the rolling MOI is found to be larger for the Flying V. This is expected as the cargo and passengers are located further away laterally from the Centre of Gravity. The pitching moment of inertia is smaller for the same reason and since the overall length of the Flying V (FV) is shorter in comparison to the Reference Aircraft (RA). The yawing MOI is found to be similar for both aircraft. At Empty weight, the latter is not the case. Here the difference in rolling MOI is found to be smaller between the aircraft, which is as expected as they have a similar wingspan.

Inertia	Flying V		Reference Aircraft		Unit
	MTOW	Empty Weight	MTOW	Empty Weight	
I _{xx}	3.9641	1.2275	2.9448	0.8525	$[\cdot 10^7 \text{ kgm}^2]$
I _{yy}	2.7619	1.0504	3.8777	2.1229	$[\cdot 10^7 \text{ kgm}^2]$
I _{zz}	6.5822	2.1437	6.6484	2.8460	$[\cdot 10^7 \text{ kgm}^2]$

Table 6.1: Principle axes Moments of Inertia at Empty and Maximum Take-Off Weight

6.2. Performance Considerations

Any centre of gravity within the defined limits should provide desirable Handling Qualities. There is however a range of recommended locations for the CG position. This range is specific to any aircraft in order to increase performance during different flight phases. For conventional aircraft in the cruise flight phase, tail down force to compensate the natural nose down pitching moment effect reduces when the CG is moved rearward. Additionally, the higher the tail down force, the higher the wing lift required to maintain level flight, further increasing induced drag and hence fuel consumption. Additionally, the more forward the CG, the higher the minimum speed required to maintain level flight (VS1G). Finally, the more forward the CG, the lower the

takeoff and landing performance. Both angle of attack and speed to maintain required Flight Path Angles increase. For the Flying V, this trim drag effect deteriorates the performance even more, as large portions of lift are lost when trying to pitch the nose up at forward positions of centre of gravity.

6.2.1. Optimization Point

Both models are optimized for a mass of 200 tons at an altitude of 13,000m and a Mach number of 0.85. The chosen deck angle in cruise is set at 2.5° for passenger comfort. The centre of gravity location for which the reference aircraft is optimized is based on the mid-point of the Weight and Balance of the A350-900 (30.5% MAC). For the reference aircraft, the Neutral Points were found at 62 and 65%. The different CG limits here are respected throughout the flight dynamics simulations for the different weights and flight phases. The Weight and Balance utilized in provided in Figure 6.1.

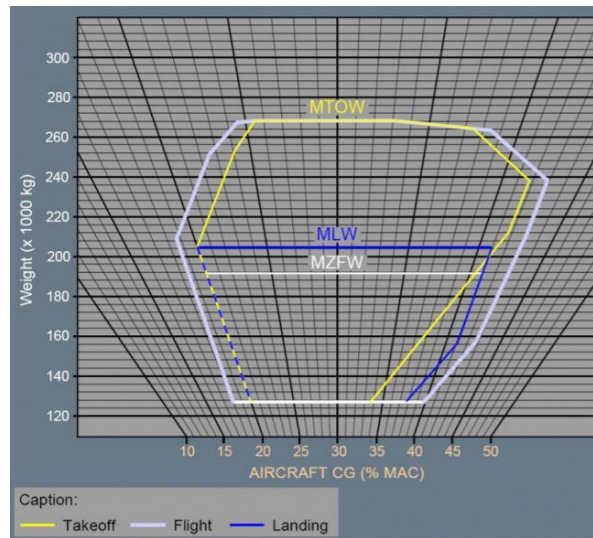


Figure 6.1: Weight and Balance of the A350-900 [3]

For the sake of comparability, about the same optimization point as Faggiano and Palermo was chosen. At this point, a static margin of 5% MAC for the Flying V is provided and a lift to drag ratio of 24 was found as given in Table 6.2. The optimization undertaken goes as follows. The reference point chosen is the conventional quarter chord location (25% MAC). Next the attitude of 2.5° is specified together with the other cruise conditions. First the wing twist is optimized, provided that airfoils are given. These allow for deducing a camber distribution. Here the twist is varied without imposing elevon deflections while maintaining the angle of attack of 2.5° . Then Odilila is ran for two different angles of attack. This is done to retrieve the moment and lift coefficients for the AOAs specified. The latter allows for retrieving the static margin through Equation 6.1. Since the reference point was placed at the quarter chord location, the Neutral point is easily retrieved. This point was found to be 33.68 m aft from the nose, which corresponds to 68% MAC at M0.85. This reduced to 32.2 m (60% MAC) at the approach conditions at M0.2. It was reasoned before by Palermo that the minimum stability margin could potentially be reduced to 2.5%. The rearward CG limit therefore becomes 57.5% MAC.

$$K_n = \frac{X_{NP}}{\bar{c}} - \frac{X_{CG}}{\bar{c}} = -\frac{C_{m\alpha}}{C_{L\alpha}} \quad (6.1)$$

Variable	Flying V	Reference Aircraft	Unit
Altitude	13,000	13,000	[m]
Mach	0.85	0.85	[-]
α	2.5	2.5	[deg]
Reference CG Position	55	30.5	[% MAC]
$\frac{C_L}{C_D}$	23.9	20.6	[-]

Table 6.2: Optimization point comparison Flying and Reference Aircraft

The twist and lift distributions of both aircraft as outputted by Odilila are provided in Figures 6.2 to 6.7. The lower lines for the reference aircraft indicate the contribution of the Trimmable Horizontal Stabilizer (THS) and the effect on the lift and twist distribution which is optimized to compensate for the THS. Be advised that the other lines are coming from the Nacelles and VTP.

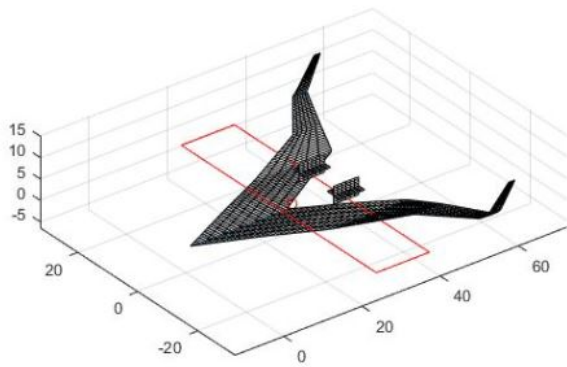


Figure 6.2: Flying V Odilila panel model

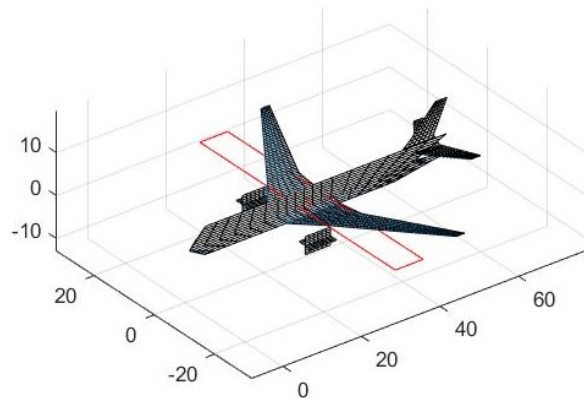


Figure 6.3: Reference Aircraft Odilila panel model

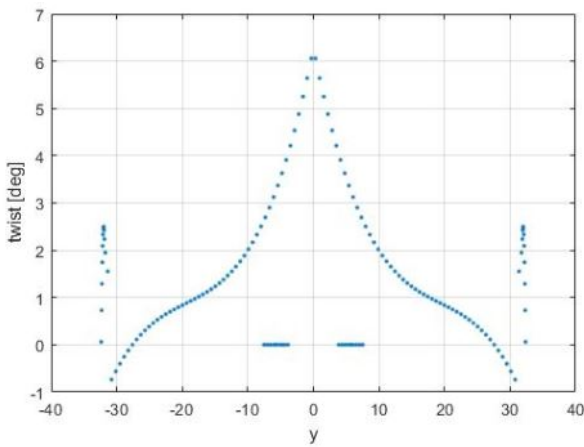


Figure 6.4: Flying V Odilila optimized twist distribution (mass=200 t)

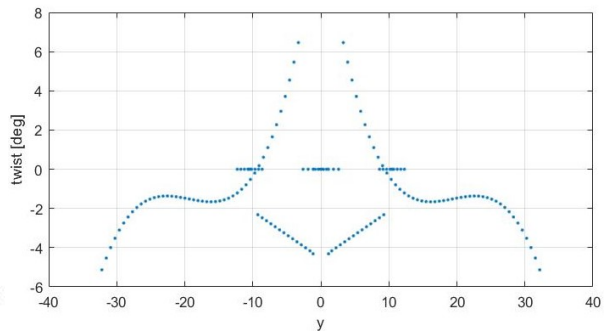


Figure 6.5: Reference Aircraft Odilila optimized twist distribution (mass=200 t)

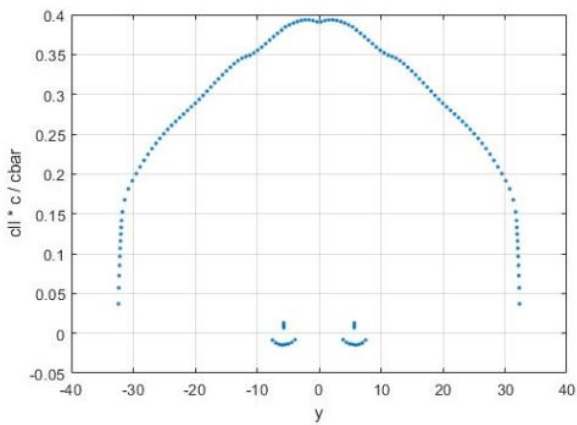


Figure 6.6: Flying V lift distribution (mass=200 t)

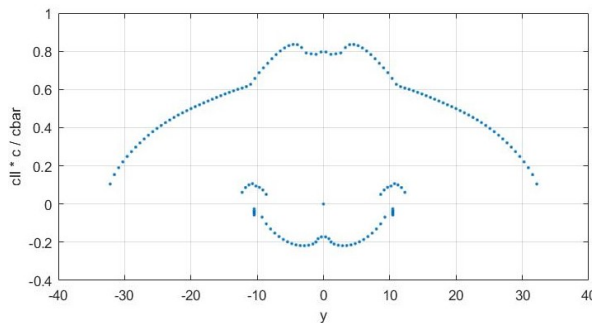


Figure 6.7: Reference Aircraft lift distribution (mass=200 t)

Results of the Aerodynamic Centre (AC) in relation to the selected Centre of Gravity (CG) range for both aircraft are summarized in Table 6.3 and are elaborated upon in the next Sections.

Variable	Flying V	Reference Aircraft	Unit
Mean Aerodynamic Chord	18.74	9.48	[m]
Reference CG Position	55	30.5	[% MAC]
Forward AC Position	60	62	[% MAC]
Rearward AC Position	68	65	[% MAC]
Forward CG Limit	45	18	[% MAC]
Rearward CG Limit	57.5	43	[% MAC]
CG Range	12.5	25	[% MAC]
CG Range	2.34	2.37	[m]
Minimum Static Margin	2.5	17	[% MAC]
Minimum Static Margin	0.47	1.6	[m]

Table 6.3: Centre of Gravity range summary in comparison to the retrieved Aerodynamic Center locations

6.2.2. Maximum Specific Range

It was shown by Faggiano that the Flying V is aerodynamically more efficient at higher lift coefficients [12]. In other words, that for the same Mach number, the Flying V becomes more efficient with altitude. Additionally, if the planform is then optimized iteratively for these higher altitudes, performance will further increase. Instead of plotting the Mach number versus the Specific Range [29], it was chosen to display the lift coefficient with its corresponding aerodynamic efficiency in Figure 6.8. Here one can see that the L/D remains constant for a certain range of lift coefficient after passing through the optimization point. As a consequence the highest aerodynamic efficiency for the Flying V is expected to be achieved at higher altitudes. This since the required lift coefficient will increase with altitude as density is decreasing, provided that the aircraft is operated at equal TAS. Margin with relation to high speed buffet, structural and powerplant effects should nonetheless be studied. Moreover, it should be noted that no compressibility effects are taken into account by Odilila. Therefore the results are overestimated for both aircraft.

The same conclusion can be made for the reference aircraft again as it could fly at higher altitudes at this weight of 200 tons and become more efficient. Or in other words, fly at the same altitudes at higher weights while increasing performance. The difference between the optimization point and the maximum efficiency is only about 0.4, while the difference for the Flying V was about 1.1 as indicated by Figure 6.9.

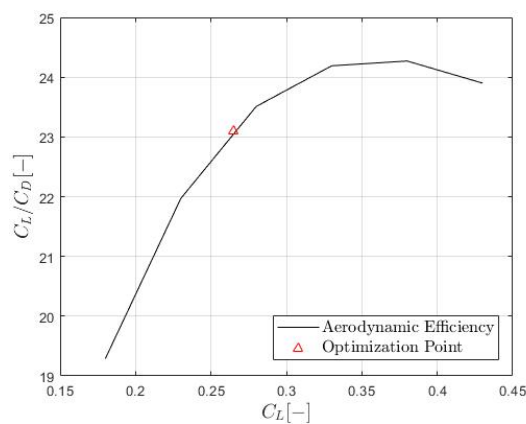


Figure 6.8: Flying V aerodynamic efficiency per lift coefficient

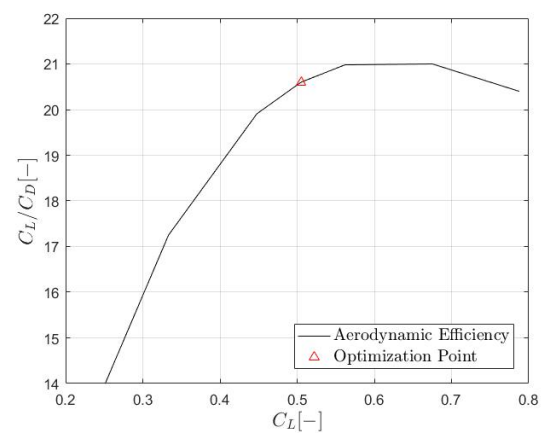


Figure 6.9: Reference Aircraft efficiency per lift coefficient

6.3. Longitudinal Handling Qualities

6.3.1. Trim on Approach

Even though the maximum lift coefficient of the Flying V is lower than that of the reference aircraft, it does not require High Lift Devices (HLD) due to its large surface area. It should however be checked whether the angle of attack and required control surface deflections are practical at approach speed with the CG placed at its forward limit. Based on the determined $C_{L_{max}}$ of 0.95, it was found that the Stall Reference Speed put the approach speed into the ICAO Aircraft Approach Categorization D (141-165 kn) [9]. This is the class of the A350-1000, the A350-900 however was able to be classified in the ICAO APC C (121-140 kn) due to its lower approach speed. The $C_{L_{max}}$ corresponds to the lift coefficient found in Odilila for an angle of attack of 18° , this in order to provide a margin of 2° to the onset of pitch-up break tendencies. With the CG placed at 45% MAC at Maximum Landing Weight (MLW) and an approach speed of 78 m/s (152 kn), the AOA amounted up to 12.7° with an elevon deflection of -7.8° when utilizing both elevons. This deflection increased to -13° and AOA to 13° when only using elevon 1. The reference aircraft with its approach speed of 72 m/s (140 kn) on a Flight Path Angle of -3° required -11° trailing edge up deflection of the Trimmable Horizontal Stabilizer and elevator in approach with an AoA of 12.2° in Configuration (CONF) FULL. Above given values are repeated in Table 6.4.

Variable	Flying V	Reference Aircraft	Unit
Mass	210	210	[t]
CG Position	45	20	[% MAC]
V_{app}	152	140	[kn]
α	13.7	12.2	[deg]
η_e	-7.8	-11	[deg]

Table 6.4: Trim on approach comparison

Figure 6.10 gives a visual representation of the control power of the elevons. This trim point was simulated in level flight at the approach speed and Maximum Landing Weight. Here it can be seen that when using Elevon 1 alone, the control surface deflection is more than halfway towards its maximum deflection. When utilizing both Elevon 1 and 2, there is plenty of range to the control deflection stops, currently set at 30° of deflection. This kind of trim plot as displayed in Figure 6.10 was utilized to ensure static stability at the rearward CG position of both aircraft for both approach and cruise conditions. More specifically, it was checked that these curves displayed negative slopes for every combination of elevator deflection and/or Configuration.

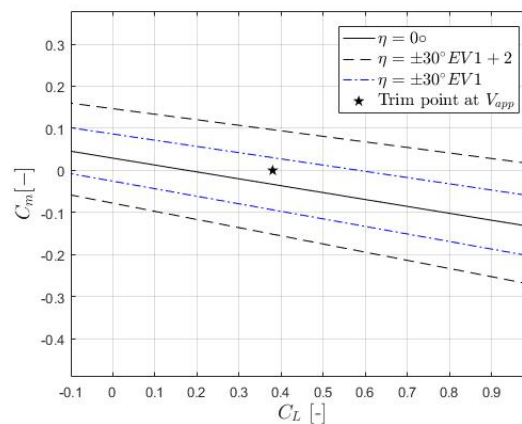


Figure 6.10: Flying V elevon control power limits

Pull-up Manoeuvre

As the static stability and control saturation have just been checked on approach, its manoeuvrability is now assessed. The requirement referred to is the minimum manoeuvring capability specified in CS 25.143, Positive (minimum) limiting load factor. The relevant part for this requirement is summarized based on Acceptable Means of Compliance Section 6.9 of CS 25 Amendment 23 [1]. From the approach speed in the highest lift configuration pull-up to 1.3 g.

The AMC specifies that the aircraft should be flown at Medium to light weight. To be on the conservative side the Maximum Landing Weight and CG at the forward limit was chosen for these tests as the aircraft will behave as sluggish as possible. For the forward limit of the Flying V initially chosen, reference is made to Claeys's thesis [8]. Here the Flying V's mass distribution variation showed that the most forward CG location was found for the Maximum Zero Fuel Weight (MZFW) sizing point. Translated to the BlackSwan parametric model, this point corresponds to 18% MAC (23.9m from the nose). It became evident that it was impossible to reach load factors over 1.1 g for any combination of elevons up to their maximum deflections. What was striking was the fact that when elevons 1 and 2 were deflected to their maximum deflections in approach, the loss in lift was so significant that the aircraft could lose up to tens of meters of altitude and initially go significantly below 1 g. After a delay of about 2 s, the angle of attack reached elevated values and the load factor and altitude increased.

From this point onward, the forward limit was moved rearward iteratively until a load factor of 1.3 g could be achieved in approach. This was found to occur at 45% MAC. The control surfaces 1 and 2 required a deflection of about -14° . At a Flight Path Angle of -3° at 78 m/s and Maximum Landing Weight, a load factor of 1.39 g can be achieved. These results are summarized in Table 6.5.

The same tests were conducted to see whether the forward limits of the weight and balance of the reference aircraft could be explained. In Configuration FULL at the same MLW of 210 tons and a V_{REF} of 72 m/s, 1.36 g is obtained. The elevator deflection was allowed to travel to its stop of -20° with the THS at 14° trailing edge up deflection. In the Clean configuration at 77 m/s, 1.53 g was obtained with again the THS at its stop. Note that this is a valid consideration as the A350 does not include the same philosophy of other Airbus aircraft on the design of the THS. In short the working principle of the THS of any other Airbus design could be said to work by the following principle. Long term inputs change the THS deflection while short term inputs are handled by the elevator. For the A350 the tail volume was reduced since the THS is also used to work more closely together with the elevator. The reaction time of course still being slower than that of the elevator alone, but this should not pose a problem for 1° extra deflection.

As a result, the forward limit of the Flying V will for now be kept at 45%. These tests formed one of the limiting factors for the determination of the forward CG limit. It was also found that in case one would like to enlarge the centre of gravity envelope and allow for more forward positioned CG, this problem could also be solved by allowing the approach speed to increase. It was found that more elevated values of this load factor could also be reached at an approach speed of 82 m/s (160 kn) at the previously defined CG location of 35% MAC. This may not be an attractive solution as the aircraft landing distance would increase drastically.

Parameter	Flying V		Reference Aircraft	Unit
	Iteration A	Iteration B	CONF FULL	
CG	35	45	20	[% MAC]
Mass	210	210	210	[t]
δ_e	-15.4 \rightarrow -20	-8 \rightarrow -14	-10.5 \rightarrow -14 (THS) -10.5 \rightarrow -20 (Elevator)	[deg] [deg]
n_z	1.2	1.4	1.4	[g]

Table 6.5: Pull-up manoeuvre conditions and obtained load factors

6.3.2. Control Anticipation Parameter

Another measure of estimating an aircraft’s manoeuvrability is assessed through the Control Anticipation Parameter (CAP). The CAP criterion does not only assure a minimum manoeuvrability but also that that the platform does not become too agile. Figures 6.11 and 6.12 represent the CAPs for both the Flying V and reference aircraft. Figure 6.11 outlines the values found during the cruise flight phase, while Figure 6.12 represents the approach flight phase. "Flight Phase A" was not considered as this is meant for highly manoeuvrable aircraft such as fighters.

The same Odilila output files for the newly defined forward CG limit and earlier defined CG limit are utilized. Since both forward and aft CG limits are tested per aircraft per flight phase, the most conservative weights are implemented. For example, the Maximum Landing Weight when checking the forward limit on approach and the lightest weight in cruise with the reference point at the rearward limit. As mentioned before, the aircraft should also not become too sensitive at lower inertia’s, lower values of the static margin and wing loading. The Flight Mechanics Model was ran and trimmed for the desired flight phase. Next the model was linearized and the frequency of the short periods was collected. Subsequently a simulation was made where at some point in time an arbitrary pitch control input was given. From this the $N_{z\alpha}$ could be deduced by collecting the angles of attack and loading factor before and after the control input.

For the reference aircraft, reference was made again to the weight and balance of the Airbus A350. Here the most forward and aft loading configuration were selected per flight phase. Changes in load factor were acquired by deflecting both THS and elevator. As can be concluded, these values all fall within level 1 limits. The CAP in approach for the reference aircraft are found on the border of the level 1 requirement. This is due to the lower approach speed and higher wing loading of the Reference aircraft. Note that with the initially defined forward CG limit of the Flying V, the approach phase CAP values were found to fall within the level 2 requirements. For clarity, the test conditions are repeated in Tables 6.7 and 6.6.

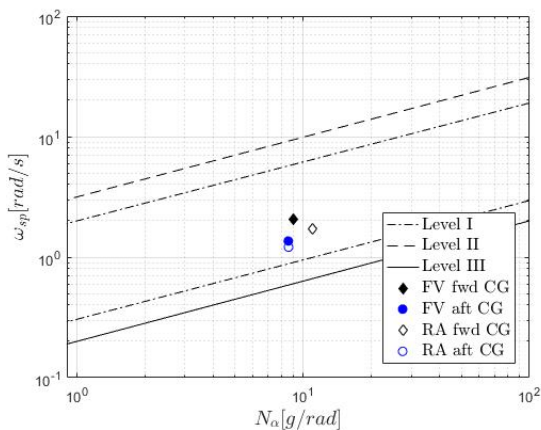


Figure 6.11: Flight Phase Category B, Control Anticipation Parameters

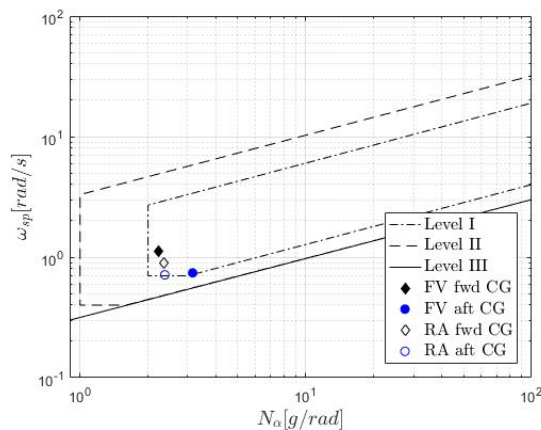


Figure 6.12: Flight Phase Category C, Control Anticipation Parameters

Variable	Flying V	Reference Aircraft	Unit
Forward CG position	45	20	[%MAC]
Aft CG position	57.5	41	[%MAC]
Mass	210	210	[t]
TAS	152	140	[kn]

Table 6.6: CAP tested condition in Flight Phase Category C (Approach)

Variable	Flying V	Reference Aircraft	Unit
Forward CG position	45	18	[%MAC]
Mass at fwd CG pos	210	210	[t]
Aft CG position	57.5	43	[%MAC]
Mass at aft CG pos	240	240	[t]
TAS	486	486	[kn]

Table 6.7: CAP tested condition in Flight Phase Category B (Cruise)

6.3.3. Eigenvalue Analyses

The longitudinal Eigenvalues of both aircraft are given in Figures 6.13 and 6.14 together with the detailed values in Tables 6.8 and 6.9. Here a comparison is given with the CG placed at their aft limits during the cruise and approach flight phases.

Phugoid

It was found that the static margin had no direct effect on the phugoid performance. Longitudinal dihedral and aerodynamic efficiency however do have an impact. The damping values found were similarly small. A Level 1 performance requires a damping of $\zeta \geq 0.04$. In order to obtain a Level 2 phugoid performance the damping has just to be positive, which is the case for all phugoid motions except for the reference aircraft in approach configuration. The time to double in this case was equal to 462 s, by which the Level 3 criteria is still acquired. In conclusion all phugoid Eigenmodes are adequate and do not pose a problem as they are easily controlled by the pilot or control system.

Short Period

Cook demonstrated that the ideal damping ratio for a Short Period Oscillation (SPO) mode is 0.7 [10]. For this value, the settling time after a disturbance is minimized while ensuring a satisfactory margin for stability. The reference aircraft scored its worst value in cruise with the CG at the forward limit with a damping value of $\zeta = 0.29$. The Flying V scored a similar result of $\zeta = 0.27$ at this condition. Resulting that they both fall just outside the Level 1 requirements for the SPO oscillation in the Flight Phase Category B (cruise). The Approach Flight Phase C results in Level 1 values for the SPO damping value for both aircraft. With the CG placed at the aft limit, Level 1 Short Period requirements are obtained.

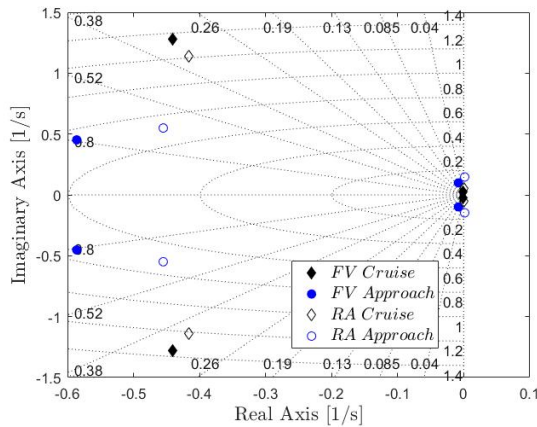


Figure 6.13: Longitudinal Eigenvalues comparison at most rearward CG position

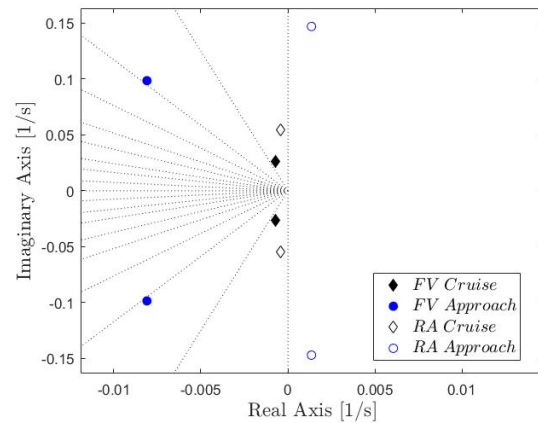


Figure 6.14: Close-up view of the Phugoid Eigenvalues at most rearward CG position

Flight Phase	Mode	Poles	Damping [-]	Natural Frequency [rad/s]
Cruise	Phugoid	$-0.0007 \pm 0.026i$	0.03	0.03
	Short Period	$-0.441 \pm 1.28i$	0.33	1.36
Approach	Phugoid	$-0.0081 \pm 0.099i$	0.08	0.10
	Short Period	$-0.586 \pm 0.452i$	0.79	0.74

Table 6.8: Flying V longitudinal Eigenvalues

Flight Phase	Mode	Poles	Damping [-]	Natural Frequency [rad/s]
Cruise	Phugoid	$-0.0004 \pm 0.055i$	0.01	0.06
	Short Period	$-0.416 \pm 1.14i$	0.34	1.21
Approach	Phugoid	$0.001 \pm 0.147i$	-0.01	0.15
	Short Period	-0.455 ± 0.549	0.64	0.71

Table 6.9: Reference Aircraft longitudinal Eigenmodes

6.4. Lateral-Directional Handling Qualities

6.4.1. Lateral Control Departure Parameter

Roll rates are conventionally limited at high angles of attack and in case of an engine failure / low speed combination. The contribution of wing sweepback becomes especially important at high values of C_L due to the sideforce acting relatively far behind the Centre of Gravity. The Flying V does not suffer from a destabilizing effect of the fuselage. In contrast the reference aircraft does have a large stabilizing vertical fin while the Flying V utilizes the two vertical fins. The desired sign of $C_{n\beta}$ is therefore positive and was found to be positive for all configurations tested. Additionally it is noted that the side force estimation of the Flying V is expected to be slightly more accurate since this VLM model does not possess a fuselage.

The designation "effective dihedral" is commonly used to refer to $C_{l\beta}$. The main influences of this parameter are found to be the dihedral, wing sweep and wing-fuselage interaction. Effects of fuselage and tailplane are less. For this derivative a negative value is sought after. A positive aileron deflection is defined as one where the right aileron's trailing edge moves down. Therefore a positive aileron deflection lifts the right wing and initiates a rolling moment to the left, therefore the derivative should have a negative value. Additionally, since the influence of the Mach number is not taken into account and no aeroelasticity is modelled, no flow separation on the wing in the area of the ailerons occurs. As a consequence $C_{l\delta_a}$ is considered independent of C_L .

The yawing moment caused by the ailerons is based on the differential drag generated by the down and up-going ailerons. The wing with the downward deflected aileron being the one with the highest drag as it is generating more lift. As a consequence a positive aileron deflection causes a positive yawing moment. The predominant test points consulted are shown in Table 6.10.

It was found that the values of the LCDP decreased with speed and the most conservative values were found at the Reference Stall Speed (V_{SR}). Here the values were still positive and LCDP does not pose adverse behaviour for both aircraft. As a result, aileron deflection at elevated angles of attack holds the desired effect.

Aircraft	Conf	Velocity [kn]/[m/s]	CG [% MAC]	LCDP
Flying V	n.a.	136/70	57.7	0.0954
	n.a.	136/70	45	0.0954
Reference Aircraft	Clean	113/58	18	0.4402
	Take-Off	113/58	20	0.4402
	Full	113/58	20	0.4461
	Clean	113/58	43	0.4406
	Take-Off	113/58	42	0.4405
	Full	113/58	41	0.4623

Table 6.10: LCDP Test Points

6.4.2. Eigenvalue Analyses

Spiral Stability

A slow and often unstable mode where the aircraft will fly a diverging spiralling path toward the ground after a lateral disturbance. Aircraft such as the A350 achieve neutral roll stability up to a bank angle of around 30° and often implement protections at higher bank angles [3]. As the MIL-HDBK criteria allows this mode to be unstable, a time to double is prescribed with a Level I minimum value of 12 s on approach and 20 s in cruise. The only unstable Spiral mode found was for the Flying V in approach conditions with the CG at the forward limit. Here the time to double was 10 times the minimum value and therefore poses no problem. The reference aircraft did not acquire positive real values for the spiral stability and therefore naturally also passes the criteria.

Flight Phase	Mode	Poles	Damping [-]	Natural Frequency [rad/s]
Cruise	Roll Subsidence	-0.7	1.0	0.7
	Spiral Stability	-0.005	1.0	0.01
	Dutch Roll	0.018±0.688	-0.03	0.69
Approach	Roll Subsidence	-1.08	1.0	1.08
	Spiral Stability	-9.06·10 ⁻⁶	1.0	-9.06·10 ⁻⁶
	Dutch Roll	0.054± 0.845	-0.06	0.85

Table 6.11: Flying V Lateral-Directional Eigenmodes

Flight Phase	Mode	Poles	Damping [-]	Natural Frequency [rad/s]
Cruise	Roll Subsidence	-0.796	1.0	0.80
	Spiral Stability	-0.018	1.0	0.02
	Dutch Roll	-0.021 ± 0.742	0.03	0.74
Approach	Roll Subsidence	-1.02	1.0	1.02
	Spiral Stability	-0.030	1.0	0.03
	Dutch Roll	-0.048 ± 0.817	0.06	0.82

Table 6.12: Reference Aircraft Lateral-Directional Eigenmodes

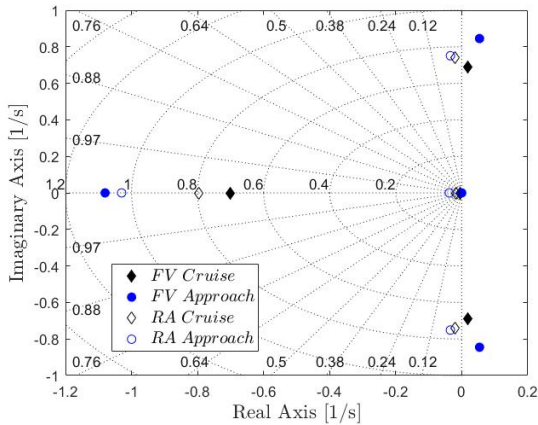


Figure 6.15: Lateral-Directional Eigenvalues comparison at most rearward CG position

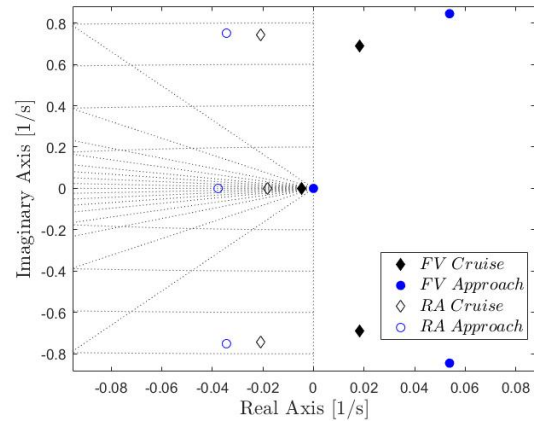


Figure 6.16: Close-up view of the Spiral and Dutch Roll Eigenvalues at most rearward CG position

Dutch Roll

A normally damped oscillation in yaw which is closely coupled with the motion in roll. When the vertical fin experiences a disturbance from straight and level flight, an oscillation in yaw is started. The vertical fin is providing aerodynamic stiffness. Due to this yaw motion, a differential in lift and drag is created. The forward moving wing is experiencing higher velocities, therefore creating higher lift and drag. As a result an oscillation in roll ϕ is started which lags ψ by approximately 90° . The sideslip created is in the direction of the low wing which is also the wing moving forward.

The minimal required damping is considered to be a function of the period of the motion. In case the period is too short, the reactions of the pilot will be too slow to stabilize the motion by suitable control deflections. In such a case a relatively high damping is required. If the period is longer, the damping of the motion may be lower. Here the pilot has less difficulty to improve the damping of the aircraft's motion via his control deflections. In the end it is key to prevent the dutch roll from developing altogether. Conventionally, Dutch roll motion of aircraft having a low wing loading, flying at relatively low altitude are relatively well damped.

In aircraft with swept-back wings, Dutch Roll can be a significant problem. Therefore a yaw damper is incorporated. This is a device which neutralizes yaw rates by a deflection of (or a portion of) the rudder. As a result the Dutch Roll never gets a chance to develop. The system exists of a yaw-rate sensor and processor that provides an actuator output connected to the rudder. Generally they are used for passenger comfort. But it's importance can be so predominant that even in case of complete electric failure on some aircraft, more basic back-ups still provide yaw damping. Should the Original Equipment Manufacturer (OEM) allow for dispatching the aircraft with the Yaw Damper inoperative, the aircraft would normally be limited in speed and altitude, dependent on the aircraft's Dutch Roll characteristics.

Figures 6.17 and 6.18 provide the performance of both aircraft w.r.t. the selected criteria. In order for the aircraft to exhibit positive dutch roll stability, the markers have to be on the right side of the vertical axis. Furthermore it is shown that the Reference Aircraft falls within the Level 3 (controllable) requirement. In case the aircraft would be operated without yaw damper, this would result in a unpleasant experience for the passengers with a large likelihood of motion sickness. The Flying V however, is not capable of operating without a yaw damper as the planform is found to be unstable. This, except for one condition, where the aircraft is flying in cruise conditions with the CG located at the forward limit. The same can be concluded from Figures 6.15 and 6.16.

This in other words means that with the current configuration, a certifiable yaw damper is required. More specifically, the yaw damper might not exhibit a failure rate larger than $1 \cdot 10^{-9}$, where a single point failure could lead to the loss of the aircraft.

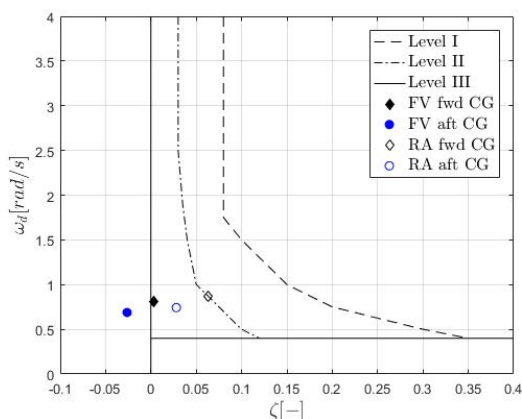


Figure 6.17: Dutch Roll Performance during Cruise

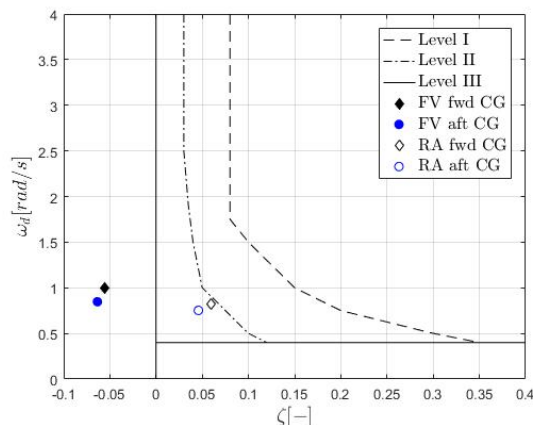


Figure 6.18: Dutch Roll Performance during Approach

An attempt was made to better understand the source of this poor Dutch Roll performance. Arbitrary design changes were made and the difference in time to double to a reference case was recorded. The reference value is from a simulation with the CG placed at the rearward limit in approach conditions. It should first be noted that no design change or combination of the changes made lead to a positively damped dutch roll in this condition, only trends could be observed. The most effective way of increasing the dutch roll performance was through decreasing the dihedral. The dihedral angles tested were provided by another student who is looking into the landing gear design. Second, increasing the winglet's length (and therefore vertical fin volume) also proved to be an effective approach. Altering the sweep would largely impact the performance and its effect is as expected, further decreasing the dutch roll stability with increasing sweep. The difficulty in making design changes to e.g. the vertical fins, lies within their compound effect on stability derivatives. More specifically, a dedicated study is required to improve the dutch roll performance where a specific design study of the vertical fins could be a good starting point. This in addition to a study of the effects of yaw rate feedback to rudder, will improve lateral-directional flying qualities.

Design Change	Time to double [s]
None (original design)	12.9
Winglet length increased from 7 to 9m	21.2
Dihedral decreased to 0° (inboard) and -7° (outboard)	22.8
Increased outboard sweep to 50°	8.6

Table 6.13: Design changes to the Flying V and their effect on the time to double of the Dutch Roll Eigenmode

Roll Subsidence

While rolling the aircraft along its longitudinal axis, the increase in lift of the down-going wing restores the rolling moment. Provided that $C_{l_p} < 0$. The minimum Eigenvalue found was on the Flying V and amounted to -0.7. No roll subsidence time constant was found which surpassed the recommended maximum values. This rolling capability is addressed in more detail in the following requirement.

6.4.3. EASA CS 25.143

Coordinated Turn Capability

The trim in coordinated turn mainly focuses on providing adequate manoeuvrability and controllability. In total 4 test points were assessed of which two included One Engine Inoperative conditions. All tests were made at the Maximum Landing Weight (MLW) and forward CG limit. The aircraft is required to be trimmed in a steep turn. In the OEI case, this turn has to be made into the conservative direction, in effect to the side of the inoperative engine. The aircraft should not exhibit stall warning during flight test and control forces within bounds. For this simulation the Angle of Attack and control surface deflections were monitored. No excessive values were found for the reference aircraft except for an elevated AOA in CONF FULL at V_{APP} and a bank angle of 40°. The aircraft however is expected to remain clear of stall and control surface deflections are well within limits. The same test point posed problems when the CG limit of the Flying V was still placed at 40% during iterations and was therefore moved to 45%. The Angle of attack now amounts up to the same value as the reference aircraft, providing a margin of over 2° to the start of the pitch-up break tendency. Note that the elevated AoA of the reference aircraft of $\alpha = 17.7^\circ$ is considered to be too elevated to remain clear of stall warning. It was however concluded that the highest lift configuration's flap setting was 2.5° too low in comparison to the actual A350-900 setting.

Furthermore the control power of the rudder of the Flying V was found to be inadequate for the test point at V_2 with a bank angle of 30° and One Engine Inoperative. Here the rudders hit their stop as a maximum deflection of 30° is required. The results are outlined in Tables 6.14 and 6.15.

Bank to Bank Manoeuvre (Roll Capability)

The roll capability with both engines running and OEI has to be demonstrated. The maximum SSA without deflecting the rudder can go up to more than 10 degrees at 100 kt for widebody Airbus aircraft, but decrease significantly with TAS. Note that currently no spoilers are modelled which would significantly increase the roll rate while limiting adverse yaw, to compensate for this, large differential deflections were added to the control mixer. The outer ailerons were assumed to be inhibited at the high speed test points. The same findings were found, demonstrating that the lateral-directional control power of the Flying V is too limited with the current control allocation and sizing. Tables 6.16 and 6.17 hold the summarized test point values. Figure 6.19 shows an extreme example of directional control power issues of the Flying V. Here a roll command of $\delta_e = 20^\circ$ was given to both elevons 1 and 2. A bank to bank manoeuvre with OEI at 80 m/s is conducted. This in order to increase the consequential yaw SAS rudder command to reduce the sideslip angle during the manoeuvre for demonstration. Here the rudder deflection can be seen to increase rapidly (because of the tuning) to the unfeasible deflection of 60° . The effect of the angular rate slope on the rudder deflection can also be seen around the 5 seconds mark.

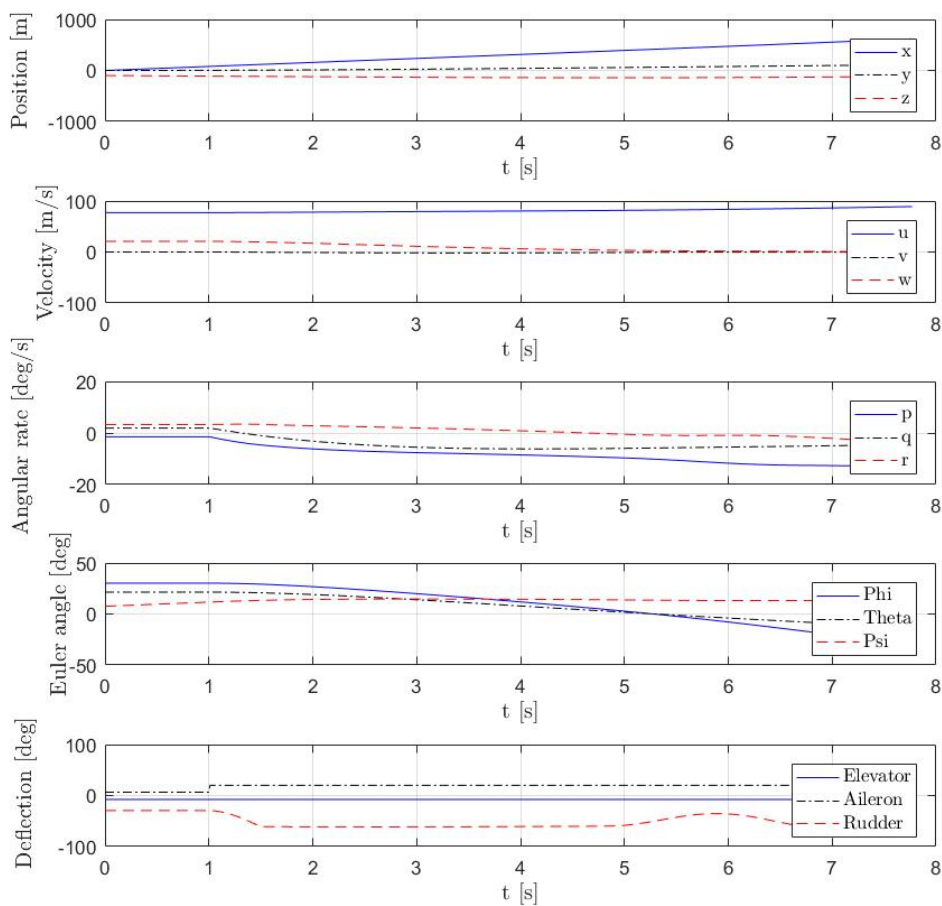


Figure 6.19: Unfeasible Flying V OEI Bank 2 Bank manoeuvre

Steady Heading Sideslip

The amount of sideslip leading to optimum trim for prompt achievement of the best drag configuration in case of an engine failure is normally displayed to the pilot. The requirement treated is the CS 25.121 Climb one-engine-inoperative. Here a constraint is put on the maximum bank angle allowed during the demonstration of a minimum climb gradient in case of One Engine Inoperative (OEI). The Acceptable Means of Compliance (AMC) state an acceptable bank angle value of 2 to 3°. The thrust of one engine was set to zero while the other engine provided an Equivalent Bare Engine Take-Off Thrust of 379 kN, as provided by the EASA E.111 Rolls Royce Trent XWB series engines Type Certificate datasheet [2]. Note that this is assumed to be an acceptable overestimation of the actual engine thrust applied as no windmilling drag is added. It was chosen to trim the aircraft with a constant True Airspeed and constant heading and allow the climb gradient to be a consequence. The target climb gradients were easily obtained due to the underestimated drag models. In total three test points were defined for both aircraft. The reference aircraft required its highest rudder deflection of 25.9° in case of a OEI SHS climb in Conf FULL at MLW at the approach speed with the CG placed at the forward limit. The Flying V reached its control stop for the same test point (without high lift devices) and failed another test point. The latter was a climb at MTOW at V_2 where a minimum value of 37° was demanded from the rudders, which is beyond its maximum deflection. The problematic values are again indicated in bold and displayed in Tables 6.18 and 6.19.

6.4.4. Proposed Solution

Flying wings, without vertical tails possess several unique lateral-directional characteristics. They include low side force in sideslip, low yaw damping, low directional stability and large ratio of dihedral to directional stability. With this and One Engine Inoperative requirements in mind, Palermo made a preliminary design for the vertical fins of the Flying V [20]. In the One Engine Inoperative tests conducted it was shown that there were four sizing cases for the Flying V's vertical fins.

Conventionally, a rudder mounted on the vertical tailplane of a conventional aircraft provides yaw control. On flying wings like the Northrop B2, however, split elevons are implemented. They create a yawing moment by creating a differential drag over a long moment arm. They are as a result conventionally installed at the wing tips. Combinations of the aforementioned control surfaces with drag rudders (e.g. Rutan Long-ez) also exist. This control allocation might become interesting in case no sufficient control power is achieved through either split elevons and/or rudders installed on the winglets. It was however kept in mind that the purpose and the benefit of a concept such as the Flying V lies in the cleanness and simplicity of its design. A possibility could be the combination of controls where the winglet rudders are combined with drag ruddervons. In case of One Engine Inoperative, the idea is to open the split rudder installed on the winglet on the side of the operative engine to reduce the thrust yaw moment by increasing drag on that side. Furthermore the sideslip angle should be kept within tolerance by deflecting the winglet rudder on the side of the engine failure. Additionally, deploying split elevons or ruddervons to a small degree during approach could hold better speed stability characteristics in e.g. approach.

When drag rudders would be installed on the winglets of the Flying V, a significant pitching moment would be created each time these rudders are operated. This since they would hold a moment arm to the Centre of Gravity along the top axis. The pitching moment created by split elevons is limited. Additionally the winglets do not have to be structurally enforced. The split elevons are easier to accommodate while adding as little complexity to the control system. This since no extra control surfaces are created. Therefore split elevons would hold the most ingenious method for providing directional control and damping for the Flying V. That is, if they are able to operate as yaw dampers and provide sufficient controllability and stability. Kindly note that the winglets will still provide significant directional stability. Split elevons are found to mainly provide favourable control power while cruising in still air while losing their effectiveness in turbulent air and lower speeds.

The importance of keeping the thrust lines as close as possible to the centreline is evident, but becomes even more significant in case of the split rudder control allocation. In this case, on top of the lost thrust due to engine failure, drag is added to maintain directional control. Due to the aerodynamically cleaner design of the Flying V, it is likely that smaller powerplants will be utilized. Reducing the directional control power constraints but possibly running into excess thrust limitations which should be able to safeguard an adequate climb gradient in case of OEI.

Figure 6.20 provides an example of a possible control allocation which could resolve the rudder control power issues found.

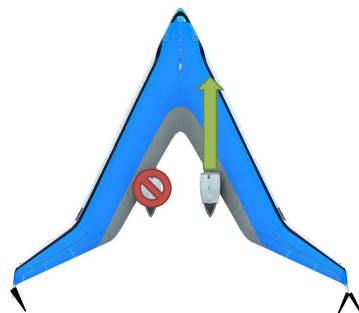


Figure 6.20: Potential control allocation in case of One Engine Inoperative

Mass [t]	CG [%MAC]	Conf	ϕ [deg]	TAS [kt]/[m/s]	AOA [deg]	δ_e [deg]	δ_a [deg]	δ_r [deg]	THR
210	45	n.a.	30	156/80	13.8	-11.2	-1.9/-20.6	29.1	OEI
210	45	n.a.	40	167/86	13.6	-11.4	-17.9/-4.8	7.1	AEO Climb FPA +7.7°
210	45	n.a.	40	220/113	5.7	-6.3	-4.9/-4.9	15.3	OEI
210	45	n.a.	40	152/78	17.7	-12.6	-20.3/-5.0	7.5	AEO FPA -3°

Table 6.14: Flying V Coordinated turn test points

Mass [t]	CG [%MAC]	Conf	ϕ [deg]	TAS [kn]/[m/s]	AOA [deg]	δ_e [deg]	δ_a [deg]	δ_r [deg]	THR
210	20	Take-Off	30	163/84	12.9	-7.4	-0.9	21.0	OEI
210	20	Take-Off	40	177/91	12.6	-7.9	-3.5	1.3	AEO Climb FPA +7.7°
210	18	Clean	40	220/113	7.1	-4.5	-0.5	13.4	OEI
210	20	Landing	40	142/73	17.7	-17 (e) θ / -11 (THS)	-6	1.8	AEO FPA -3°

Table 6.15: Reference Aircraft Coordinated turn test points

Mass [t]	CG [%MAC]	Conf	TAS [kn]/[m/s]	β [deg]	$\delta_{r_{max}}$ [deg]	δ_a [deg]	Time to roll [s]	THR
260	57.5	n.a.	156/80	10	60	20	9.5	OEI
260	57.5	n.a.	485/250	-0.3	20	10 (EV1)	6.1	AEO FPA -5%
260	57.5	n.a.	152/78	10.8	60	20	5.3	AEO FPA -5%

Table 6.16: Flying V Bank to Bank test points

Mass [t]	CG [%MAC]	Conf	TAS [kn]/[m/s]	β [deg]	$\delta_{r_{max}}$ [deg]	δ_a [deg]	Time to roll [s]	THR
260	38	Take-Off	163/84	8	30	20	11.0	OEI
260	38	Clean	485/250	0	3.1	20 (inboard)	3.3	AEO FPA -5%
260	38	Landing	142/73	-1.9	20	30	6.5	AEO FPA -5%

Table 6.17: Reference Aircraft Bank to Bank test points

Mass [t]	CG [%MAC]	Conf	TAS [kn]/[m/s]	ϕ [deg]	β [deg]	δ_r [deg]	δ_a [deg]	THR
260	45	n.a.	156/80	3	-23.7	4.4	36.8	OEI
260	45	n.a.	220/113	3	-12.5	3.7	15.4	OEI
210	45	n.a.	152/78	3	-13.4	2.4	30.1	OEI

Table 6.18: Flying V OEI Steady Heading Sideslip test points

Mass [t]	CG [%MAC]	Conf	TAS [kn]/[m/s]	ϕ [deg]	β [deg]	δ_r [deg]	δ_a [deg]	THR
260	25	Take-Off	163/84	3	-1.9	-1.9	20	OEI
260	25	CLEAN	220/113	3	-1.6	0.9	12.3	OEI
210	20	n.a.	142/73	3	-2.5	1.7	25.9	OEI

Table 6.19: Reference Aircraft OEI Steady Heading Sideslip test points

Conclusion & Recommendations

7.1. Conclusion

A flight mechanics toolbox is created to assess the Handling Qualities of a Flying V configuration with respect to the selected criteria. The analysis is repeated for a reference aircraft based on the Airbus A350-900. The most significant results are presented to demonstrate the capabilities of the Flying V and toolbox. Classic Handling Qualities requirements were demonstrated to be applicable to the Flying V. The most forward and rearward Centre of Gravity locations were motivated to be at 45% and 57.5% Mean Aerodynamic Chord. This CG range results in about the same total distance of CG travel on the reference aircraft. The Mean Aerodynamic Chords and CG limitations are repeated in Figures 7.1 and 7.2. The effect of Centre of Gravity location on the Flying V was investigated for each requirement specified.

Limited lateral-directional controllability was found to postulate in the One Engine Inoperative tests at low speed for the Flying V. Moreover the limiting requirements were identified to mainly be within the controllability and manoeuvrability requirements of CS 25.143. The effect of design changes like dihedral and vertical fin size were analyzed and sensitivities on the dutch roll were demonstrated.

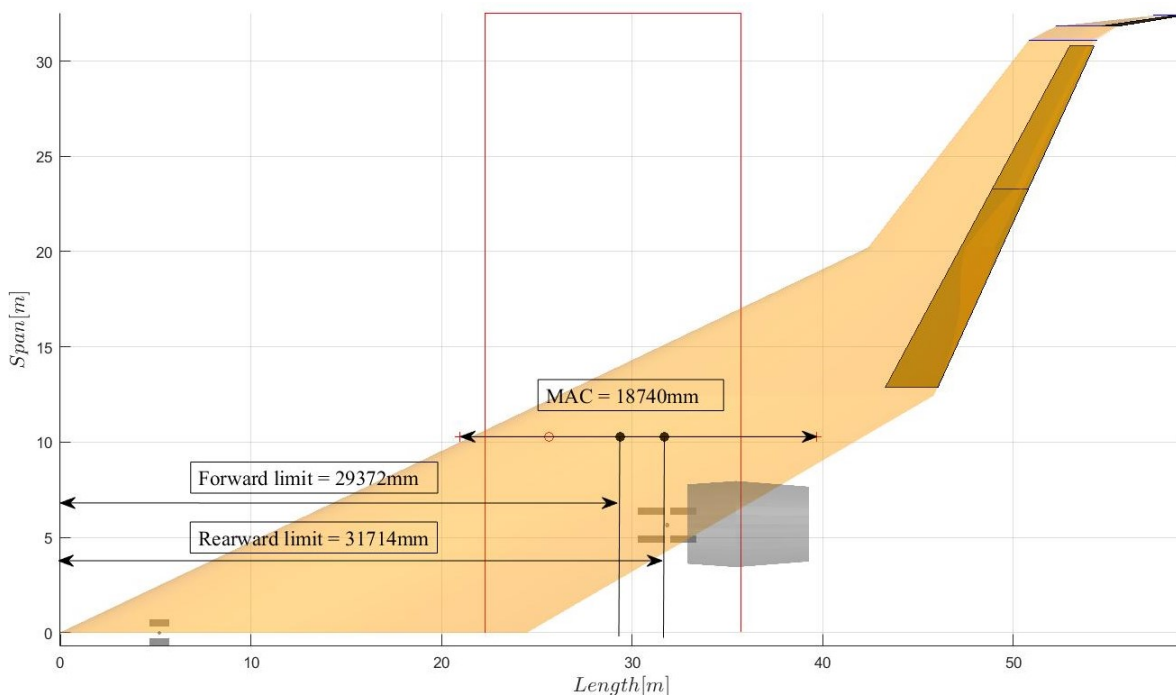


Figure 7.1: Flying V Centre of Gravity limitations

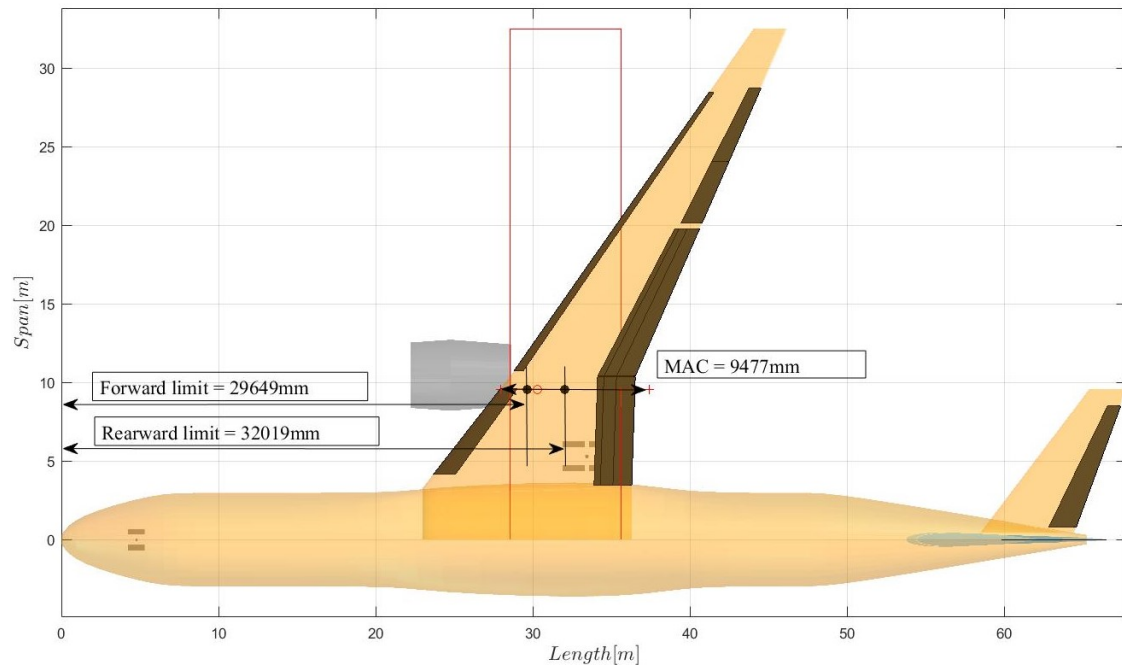


Figure 7.2: Reference Aircraft Centre of Gravity limitations

7.2. Recommendations

7.2.1. Flight Mechanics Toolbox

Up to this point, not all capabilities of the toolbox developed have been exploited. The unexploited capabilities lay mainly within the landing-gear model and its effects on the aircraft's behaviour. Moreover, in the current model, a change in centre of gravity location was implemented through the parametric models which resulted in altered aero and inertia models. It is however also possible to change the centre of gravity location in the Equations of Motion themselves. Additionally no fuel or mass imbalance in the lateral direction has been investigated even though this can be taken into account in the equations of the model.

Potentially crucial test points to be undertaken in the future are the rotation behaviour/control power and Minimum Control Speed on ground. Here it has to be shown that the aeroplane can be controlled using rudder alone (without nose wheel steering). Hereby enabling the take-off to be safely continued in case of an engine failure while the aircraft may not deviate more than 9.1 m laterally from the centreline. For this reason and for future investigation through the toolbox, modifications are required to increase the fidelity of the model. Specific to the landing gear model, bending modes and friction forces should be implemented.

The Vortex Lattice Method could in the future be extended with more accurate estimates for parasite and wave drag. Aerodynamic data in general could be improved through using combinations of tools such as VLM, CFD, windtunnel data. This since it is not uncommon for toolboxes to use different choices of the adequate aerodynamic model dependent on the purpose of the model. During the course of 2020, it is also planned to implement spoilers and split elevons and ruddervons to the capabilities of the VLM which allows for higher fidelity control allocation studies.

The propulsion model could be enhanced to a static engine model, where the thrust vector is based on the flight condition. This makes the thrust dependent on Mach number, altitude and fuel flow. Analyzing OEI conditions or manoeuvres where engine dynamics affect the performance requires dynamic models. This could be assessed through a Gas Turbine Simulation program.

Currently the model does not incorporate failure cases. Should they in the future be considered the idea is that the more likely a failure, the better the consequent-and-subsequent flying qualities should be. As the model is linearized, the investigations undertaken currently only hold valuable information within the flight envelope encompassing linear flight characteristics. No research was undertaken at the corners of the flight envelope where behaviour is expected to be nonlinear.

Aeroelastic effects will affect the stability and control derivatives together with the general performance of the airframe. Therefore these deformations and bending modes should be taken into account. This will also result in a different parametric model as the difference in between jig shape and loaded model is taken into account.

7.2.2. Flying V

The split line between elevon 1 and 2 was chosen rather arbitrarily. Through the implementation of a control mixer, where the elevons take up more than one primary control surface task, this did not pose any problem. The total control surface volume of elevons 1 and 2 was found to be sufficient. The sizing cases were found to be longitudinal control power driven. Criteria such as the pull-up manoeuvre, trim in coordinated turn and trim on approach lead to this conclusion. This since the use of the inner elevon alone did not result in sufficient control surface deflection margin to its maximum deflection.

A specific control allocation study should be undertaken as the number of control surfaces has to increase for redundancy and optimized control allocation. In the future, as split elevons might get introduced together with spoilers, the lateral directional control power issues can be further investigated. This together with a design study for the vertical fins.

Claeys' [8] mass estimations were utilized throughout the investigation. The current Centre of Gravity range determined and mass distribution of the Flying V are found not to match. Therefore the internal design configuration should be revised.

Eigenmodes, specific to Flying wing designs, such as tumbling, should be investigated. Speed stability (on approach) is another topic to investigate in the future together with a control configuration to increase drag on glideslope and perform emergency descents. Currently the approach speed is limited by the lift coefficient found at an angle of attack of 18° . This in order to provide sufficient margin in comparison the pitch break tendencies found to postulate around 20° of Angle of Attack.

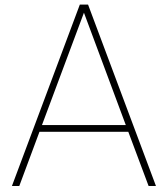
A full investigation into the handling qualities of the Flying V should be made for a wide range of aircraft configurations spanning across the flight envelope. Future design work could focus on the limited lateral-directional controllability which was found to postulate in the One Engine Inoperative tests at low speed. Optimized control allocation and implementing spoilers and/or split elevons or ruddervons are likely to resolve this problem. Additionally a design change certifiable yaw damper should be developed to ensure Dutch Roll stability in all phases of flight for the specified Centre of Gravity envelope.

In summary, the research objectives of Airbus Future Projects Office were obtained and the research questions were answered. A solid foundation in the form of a flexible Flight Mechanics Model is provided for future work. Lastly a relevant direction for future research was proposed.

Bibliography

- [1] European Union Aviation Safety Agency. *Certification Specifications for Large Aeroplanes CS-25 - Amendment 23*. European Union Aviation Safety Agency, Konrad-Adenauer-Ufer 3, 50668 Köln, Germany, 2019.
- [2] European Union Aviation Safety Agency. Type certificate data sheet no.easa e.111 for trent xwb series engines. page 19, 2019.
- [3] Airbus. A350-900 flight deck and systems briefing for pilots. URL <http://www.smartcockpit.com/docs/a350-900-flight-deck-and-systems-briefing-for-pilots.pdf>.
- [4] Barton J. Bacon and Irene M. Gregory. General equations of motion for a damaged asymmetric aircraft. *NASA Langley Research Center, Hampton, VA, 23681*. doi: 10.2514/6.2007-6306.
- [5] J. Benad. The flying v, a new aircraft configuration for commercial passenger transport. *Airbus Operations GmbH*, 2015 .
- [6] K. Bender. Analyse der handling qualities im flugzeugvorentwurf. *Diplomarbeit, Institut für Flugzeugbau der Universität Stuttgart*, 2002 .
- [7] Martin Carrizales, Mohammad Lone, and Estela Bragado Aldana. Non-elliptic wing lift distribution wings to decrease vertical tailplane size in commercial aircraft. 01 2019. doi: 10.2514/6.2019-0265.
- [8] M.B.P. Claeys. Flying v and reference aircraft structural analysis and mass comparison. page 46, August 2018 .
- [9] Airbus Airport Compatibility. Icao / easa aerodrome reference code, faa airplane design group and aircraft approach category for airbus aircraft. September 2019 .
- [10] W. V. Cook and H. V. de Castro. The longitudinal flying qualities of a blended-wing-body civil transport aircraft. *The Aeronautical Journal, Vol. 108, No. 1080*, pages 75–84, 2004 .
- [11] G. Cooper and R. Harper. The use of pilot rating in the evaluation of aircraft handling qualities. *Technical Report TN D-5153, NASA*, April 1969 .
- [12] F. Faggiano. Aerodynamic design optimization of a flying v aircraft. *TU delft repository*, November 2016 .
- [13] Antonio Filippone. *Advanced Aircraft Flight Performance*. 01 2012. doi: 10.1017/CBO9781139161893.
- [14] Airbus Product Safety Department (GS). Control your speed...at take-off. *Airbus Safety magazine, Safety First*, page 19, July 2014 .
- [15] J. Hodgkinson. *Aircraft Handling Qualities*. AIAA education series. Blackwell Science, 1999. ISBN 9780632038169. URL <https://books.google.be/books?id=vPFHswEACAAJ>.
- [16] Steven B. Jacobson and Thomas D. Colangelo. B-2 flight control system development flight test lessons learned.
- [17] Anthony Brabazon Jonathan Byrne, Philip Cardiff and Michael O'Neill. Evolving an aircraft using a parametric design system. *Natural Computing Research & Applications Group University College Dublin, Ireland*, 2014 .
- [18] Dimitri N. Mavris. Probabilistic analysis of an hsct modeled with an equivalent laminated plate wing. *Copyright © 1997 Society of Automotive Engineers, Inc.*, August 1999 .
- [19] Department of Defense Handbook. Mil-std-1797a flying qualities of piloted aircraft. *Interface Standard*, pages 2–18, 1997 .

- [20] M. Palermo. The longitudinal static stability and control characteristics of a flying v scaled model, an experimental and numerical investigation. *TU delft repository*, February 2019 .
- [21] Berta Rubio Pascual. Engine-airframe integration for the flying-v. *TU Delft Repository*, November 2018 .
- [22] Daniel Raymer. *Aircraft Design: A Conceptual Approach, Sixth Edition*. 09 2018. ISBN 978-1-62410-490-9. doi: 10.2514/4.104909.
- [23] J. Roskam. *Airplane Design, Part V: Component Weight Estimation*. Number dl. 5 in Airplane Design. DARcorporation, 1985. ISBN 9781884885501. URL <https://books.google.de/books?id=mMU47Ld7yQkC>.
- [24] Jan Roskam. *Airplane Design: Preliminary Calculation of Aerodynamic, Thrust and Power Characteristics. Determination of Stability, Control and Performance Characteristics: Far and Military Requirements. Airplane Cost Estimation, Design, Development, Manufacturing and Operating*. DARcorporation, 1440 Wakarusa Drive, Suite 500, Lawrence, Kansas 66049, U.S.A., 2006.
- [25] Airbus S.A.S. *A350 Airplane Characteritics, Airport and Maintenance Planning*. Airbus S.A.S. Customer Services Technical Data Support and Services, 31707 Blagnac Cedex, France, 2002.
- [26] Airbus S.A.S. *A300-600 Airplane Characteritics For Airport Planning AC*. Airbus S.A.S. Customer Services Technical Data and Services, 31707 Blagnac Cedex, France, 2002.
- [27] H. Schlichting and E. A. Truckenbrodt. Aerodynamik des flugzeuges. Erster Band:480, 2000.
- [28] H. Schlichting and E. A. Truckenbrodt. Aerodynamik des flugzeuges. Zweiter Band:480, 2000.
- [29] Airbus Customer Services. *Getting to grips with aircraft performance*. Airbus Flight Operations Support & Line Assistance, 1, rond-point Maurice Bellonte, BP 33 31707 BLAGNAC Cedex FRANCE, 2002.
- [30] J.A. Mulder / W.H.J.J. van Staveren / J.C. van der Vaart / E. de Weerd / C.C. de Visser / A.C. in 't Veld / E. Mooij. *Flight Dynamics Lecture Notes*. Control and Simulation division, Delft University of Technology, Kluyverweg 1, 2629 HS Delft, Netherlands, 2013.



Cooper-Harper Rating Scale

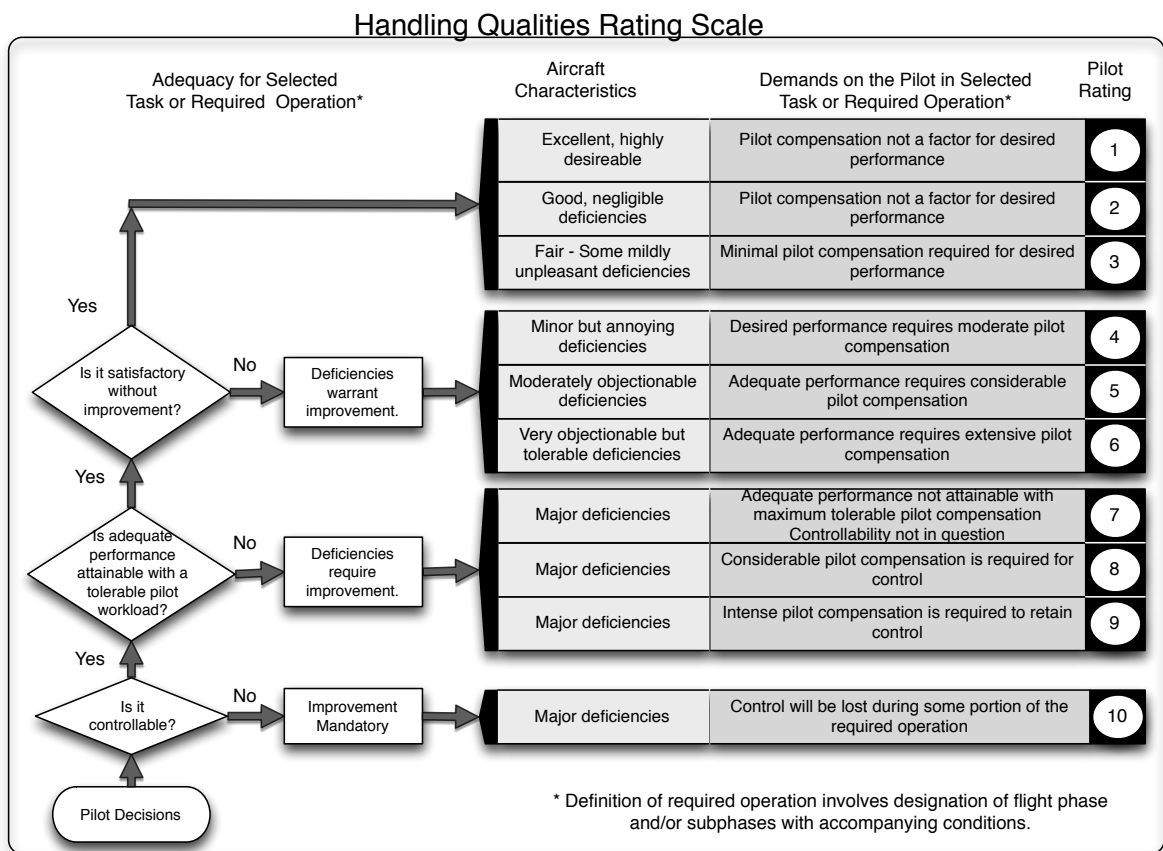


Figure A.1: Cooper Harper Rating Scale, G. Cooper and R. Harper. The use of pilot rating in the evaluation of aircraft handling qualities. Technical Report TN D-5153, NASA, April 1969 [11]

B

MIL-HDBK-1797A Extractions

Level/Degree	Definition	HQR
1/Satisfactory	Flying qualities clearly adequate for the mission Flight Phase.	≥ 3.5
2/Adequate	Flying qualities adequate to accomplish the mission Flight Phase, but some increase in pilot workload or degradation in mission effectiveness, or both, exists.	≥ 6.5
3/Controllable	Flying qualities such that the airplane can be controlled safely, but pilot workload is excessive or mission effectiveness is inadequate, or both. Category A Flight Phases can be terminated safely, and Category B and C Flight Phases can be completed.	≥ 9.5

Table B.1: Handling Qualities definition and their rating in MIL-HDBK-1797A [19]

Class	Aircraft
I	Small, light airplanes
II	Medium weight, low-to-medium manoeuvrability airplanes
III	Large, heavy, low-to-medium manoeuvrability airplanes
IV	High-manoevrability airplanes

Table B.2: Aircraft Classes definition in MIL-HDBK-1797A [19]

Category	Flight Phase
A	Flight Phases that require rapid manoeuvring
B	Non terminal Flight Phases (Climb, Cruise, Loiter)
C	Terminal Flight Phases

Table B.3: Flight phases definition in MIL-HDBK-1797A [19]

Level	Flight Phase Category	
	A,C	B
1	$0.35 \leq \zeta \leq 1.30$	$0.3 \leq \zeta \leq 2.00$
2	$0.25 \leq \zeta \leq 2.00$	$0.20 \leq \zeta \leq 2.00$
3	$\zeta \geq 0.15$	$\zeta \geq 0.15$

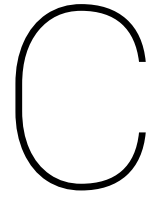
Table B.4: Short period requirements in MIL-HDBK-1797A [19]

Level	Applies to all Categories
1	$\zeta \geq 0.04$
2	$\zeta \geq 0$
3	$T_2 \geq 55s$ (Unstable)

Table B.5: Phugoid requirements in MIL-HDBK-1797A [19]

Level	Flight Phase Category	Class	Min ζ_d [-]	Min $\zeta_d \omega_d$ [rad/s]	Min ω_d [rad/s]
1	A (CO,GA,PR, TFRC,FEAS)	I, II, III, IV	0.4	0.4	1.0
		I, IV	0.19	0.35	1.0
	A	II, III	0.19	0.35	0.4
	B	All	0.08	0.15	0.4
	C	I, II-C IV	0.08	0.15	1.0
		II-L, III	0.08	0.1	0.4
2	All	All	0.02	0.05	0.4
3	All	All	0	-	0.4

Table B.6: MIL-HDBK-1797 Recommended minimum dutch roll frequency and damping [19]



Parametric Model Values

Flying V model Planform Class

Description	Value	Unit
Wing span	62.2	[m]
Wing area	875.7	[m ²]
Taper ratio	0.146	[-]
Leading edge sweep up to the 1 st kink position	64.4	[deg]
Leading edge sweep up to the 2 nd kink position	37.8	[deg]
Relative spanwise kink 1 location	40	[%]
Relative spanwise kink 2 location	65	[%]
Dihedral of the inboard wing	0	[deg]
Dihedral of the outboard wing	7	[deg]
Twist at spanwise Kink 2 location	-4.3	[deg]
Twist at the tip location	-4.4	[deg]

Table C.1: The initial values utilized to define the Flying V's planform in the BlackSwan Class

Winglet Class

Description	Value	Unit
Leading edge sweep	36	[deg]
Taper ratio	0.45	[-]
Winglet root to planform tip ratio	1	[-]
Winglet length	7	[m]
Cant angle	8	[deg]
Radius	0.48	[m]
Delta twist from root to tip	0	[m]

Table C.2: The initial values utilized to define the Flying V's winglet in the BlackSwan Class

Landing Gear Class

Description	NLG value	MLG value	Unit
Pintle axis length	4	5.2	[m]
Wheel diameter	1.05	1.4	[m]
Wheel width	0.395	0.53	[m]
Wheels per axle	2	2	[-]
Number of axles	1	2	[-]
Axle spacing	n.a.	1.2	[m]
Wheel spacing	1.05	2.65	[m]
Axle compression	0.3	0.3	[m]
Global x coordinate of central wheel contact patch	5.19	31.85	[m]
Global y coordinate of central wheel contact patch	0	5.65 (RHS)	[m]
Global z coordinate of central wheel contact patch	-5	-6.384	[m]

Table C.3: The initial values utilized to define the Flying V's Landing Gear in the BlackSwan Class

Reference Aircraft Model

Wing Class

Description	Value	Unit
Span	65	[m]
Area	442	[m^2]
Taper ratio	0.2	[-]
Leading edge sweep	35	[deg]
Dihedral angle	7.12	[deg]
Delta dihedral outboard section	-1.3	[deg]
Kink eta	32	[%]
Yehudi angle	22	[deg]
Leading edge extension angle	4.9	[deg]
Spanwise location of the root	10	[%]

Reference Aircraft Wing Class

Horizontal Tailplane Class

Description	Value	Unit
Span	18.3	[m]
Area	77	[m^2]
Taper ratio	0.4	[-]
Leading edge sweep	37	[deg]
Dihedral angle	4.6	[deg]

Table C.4: Reference Aircraft Horizontal Tailplane Class

Vertical Tailplane Class

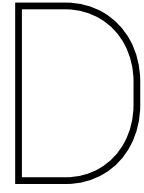
Description	Value	Unit
Height	9.42	[m]
Area	49.7	[m ²]
Taper ratio	0.39	[-]
Leading edge sweep	44	[deg]
Leading edge extension spanwise location	30	[%]
Leading edge extension angle	15	[deg]

Table C.5: Reference Aircraft Vertical Tailplane Class

Fuselage Class

Description	Value	Unit
Width	5.96	[m]
Height	6.09	[m]
Length	65.3	[m]
Nose length ratio	1.01	[-]
Nose height ratio	-0.23	[-]
Tail length ratio	1.74	[-]
Tail height ratio	0.24	[-]
Body fairing length ratio	0.31	[-]
Body fairing position ratio	0.31	[-]
Body fairing sharpness	0.173	[-]
Body fairing forward width ratio	1.13	[-]
Body fairing forward height ratio	1.04	[-]
Body fairing rearward width ratio	1.31	[-]
Body fairing rearward height ratio	1.19	[-]

Table C.6: Reference Aircraft Fuselage Class



A300-600 Mass & Inertia Model

The airplane characteristics for airport planning [26] is property of Airbus S.A.S. and can be retrieved by the public, providing high fidelity characteristics of the A300-600. The above mentioned values together with a three view were utilized to set-up the BlackSwan model of the A300-600. Additionally, a document by FedEx¹ on the A300-600 Airframe Systems for the Air Transport Association provided detailed landing gear weights.

As most weights could be deduced from documentation, it was only required to find weights for the:

- Fuselage (including furniture, operational equipment, systems and structure)
- Wing structure and systems
- Empennage structure and systems

Therefore following equations were adopted from Roskam's Airplane Design series on Component Weight Estimation.

$$M_w = 0.0017 \cdot W_{MZF} (b / \cos(\lambda_{1/2}))^{0.75} (1 + 6.3 \cdot \cos(\lambda_{1/2}) / b^{1/2}) \times (n_{ult})^{0.55} (bS / t_r W_{MZF} \cos(\lambda_{1/2}))^{0.3} \quad (D.1)$$

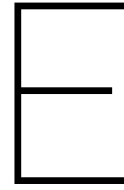
$$M_h = K_h S_h [3.81 (S_h)^{0.2} V_D / 1,000 (\cos(\lambda_{1/2_h}))^{1/2} - 0.287] \quad (D.2)$$

$$M_v = K_v S_v [3.81 (S_v)^{0.2} V_D / 1,000 (\cos(\lambda_{1/2_v}))^{1/2} - 0.287] \quad (D.3)$$

Kindly note that the equations utilize British Imperial Units, additionally Roskam's notation is adopted as well as possible. Following definition of terms apply:

- M_w : mass of the wing
- M_h : mass of the horizontal tailplane
- M_v : mass of the vertical tailplane
- M_{MZF} : maximum zero fuel weight
- $\lambda_{1/2}$: wing semi-chord sweep angle
- t_r : maximum thickness of wing root chord
- b : wing span
- S : wing area
- K_h : 1.1 for variable incidence stabilizers
- K_v : 1.0 for fuselage mounted horizontal tails
- V_D : Design dive speed [kts]

¹<https://de.scribd.com/doc/287052535/Airbus-32-A300-A310-Landing-Gear>



Odilila Delta Wing Validation

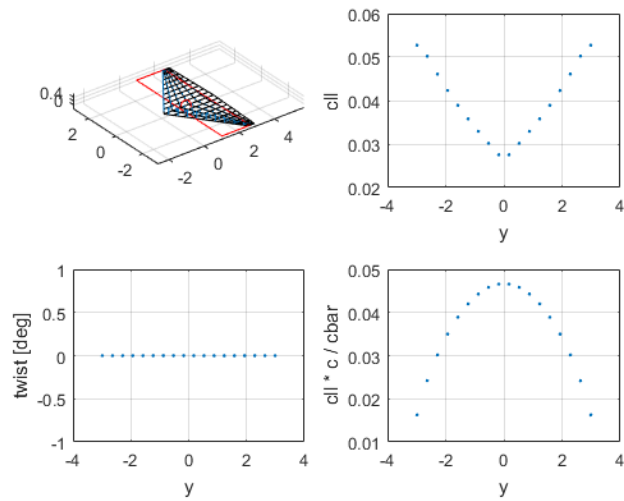


Figure E.1: Odilila delta wing panel model and lift distribution without wing twist

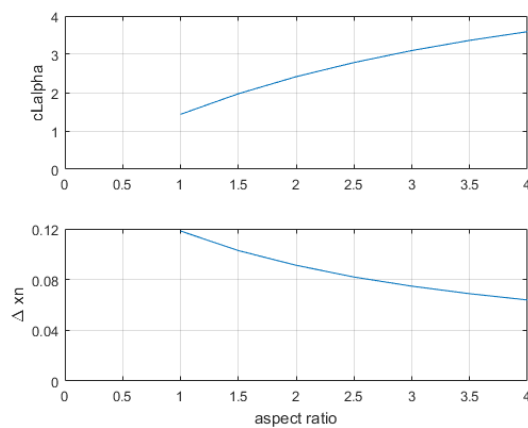


Figure E.2: Lift gradient and Neutral Point shift for varying aspect ratio of delta wings